



UNIVERSITY OF CAPE TOWN
CENTRE FOR MINERALS RESEARCH

**ON-LINE SENSORS FOR MEASURING THE TOTAL BALL AND CHARGE
LEVEL IN TUMBLING MILLS**

by

SARPONG BISMARCK DONKOR

BSc. Mineral Engineering, University of Mines and Technology Tarkwa- Ghana, 2009.

A thesis submitted in fulfilment of the requirements for the award of the degree of
Master of Sciences in Engineering, MSc (Eng.)

Centre for Minerals Research - Comminution Group

Department of Chemical Engineering

April 2014

The copyright of this thesis vests in the author. No quotation from it or information derived from it is to be published without full acknowledgement of the source. The thesis is to be used for private study or non-commercial research purposes only.

Published by the University of Cape Town (UCT) in terms of the non-exclusive license granted to UCT by the author.

DECLARATION OF ORIGINALITY

This is to certify that the work is entirely my own, not that of any other person, unless explicitly acknowledged. The work has not been submitted in any form to the University of Cape Town or to any other institution for assessment for any purpose.

Signed

SARPONG B. DONKOR

Date

ABSTRACT

Tumbling mills are still the mostly used milling device in the mineral processing industry for both coarse and fine grinding applications. A number of factors affect the performance of tumbling mill. One of these factors is volumetric filling which is the volume of charge in the mill expressed as a fraction of the total volume available. The volumetric filling controls the mill throughput, power draw and product size. The common method of measuring volumetric filling is by taking in situ measurements when the mill is stationary. This method is disruptive to production due to the mill downtime involved. The use of on-line sensors for measuring the volumetric filling using acoustic, inductive proximity and conductive sensors are the new technologies attempting to monitor volumetric filling in situ. The methods are non-intrusive and low cost approach for direct monitoring of dynamic volumetric filling conditions in the tumbling mill. The dynamic volumetric filling was assumed to be directly related to static mill filling conditions.

In this study, the volumetric filling was calculated from the toe and shoulder angles estimated by the CSIRO monitor (acoustic) and the Magotteaux Sensomag (inductive proximity and conductive) sensors. The CSIRO acoustic sensor was installed on a run-of-mine (RoM) ball mill at Angloplatinum UG2 Concentrator at Rustenburg, South Africa. The toe and shoulder angles were obtained from the surface vibration caused by the impact of the charge on the mill shell. The industrial scale experiments were performed at varied mill feed rate at constant ball load of 28%. In the pilot scale experiments, the Magotteaux ball mill at Frank Concentrator was equipped with a Sensomag sensor for measuring the toe and shoulder angles of the slurry and ball load based on the principle of conductance and induction, respectively. The mill was configured to operate as a RoM ball mill. The experiments were conducted at varying mill speeds (75%-85% critical speed), feed rate (1200-2800kg/hr) and ball loads (15-26%). The static mill filling was determined from physical measurements after crash stopping the mill.

The results indicated that the two sensors tested are capable of providing continuous measurements of the toe and shoulder angle of the mill charge on-line, which can be used to estimate the dynamic volumetric filling. The results obtained from the experiments on industrial and pilot scale mill show satisfactory agreement between the static volumetric filling measurements and the dynamic volumetric filling. A direct relationship was observed

between the shoulder angle and volumetric filling, while an inverse relationship was observed between the toe angle and dynamic volumetric filling. In addition, it was found that there is an inverse relationship between the material passing percentage $75\mu\text{m}$ and the dynamic volumetric filling. This is due to the decreased in impact force on the charge as a result dropped in the impact height of the charge from the shoulder region. This study found that the information from the sensors can be used in the control strategy of the grinding circuit and that they will reduce mill down time and hence increase throughput.

DEDICATION

I dedicate my dissertation work to my family and many friends. A special word of gratitude goes to my loving wife, Evelyn Blankson whose words of encouragement and push for tenacity ring in my ears.

ACKNOWLEDGMENTS

First, I would like to express my sincere gratitude to the Almighty God, my Creator and Saviour, for the strength to complete this work.

I would like to express my great thanks to those who have made my work possible and contributed with support, encouragement and valuable advice. Special thanks go to my supervisor, Associate Professor Aubrey Mainza, for his patience, encouragement, guidance and support for the completion of this work. To Mussa Lisso, Umut Kadir Erol and Paul Bepswa and all the members of the Centre for Mineral Research – Comminution group for their assistance with various aspects of this research project.

I would like to appreciate Mauritz, Benoit Clermont and Bernard de Haas from Magotteaux and Anglo Platinum UG2 Waterval Concentrator for allowing me to conduct my research work using their facilities. Special thanks to Peter Dawson and Naressa Naicker for their hospitality.

Finally, I acknowledge my parents and family for their encouragement, and the emotional and social support with which they provided me throughout this work.

TABLE OF CONTENTS

DECLARATION OF ORIGINALITY	i
ABSTRACT.....	ii
DEDICATION.....	iv
ACKNOWLEDGMENTS	v
TABLE OF CONTENTS.....	vi
LIST OF FIGURES	ix
LIST OF TABLES.....	xi
NOMENCLATURE	xii
CHAPTER ONE: INTRODUCTION	1
1.1 Hypothesis.....	2
1.2 Scope of this study.....	2
1.3 Thesis layout.....	3
CHAPTER TWO: LITERATURE REVIEW	4
2.1 Introduction.....	4
2.2 General application of tumbling mills.....	4
2.3 Types of tumbling mills	4
2.3.1 Autogenous (AG) mills.....	5
2.3.2 Semi-Autogenous (SAG) mills.....	5
2.3.3 Ball mill	5
2.3.4 RoM ball mill.....	5
2.4 The Motion of the charge in the tumbling mill.....	5
2.5 The shape of the charge in the tumbling mill	6
2.5.1 The methods for determining of shape of the charge	6
2.5.1 Morrell’s charge shape.....	6
2.5.2 Discrete Element Method (DEM)	10
2.6 Tumbling mill load behaviour measuring technologies	10
2.6.1 Conductivity probe technology.....	11
2.6.2 Strain gauge sensors	14
2.6.3 Inductive proximity probe	18
2.6.4 The Magotteaux Sensomag sensor	20
2.6.5 Piezo-electric strain transducer	20
2.6.6 Acoustic Emission Measuring Technology (AE).....	24
2.6.7 The CSIRO Acoustic sensor.....	24
2.7 The method of measuring volumetric filling in tumbling mills	26
2.8 Conclusion	28

CHAPTER THREE: THE DESCRIPTION OF EXPERIMENTAL APPARATUS AND METHOD FOR ACOUSTIC SENSOR	29
3.1 Introduction	29
3.2 Flowsheet of UG2 primary grinding circuit	29
3.3 Experimental Apparatus (Acoustic sensor)	31
3.3.2 Accelerometer module	32
3.3.3 Angular position for each accelerometer	32
3.4 Experimental methodology	33
3.4.1 Sampling the vibratory screen oversize	34
3.4.2 Vibratory screen undersize	35
3.4.3 Trommel oversize stream	35
3.4.4 Mill grind-out	35
3.4.5 Sample processing	36
3.4.6 Wet screening of sub -1mm samples	37
CHAPTER FOUR: INDUSTRIAL SCALE EXPERIMENTAL RESULTS AND ANALYSIS OF THE ACOUSTIC SENSOR	39
4.1 Introduction	39
4.2 The total vibration power	39
4.3 The profile of the toe and shoulder angle	41
4.4 The results for calculation of the dynamic volumetric filling	43
4.4.1 Relationship between the dynamic volumetric filling and mill mass.....	45
4.4.2 The results of the dynamic ball filling calculations.....	46
4.5 Relationship between grind and the toe and shoulder angle	47
4.6 Relationship between dynamic mill filling and dynamic positions	49
4.7 Relationship between mill power and grind	51
4.8 Conclusions	53
CHAPTER FIVE: THE DESCRIPTION OF EXPERIMENTAL APPARATUS AND METHODOLOGY FOR PILOT SCALE USING THE SENSOMAG SENSOR	54
5.1 Introduction	54
5.2 The description of the Magotteaux pilot plant	54
5.3 The experimental device (Sensomag sensor)	56
5.4 Experimental programme	58
5.4.1 The feed sample preparation	58
5.4.2 Experimental conditions.....	59
5.5 Sampling procedure	60
5.5.1 Trommel screen undersize	61
5.5.2 Trommel screen oversize	61

5.5.3 The mill crash stop	62
CHAPTER SIX: PILOT PLANT TEST RESULTS FROM THE SENSOMAG SENSOR	63
6.1 Introduction.....	63
6.2 Effect of mill speed on the toe, shoulder angle and mill performance	63
6.2.1 The results for the calculations dynamic volumetric filling	65
6.2.2 Effect of mill speed on the toe and shoulder position	66
6.2.3 The relationship between volumetric filling and toe and shoulder angle	71
6.2.4 The relationship between toe and shoulder angles and mill power draw	74
6.2.5 The relationship between percentage passing 75μm, toe and shoulder angle	77
6.3 The effect of ball filling on the toe, shoulder angle and mill performance	81
6.3.1 Relationship between dynamic volumetric filling, toe and shoulder angle	81
6.3.2 The relationship between ball load and the material passing percentage 75μm	84
6.4 Conclusion	87
CHAPTER SEVEN: OBSERVATIONS AND CONCLUSIONS	88
7.1 Summary of observations from inductive proximity and conductive sensor at the pilot plant scale.....	88
7.1.2 Conclusions.....	89
7.2 Summary of observations from acoustic sensor for the industrial scale test work.....	89
7.2.1 Conclusions.....	90
REFERENCES	91
APPENDICES	96

LIST OF FIGURES

Figure 2:1-Schematic of the Laboratory mill used by Morrell (1993)	7
Figure 2:2-The shape of the charge in the tumbling mill described by Morrell (1993)	7
Figure 2:3-The variation of shoulder angle with speed at varying mill filling (Morrell, 1993) 9	
Figure 2:4- The variation of toe angle with speed at varying mill filling (Morrell, 1993).....	9
Figure 2:5-Conductivity probe assembly used by Moys et al., (Moys, 1988).....	12
Figure 2:6-Fraction of toe and shoulder position as a function of mill speed (Moys, 1988)...	13
Figure 2:7- the right a cross section of a mill with a horizontal reference line, the left part shows the lifter bar (1) with a strain gauge sensor embedded (2), (Tano, 2005).....	14
Figure 2:8-Pilot mill equipped with CCM sensor (Tano, 2005).....	15
Figure 2:9-The movement of the CCM sensor through mill charge (Tano, 2005).....	15
Figure 2:10-The variation of toe angle and charge level (Tano, 2005)	17
Figure 2:11-The variation of shoulder angle and charge level (Tano, 2005)	17
Figure 2:12-The variation of toe angle with mill speed (Tano, 2005).....	18
Figure 2:13-Photograph of the inductive proximity probe on the pilot mill (Kiangi <i>et al.</i> , 2006)	19
Figure 2:14-Relationship between angular positions and power as a function of mill filling (Kiangi et al 2011)	20
Figure 2:15-Piezoelectric strain transducer (Vermeulen et al., 1985)	21
Figure 2:16-To the left the angular positions calculated from the signal and right part shows the schematic plotted on the mill shell modified after Vermeulen et al., (1985).....	22
Figure 2:17-Principle of measurement of the mill filling using a strain transducer (Kolacz, 1997)	23
Figure 2:18- The strain transducer reading for each mill revolution (Kolacz, 1997)	24
Figure 2:19-Vibration in the angular position of the maximum vibration point on the mill shell with the mill filling (Huang <i>et al.</i> , 2009)	25
Figure 2:20-A cross –section view of the tumbling mill charge (Napier–Munn <i>et al.</i> , 1996).27	
Figure 3:1-A schematic of the Primary grinding circuit at Angloplatinum UG2 Waterval concentrator.....	30
Figure 3:2-The location of Transmitter box on the mill (Davey et al., 2012)	31
Figure 3:3-A photograph of the accelerometer mounted on the mill lifter.....	32
Figure 3:4-Specification location of each accelerometer on the mill	33
Figure 3:5- A picture showing the sampling point for the vibratory screen oversize.....	34
Figure 3:6-An auto-sampler for cutting vibratory screen undersize	35
Figure 3:7-A photograph of the ball charge after grind-out	36
Figure 3:8-Wet screening of sub 1mm.....	38
Figure 4:1-The variation of total vibration power with mill mass.....	41
Figure 4:2-The variation of toe and shoulder position with time	42
Figure 4:3-Variation of toe position and mill power draw	43
Figure 4:4-The relationship between calculated mill filling and mill load.....	45
Figure 4:5- The filling and mill load relationship (Powell <i>et al.</i> , 2006).....	46
Figure 4:6-A schematic of the mill cross-section showing the toe and shoulder angles and the corresponding volumetric filling.....	48
Figure 4:7-The variation of grind and shoulder angle	48

Figure 4:8- The variation of grind with toe angle.....	49
Figure 4:9-Variation of calculated dynamic filling with shoulder angle.....	50
Figure 4:10-Variation of calculated dynamic filling with toe angle.....	50
Figure 4:11-Variation in power, feed rate, grind with dynamic volumetric filling	51
Figure 4:12- The grind curve methodology developed for a SAG mill (Powell <i>et al.</i> , 2012).	53
Figure 5:1-Flow sheet of the Magotteaux RoM Ball mill pilot plant	55
Figure 5:2-Polyurethane sensor beams for the Sensomag (Keshav <i>et al.</i> , 2011)	57
Figure 5:3-The external installation of Sensomag on the pilot mill	57
Figure 5:4- The reference point for the Sensomag and the angular positions of the slurry and ball load.....	58
Figure 5:5-A picture showing the fine feed (a) and coarse (b) feed stockpile.....	59
Figure 5:6-Sampling of trommel undersize discharge.....	62
Figure 6:1-The variation of slurry shoulder angles with mill speed at feed rate of 2400kg/hr	68
Figure 6:2-The variation of ball shoulder angles with mill speed at feed rate of 2400kg/hr...	68
Figure 6:3-The variation of slurry toe angles with mill speed at feed rate of 2400kg/hr	69
Figure 6:4-The variation of ball toe angles with mill speed at feed rate of 2400kg/hr.....	69
Figure 6:5-Schematic showing the toe and shoulder angles at 75% critical speed	70
Figure 6:6-Schematic showing the toe and shoulder angle at 80% critical speed	70
Figure 6:7-Schematic showing the toe and shoulder positions at 85% critical speed	71
Figure 6:8-The variation of dynamic volumetric filling with shoulder angles at 75% critical speed	72
Figure 6:9- The variation of dynamic volumetric filling with shoulder angles at 85% critical speed	72
Figure 6:10-The dynamic volumetric filling with the toe angle at 75%.....	73
Figure 6:11- The dynamic volumetric filling with the toe angle at 85% critical speed.....	74
Figure 6:12-The relationship between power draw and shoulder positions for the ball and slurry at 75% critical speed.....	75
Figure 6:13-The relationship between power draw and shoulder positions for the ball and slurry at 85% critical speed.....	75
Figure 6:14-The relationship between power draw and toe positions for the ball and slurry at 75% critical speed	76
Figure 6:15-The relationship between power draw and toe positions for the ball and slurry at 85% critical speed	76
Figure 6: 16-The relationship between 75 μ m and shoulder position for the ball and slurry load at 75% critical speed	77
Figure 6:17-The relationship between 75 μ m and shoulder position for the ball and slurry load at 85% critical speed	78
Figure 6: 18-The relationship between 75 μ m and toe position for the ball and slurry load at 85% critical speed	79
Figure 6:19- The relationship between 75 μ m and toe position for the ball and slurry load at 85% critical speed	80
Figure 6:20-Particle size distribution of the feed and the mill discharge product at varying feed rate.....	80
Figure 6:21-Dynamic mill filling and ball shoulder position at varying ball load	82
Figure 6:22-Dynamic mill filling and slurry shoulder position at varying ball load	83

Figure 6:23-Dynamic mill filling and ball toe position at varying ball load	83
Figure 6:24-Dynamic mill filling and slurry toe angle at varying ball load	84
Figure 6:25-Variation of mill grind as a function of varying ball load	85
Figure 6:26- Relationship between grind and slurry shoulder at 23% and 26% ball load.....	86
Figure 6:27- Relationship between grind and slurry shoulder at 23% and 26% ball load.....	86

LIST OF TABLES

Table 3:1-Primary mill specifications.....	30
Table 3:2-Primary mill operating conditions	30
Table 3:3-The conditions of the experiment at the Waterval UG2 Concentrator.....	33
Table 3:4-The screen size used for the dry and wet screening procedure	37
Table 4:1- The mill parameters for calculating the volumetric filling B.....	44
Table 4:2-Calculated mill filling using Morrell mill filling and power equation	44
Table 4:3-Comparison between the static and dynamic ball filling degree.....	47
Table 5:1-The Specifications of the Magotteaux Pilot RoM ball mill.....	54
Table 5: 2- The operating conditions of the Magotteaux Pilot RoM ball mill	55
Table 5:3-Experimental conditions for the mill speed test	60
Table 5:4-Experimental conditions for the ball load test.....	60
Table 6:1-Average values for the mill filling toe and shoulder positions from the Sensomag power and grind for varying speed test.....	64
Table 6:2-The mill performance data from the varying speed test	64
Table 6:3-Calculated volumetric filling for the slurry load from the toe and shoulder positions from the Sensomag for the varying speed test	65
Table 6:4-Comparison between volumetric fillings estimated from the crash stop measurements and the sensor toe and shoulder angles.	66
Table 6:5-Results obtained from second experimental campaign	81
Table 6: 6- The average values of the Sensomag values converted using the CSIRO acoustic reference.....	96

NOMENCLATURE

UG2 – Second Upper Group

RoM – Run-of -Mine

Toe position – This is a position on the shell where the charge comes into contact with the mill liner

Shoulder position – This is the position on the mill shell where the mill charge depart from the mill liner

Comminution – processing technique of reducing large particles to smaller sizes in order to liberate or free the minerals of interest

CSIRO – Commonwealth of Scientific and Industrial Research Organization

Acoustic sensor - Acoustic sensor is a device for measuring transient elastic waves within a material that are generated by an external force

Sensomag sensor - The Sensomag sensor is a device used for continuous measuring of both ball load and slurry positions inside a running mill.

RoM ball mill – The run-of-mine (RoM) ball mill is a type of mill which use steel balls between 30-35% and part of the coarse rocks in the charge for comminution

Mill charge – Mill charge consists of loosely packed grinding media (steel balls or rod), rock material and water.

Volumetric filling – Volumetric filling is the fraction of the total mill volume that is occupied by the charge.

Critical speed – Critical speed is the theoretical rate of rotation of the mill at which centrifuging of the mill charge.

Grind-out – Grind-out is perform to get rid of slurry and rock materials in the charge.

Centrifuging – Occurs at mill speed in excess of the critical speed above 100% of critical speed. The outermost layer of charge, which is in contact with the mill shell, rotates with the mill shell.

Cataracting – Occurs at mill speeds above 80% of the critical speed. A portion of the charge is raised high in the mill and fall back to the toe of the charge.

Cascading – Occurs at speed below 60% of the critical speed. The charge material emerged from the shoulder of the load it then rolls down the free surface of the charge to the toe of the load.

Slurry- The slurry is a mixture of ground rock materials and water

CHAPTER ONE: INTRODUCTION

The intension of this thesis is to estimate the dynamic volumetric filling on-line using the toe shoulder angles of the mill charge, instead of the usual in situ measurements after mill crash stop, and grind-out. This required installing conductance, inductance, and acoustic sensors on a run-of-mine ball mill (ROM) to estimate the toe and shoulder angle of the charge online.

Grinding is an essential unit operation in the mineral processing industry, which influences the performances of downstream processes such as leaching and flotation (Wills, 2006; Rajamani *et al.*, 2000). Tumbling mills are traditionally used for both primary and secondary grinding applications. Tumbling mills are energy intensive and consume about 70% of the total energy used at the concentrator (Napier-Munn *et al.*, 1996; Tano, 2005; Clermont *et al.*, 2010). A number of variables such as mill speed, feed size, ball load, ball size, and volumetric filling affect the efficiency of a tumbling mill (Morrell *et al.*, 1996, 2004; Moys, 2003; Powell *et al.*, 2001, 2006). The variable of interest in this study is volumetric filling, which is the total volume of the charge (ore, water, and steel balls) in the tumbling g mill (Morrell, 1993). It has been shown that the performance of the tumbling mill is sensitive to volumetric filling and key considerations in terms of operation and design such as the power draw, throughput, and quality of ground products (Powell *et al.*, 2006, 2009, 2011).

The common method of measuring volumetric filling on the plant is by taking in situ measurements after mill crash stop. The mill crash stop involves running the tumbling mill under steady state by stopping all feed streams into the mill and de-energizing the mill motor simultaneously. This method is disruptive to production due to the mill downtime involved (Napier-Munn *et al.*, 1996; Powell *et al.*, 2006; Clermont *et al.*, 2010).

Researchers have indicated that there is a direct relationship between the behaviour of the charge (toe and shoulder position) and the volumetric filling (Moys *et al.*, 1988; Morrell, 1993; Agrawala *et al.*, 1997; Clermont *et al.*, 2010; Keshav *et al.*, 2010). Other workers have also shown that the toe and shoulder positions represent the interaction between the grinding media, slurry, and the mill shell (Spencer *et al.*, 2000; Mishra *et al.*, 2007). The aim of this thesis is to estimate the volumetric filling from the toe and shoulder positions of the mill charge. The toe and shoulder positions are the boundaries of contact of the charge on the mill shell. Therefore, measuring the behaviour of the charge facilitates the development of effective control and optimization for the grinding circuit. Furthermore, the relationship

between the behaviour of the charge and mill performance has been strongly sought after in the mineral processing industry (Apelt *et al.*, 2000, 2001, 2002; Spencer and Liu, 2005; Rajamani *et al.*, 2006, 2007; Huang *et al.*, 2010; Davey *et al.*, 2012).

In recent times, various techniques and computer simulation packages have been developed to measure and study the behaviour of the mill charge (Agrawala *et al.*, 1997; Gugel *et al.*, 2003; Zhao *et al.*, 2010). However, some of these techniques pose difficulties to plant operators. Firstly, the information provided are in the raw state that has to be fed into a control system before actions can be implemented. Secondly, in some cases the signal containing the information related to the grinding process remains concealed in the raw state, which needs complex interpretations of the signal to be meaningful (Kolacz, 1997; Dupont *et al.*, 2001). Computer simulation packages, though important, only help in understanding the influence of dynamic behaviour on mill performance but cannot be applied to the operation of industrial and pilot scale mill.

To address these limitations, this thesis intends to use on-line sensors for estimating the toe and shoulder positions of the charge. These are potential key features for estimating the volumetric filling. The online measurements of the toe and shoulder position of the mill charge can be used as a tool by plant operators to make timely decision on abnormal warnings such as changes in the total charge level. The information obtained would enhance the effective control and optimization of the grinding circuit. This study was commissioned, to assess efficiency of the on-line sensor technologies in monitoring volumetric filling, and subsequent mill performance at both the industrial and pilot scales.

1.1 Hypothesis

It is hypothesised that the dynamic toe and shoulder positions of the mill charge can be used to estimate the dynamic volumetric filling because the toe and shoulder positions constitutes boundary conditions of the mill charge.

1.2 Scope of this study

The objectives of this thesis are firstly, to estimate the volumetric filling from the toe and shoulder positions of the mill charge. Secondly, to determine the efficiency of the grinding circuit using the mill performance data and the toe and shoulder positions of the mill charge.

1.3 Thesis layout

In addition to the introduction, the thesis comprises of seven chapters. A review of published work on motion of the charge and online sensors technologies for measuring the behaviour of the load in the tumbling mills is given in chapter 2. The experimental methodology employed when using the acoustic monitor on the industrial scale grinding application is described in Chapter 3. Chapter 4 presents the discussion of the results obtained from the acoustic sensor on the industrial scale work. Chapter 5 describes the Sensomag equipment used for estimating the media and slurry load position and as well as the experimental methodology applied on the pilot plant. Chapter 6 presents the results obtained from measurements of media and slurry dynamic behaviour using the Sensomag. The volumetric filling was deduced from the toe and shoulder position. The mill performance indicators were related to the toe and shoulder positions of the media and slurry load estimated from the Sensomag. The observations and conclusions drawn in this study are presented in Chapter 7.

CHAPTER TWO: LITERATURE REVIEW

2.1 Introduction

The objective of this chapter is to provide a review of the literature related to different methods of studying the dynamic behaviour of the charge in the tumbling mill. Background knowledge on the general application and the types of tumbling mills used in the mineral processing industry are presented. The motion of the charge was studied in a laboratory mill using photographic technique (Morrell, 1993). Numerical methods has been used to extract charge behavior in laboratory, pilot, and industrial mills include Discrete Element Methods (DEM) (Powell et al., 1996; Cleary, 1998, 2000, 2001; Mishra and Rajamani, 1992, 1994, 2003). These numerical methods provide information about the trajectories of the charge in the tumbling mill, which can be used as a tool for mill control and optimisation. Papers dealing with hardware sensors for inferring the dynamic behaviour of the charge in the tumbling mills were included in the review. These sensors are reviewed to assess the validity of the data obtained from Sensomag (Clermont *et al.*, 2010, 2012) and acoustic sensors used in this study (Spencer *et al.*, 2000; Campbell *et al.*, 2001,2003; Davey *et al.*, 2012).

2.2 General application of tumbling mills

Tumbling mills are widely used in the grinding application in cement, pharmaceutical, paint and the mineral processing industries for both coarse and fine grinding (Wills, 2006; Austin *et al.*, 1984, 1987). Tumbling mills are made up of cylindrical shells, sometimes with a conical section at the feed and discharge end, and have liners with lifter elements attached to the shell surface. The grinding media is either made up of steel balls, rods, or rock itself that form part of the bulk load (Wills and Napier-Munn *et al.*, 2006). The rock, water, and steel balls constitute the charge material. The tumbling mill rotates with a certain speed and the media and particles collide with each other to cause size reduction. The grinding can be carried out wet or dry, in either batch, or continuous modes. In the continuous grinding process, feed materials enter on one side and exist on the opposite side of the mill.

2.3 Types of tumbling mills

Tumbling mills are classified according to the types of grinding media used for comminuting the particles. This includes autogenous (AG), semi-autogenous (SAG), ball mill and RoM ball mills.

2.3.1 Autogenous (AG) mills

Autogenous (AG) mills are similar in operation to the SAG mills but do not use steel balls in grinding of particles. AG mills use part of the rock materials as the grinding media for grinding.

2.3.2 Semi-Autogenous (SAG) mills

Semi-Autogenous (SAG) mills are used for primary grinding application in the mineral processing industry. They utilize between 6-18% steel balls (Spencer *et al.*, 1999) for breakages of the particles (Austin *et al.*, 1984, 1987;; Wills, 2006). SAG mills are characterized by their large diameter and short length.

2.3.3 Ball mill

Ball mills are typically use for secondary grinding applications. The grinding media used is steel balls, which occupy between 30-40% of the mill volume. Ball mills normally have a smaller diameter and longer length as compared to SAG mill (Napier-Munn *et al.*, 1996; Wills, 2006).

2.3.4 ROM ball mill

The other type of tumbling mill is the run-of-mine (ROM) ball mill which is common to the South African industry (Hulbert *et al.*, 1990; Mainza *et al.*, 2006). The run-of-mine (RoM) ball mills use steel balls between 30-35% and part of the coarse rocks in the charge for comminution. In this study, the RoM ball mills were employed at the pilot and industrial scales equipped with Magotteaux Sensomag (Clermont *et al.*, 2010) and CSIRO acoustic sensor for measuring the toe and shoulder positions of the charge(Davey *et al.*, 2012).

2.4 The Motion of the charge in the tumbling mill

The Motion of the charge in the tumbling mill in wet milling is different because the slurry occupies the void space between the balls. The motion of the charge in the tumbling mill has been described as cascading, cataracting and centrifuging (Wills, 1996, 2006; Cleary, 1998, 2001, Kiangi *et al.*, 2006, 2011; Maleki-Moghaddam *et al.*, 2013). The cascading motion occurs at low speeds, where the charge rises to a certain height along the mill shell and rolls over the free surface to the toe region of the charge. The cataracting motion occurs at high speeds, but less than the critical speed. The charge, after departing from the shoulder region,

assumes a parabolic path before rolling down to the toe region of the charge. The shape of the charge is determined from the motion within the tumbling mill.

2.5 The shape of the charge in the tumbling mill

Different researchers have explored the motion of charge within the tumbling mill for both wet and dry milling applications. Rose and Sullivan (1958) studied the motion of the charge in a laboratory mill fitted with a transparent window to study the condition of dynamic surging in the mill. The motion of the charge was described as a pendulum-like oscillation of the whole charge about the centre of the charge. The work of these authors was limited to the dry milling environment

The shoulder position is the maximum height reached by the charge on the mill shell. The toe position is where the mill charge comes into contact with the mill shell (Spencer *et al.*, 2001, 2005; Almond *et al.*, 2004). The toe and shoulder positions of the charge are the boundary of contact on the mill shell. These can be used for calculating the volumetric filling of the mill charge and these are important variables in mill power modelling.

2.5.1 The methods for determining of shape of the charge

A number of people performed experiments, involving the extraction of the shape of the charge. These include Moys, (1988), Morrell, (1993), Powell, (1995) and Govender (2005). These researchers used different experimental techniques to study the charge shape. The measurement of the charge shape is essential for understanding the dynamic of the charge in the mill. Section 2.5.1 and 2.5.2 review different methods for determining the shape of the charge in the tumbling mill.

2.5.2 Morrell's charge shape

Morrell (1993) determined the shape of the charge motion by using a variable speed laboratory mill equipped with a glass window. Figure 2:1 shows a schematic of the laboratory mill used in the study. A slow shutter camera was used to capture the motion of the charge through the glass end. The effect of mill speed and mill filling on the toe and shoulder angle of the mill charge were investigated. Snapshots of the charge motion were taken between 73-112% of the critical speed and at mill fillings ranging between 15-45%. The toe and shoulder angles were determined from the photographs of the taken. The proposed charge shape relative to a cartesian co-ordinate is illustrated in Figure 2:2.

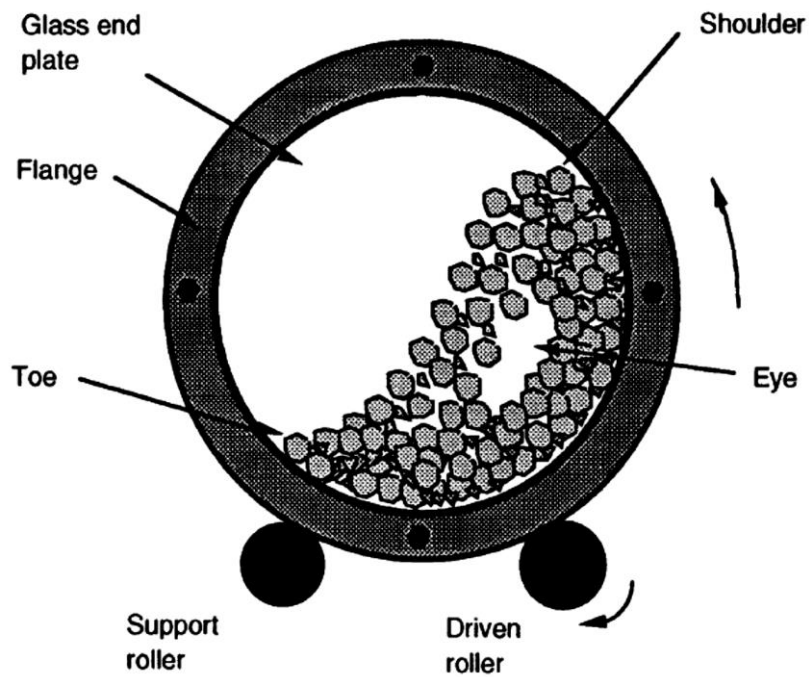


Figure 2:1-Schematic of the Laboratory mill used by Morrell (1993)

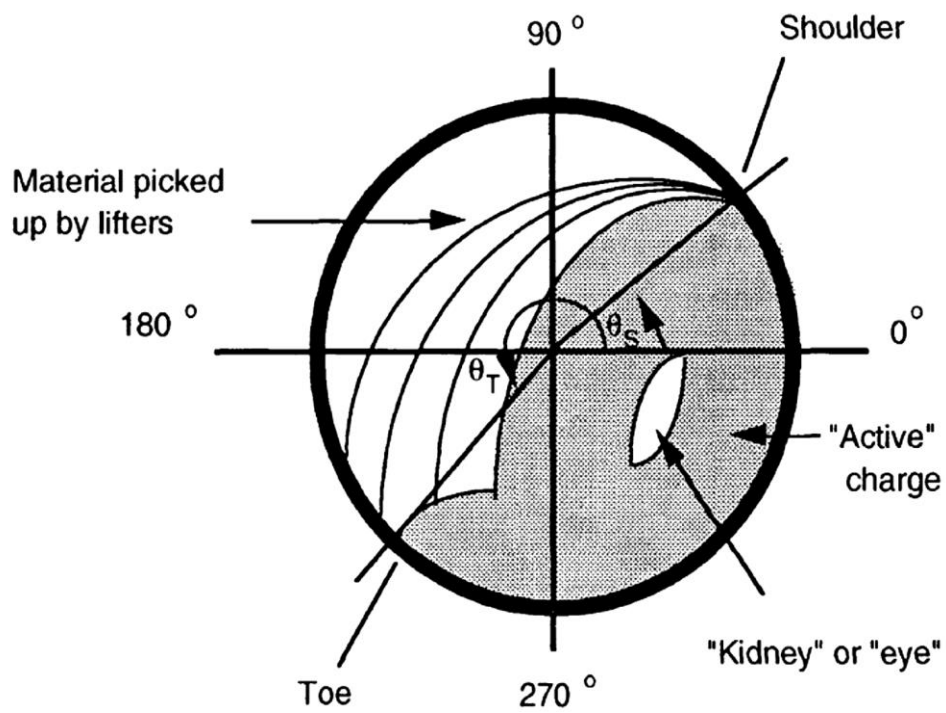


Figure 2:2-The shape of the charge in the tumbling mill described by Morrell (1993)

Based on experiments performed using a laboratory mill, Morrell proposed the following empirical equations to relate the toe and shoulder angle of the charge to the mill speed and volumetric filling. The volumetric filling can be estimated when the toe and shoulder positions of the mill charge are known. These equations are employed in this study for calculating the volumetric filling from the toe and shoulder angle estimated using on-line sensor technology. Equations 2-1 to 2-4, were established to help calculate the toe and shoulder angles and the volumetric filling.

$$\theta_S = \frac{\pi}{2} - \left(\theta_T - \frac{\pi}{2} \right) \left((0.3386 + 0.1041\phi_c) + (1.54 - 2.5673\phi_c)J_t \right) \quad (2-1)$$

Equation 2-2 uses only the toe position and the experimentally determined fraction of the theoretical critical speed at which centrifuging was fully established, and the critical speed of the mill.

$$\theta_T = 2.5307(1.2796 - J_t)(1 - e^{-19.42(\phi - \phi_c)}) + \frac{\pi}{2} \quad (2-2)$$

$$\phi_c = \phi \quad \phi > 0.35(3.64 - J_t) \quad (2-3)$$

$$\phi_c = 0.35(3.64 - J_t) \quad \phi \leq 0.35(3.64 - J_t) \quad (2-4)$$

where

J_t is the volumetric filling

ϕ is the experimentally determined fraction of the theoretical critical speed at which centrifuging was fully established.

ϕ_c is the percentage of the critical speed, at which the mill is operated.

The toe and shoulder angles were related to mill operating variables namely mill rotational speed and mill filling. Figure 2:3 and Figure 2:4 shows the variation of the shoulder and toe angle with changes in the mill filling and mill speed, respectively. It can be observed that increasing the mill filling resulted in increase in the shoulder angle of the mill charge. The increase in shoulder angle was due to the expansion of the charge in the mill. In contrast, the toe angle decreased with an increased in mill filling Morrell (1993). As the mill rotates, the charge is lifted along the rising side of the mill shell until a maximum point is reached on the shell where it falls to the toe of the charge.

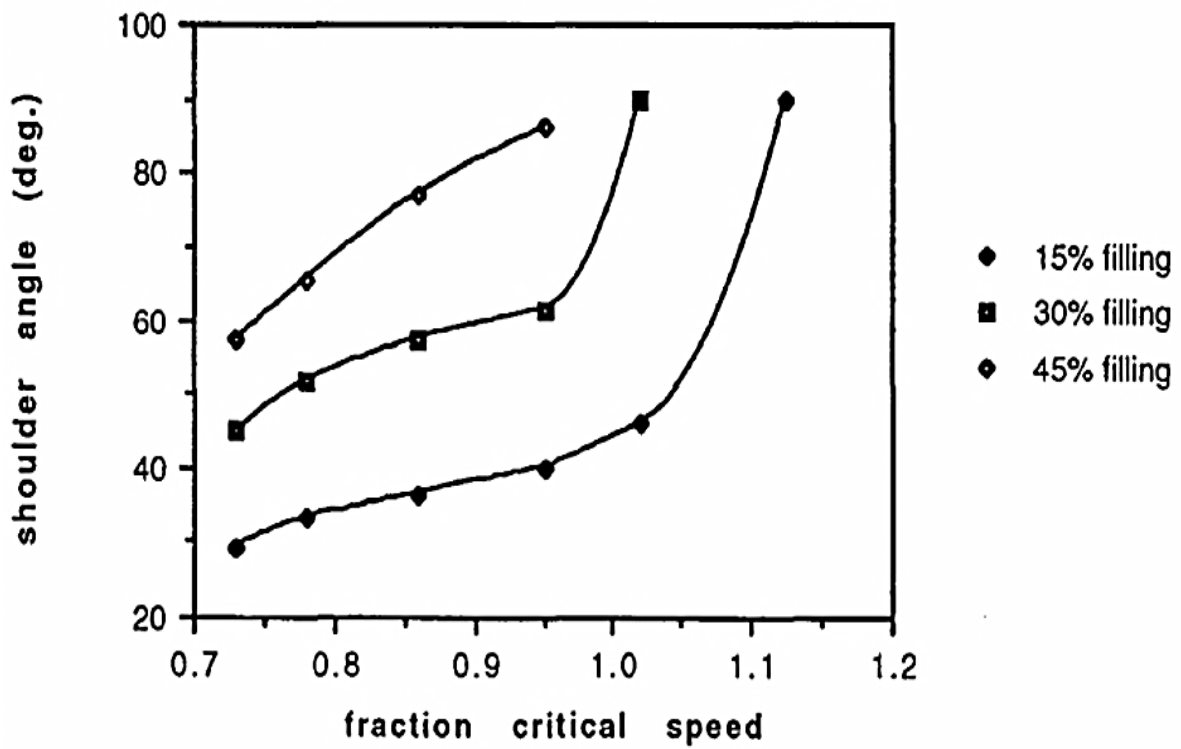


Figure 2:3-The variation of shoulder angle with speed at varying mill filling (Morrell, 1993)

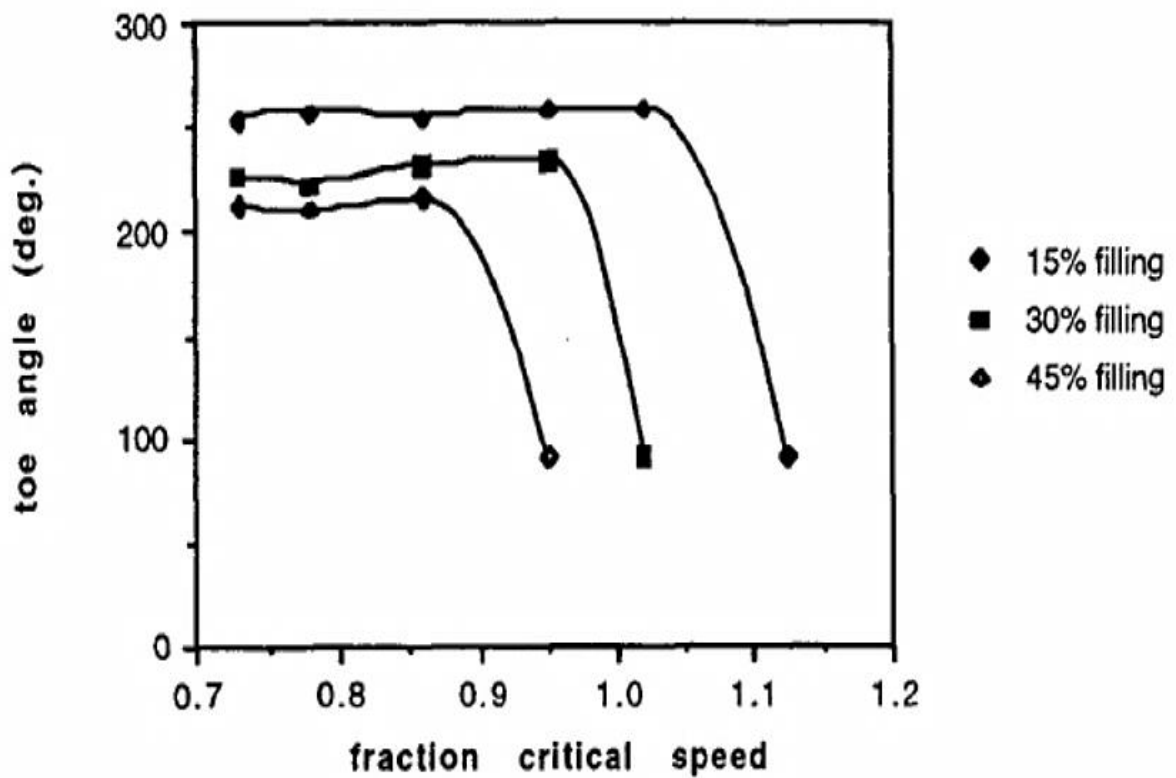


Figure 2:4- The variation of toe angle with speed at varying mill filling (Morrell, 1993)

The limitations in Morrell's work are firstly, the method of estimating the charges shape from the photographic snapshots is not applicable to industrial scale mills due to the harsh conditions prevailing within the milling environment. Secondly, the toe and shoulder positions cannot be determined online. However, with the current advances in online sensor technology, improvements can be made that would allow for direct measurement of the load behaviour inside industrial mills which this work seeks to address. Discrete Element Method (DEM) simulation offers the opportunity of better understanding charge trajectory for developing improvements to mill design and operation as reviewed in section 2.5.3.

2.5.3 Discrete Element Method (DEM)

The Discrete Element Method (DEM) is a numerical method for studying the motion of small and larger particles. Cundall and Strack (1979) appear to be the first to apply DEM to study granular flow of materials. Mishra and Rajamani *et al* (1992, 1994, 2007) pioneered the use of DEM to study the motion of the charge in tumbling mills. DEM has been used extensively to extract charge shape features by different researchers to study the motion of the charge in 2D and 3D for the prediction of charge shape and trajectory of the charge in industrial mills (Moys *et al.*, 1993). In addition, it has been used for the prediction of charge motion, power draw, segregation and wear rate in ball mills as well as charge motion in a rotary mills (Powell *et al.*, 1995 I, II, III). Cleary, (1998,2000,2001) used DEM to study the effects of changes in mill operating parameters and particle properties on the charge shape and power draw of ball mill of length 5m long. The use of DEM is very expensive due to the computational expenses involved. Particle breakage of the material is also not included in most of the tumbling mill DEM codes, which makes it difficult to evaluate the effect of charge features on mill performance. This has led to an increased interest in obtaining direct measurements of the toe and shoulder positions of the mill charge. Section 2.6 review papers on the different hard ware sensor technologies for measuring the dynamic behaviour of the charge in the tumbling mill.

2.6 Tumbling mill load behaviour measuring technologies

For the past decade, different methods have been proposed for studying the dynamic behaviour of the charge in tumbling mills. The use of the Sensomag and acoustic sensor to measure the toe and shoulder position of the mill charge is a consideration that constituted part of the motivation for this study. Methods for measuring the dynamic behaviour of the

mill charge have been classified into two categories, on shell or off-shell method (Dupont *et al.*, 2001; Tano, 2005; Kiangi, 2011). On-shell sensors rotate with the mill and are able to provide direct information related to the condition of the mill charge at every point on the mill shell. On-shell type sensors include the conductivity probe (Moys, 1988), the piezoelectric strain transducer (Kolacz, 1997), the acoustic (Campbell *et al.*, 2003), the strain gauge (Tano, 2005) and the Sensomag (Clermont *et al.*, 2010; Keshav *et al.*, 2011). The off-shell devices are normally mounted adjacent to the mill shell and do not rotate with the mill. Examples include the load cell, bearing pressure and acoustics sensors such as accelerometer and an array of microphones (Vermeulen, Ohlson *et al.*, 1984; Kemmerer, 2003). Sections 2.6.1 to 2.6.7 discuss the available sensor technologies for measuring the dynamic behaviour of the mill charge.

2.6.1 Conductivity probe technology

The conductivity probe consists of two main parts: an anode and a cathode. The probe measures fluid conductance when a voltage is applied across it. The voltage forces the negatively charged ions to move towards the anode, while the positive ions move towards the cathode. The movement of these ions is a measure of conductivity. The conductivity probe has been applied by researchers in the mineral processing industry for measuring the slurry density as well as toe and shoulder positions of the mill charge (Moys *et al.*, 1988; Kiangi *et al.*, 2006, 2011; Alatalo *et al.*, 2011).

Moys *et al.* (1985) pioneered the use of the conductivity probe. They studied the behaviour of the mill charge in terms of toe and shoulder positions using the probe in a laboratory mill. The conductivity probe was inserted through the mill liner bolts and the sensing face was parallel to the mill axis of rotation. The probe was insulated from the mill liner and shell by an epoxy coating to prevent the loss of electrical currents from the probe. The effects of mill speed and volumetric filling on the load behaviour were investigated. Figure 2:5 shows the conductivity probe assembled. The mill was operated in a batch mode with steel balls of varying size from 10 to 40mm.

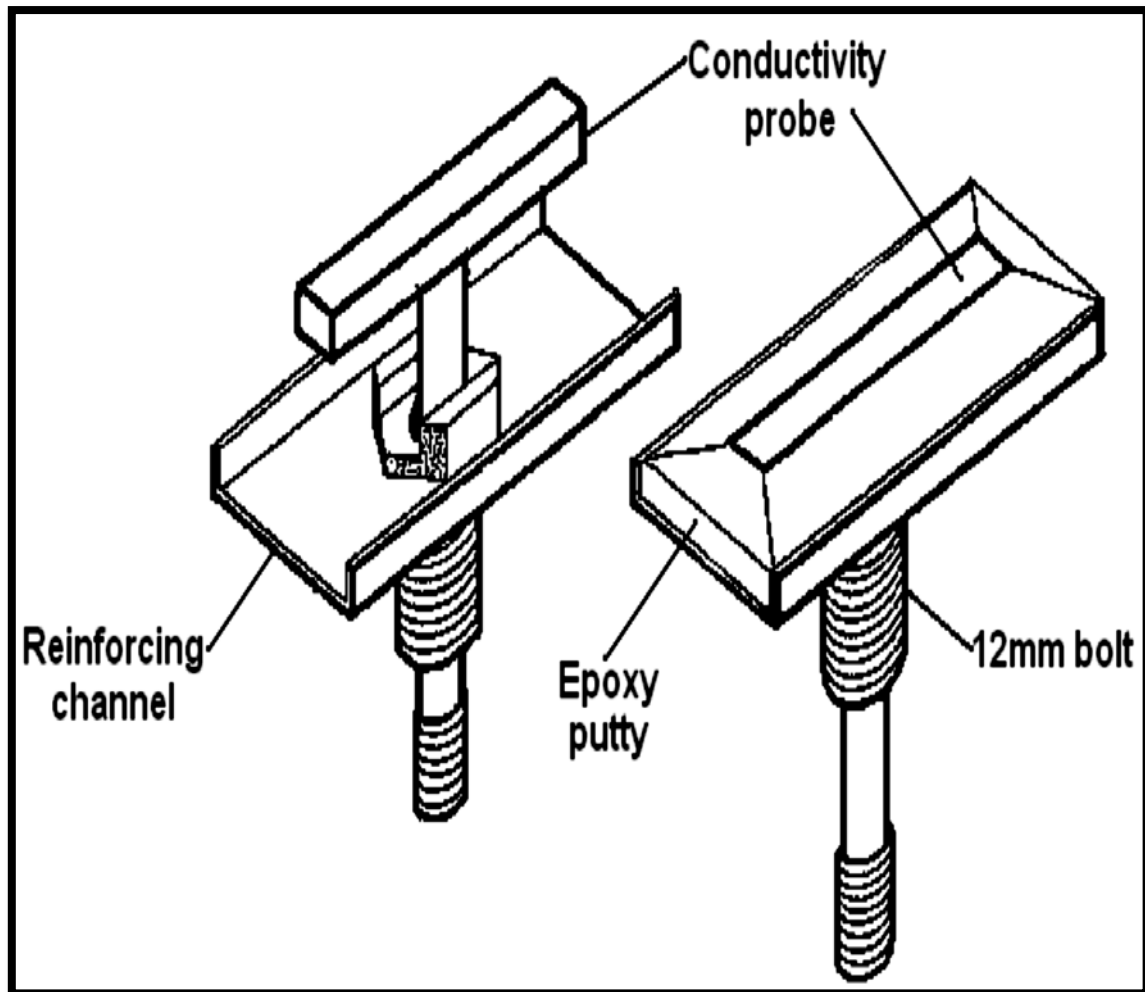


Figure 2:5-Conductivity probe assembly used by Moys et al., (Moys, 1988)

The toe and shoulder positions were expressed as fractions of the mill circumference in the direction of mill rotation. Moys (1985, 1988) then developed performance curves using the toe and shoulder position of the mill charge. Figure 2:6 represents the relationship between the toe and shoulder positions as a function of mill speed at varying mill filling. It was observed that the shoulder position varies uniformly with mill filling and mill speed due to the expansion of the mill load. The toe position decreases as the mill speed increases. As the mill speed increases above 80% critical speed, the motion of the charge is predominantly cascading resulting in the reduction of effective mass of the load in the mill.

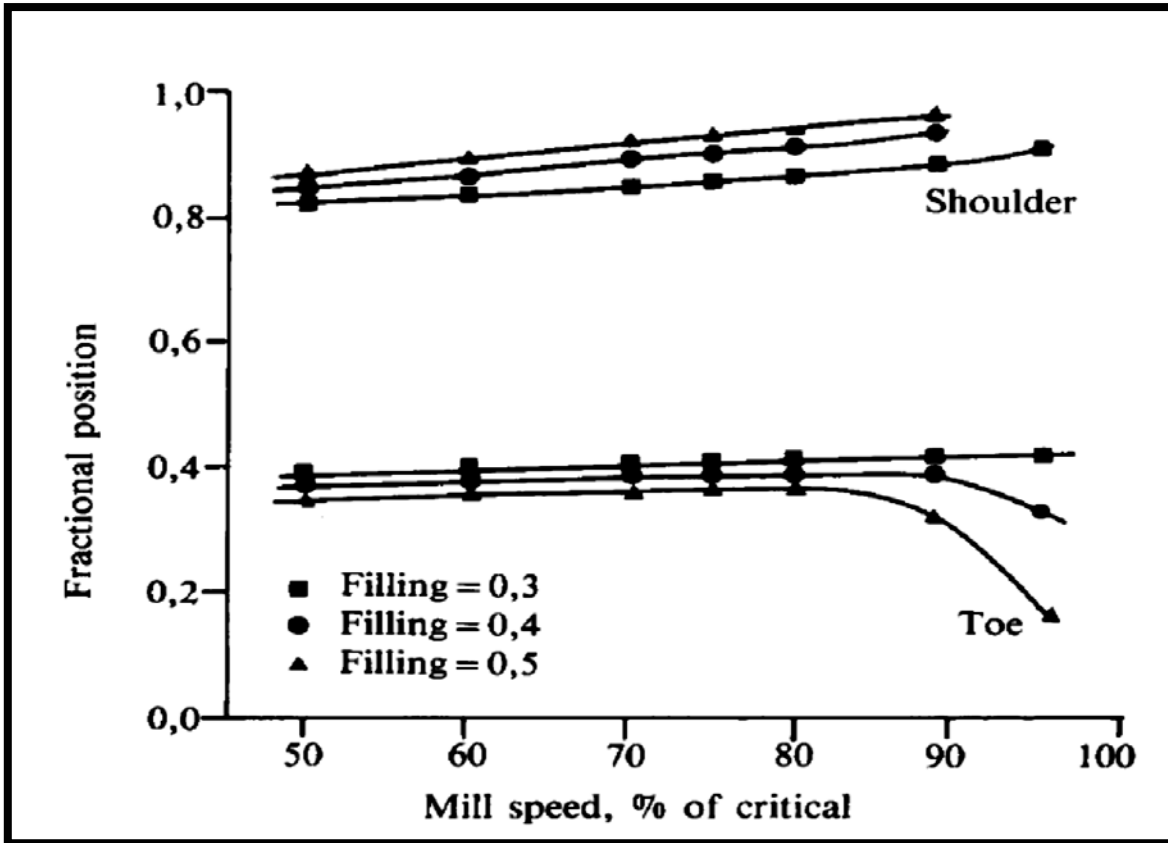


Figure 2:6-Fraction of toe and shoulder position as a function of mill speed (Moys, 1988)

Van Nierop *et al* (1997) used conductivity probes to measure the load behaviour on industrial grinding mill. The factors of the experiment were mill speed, solid feed rate and mill rotational speed. The toe and shoulder positions of the charge that were obtained from the conductivity probe signals were used to calculate the load angle of repose (α). The angle was then used to estimate the volumetric filling. Van Nierop *et al* (1997) observed that the toe and shoulder position varies with mill speed, volumetric filling, and mill load. The toe position of the charge increased as the mill mass decreased while the shoulder position increased as the load in the mill increased. This was due to increasing depth of the load in the mill.

The information from the conductivity probe has been used to improve the power draw prediction of the tumbling mill. Nonetheless, the use of the conductivity probe has the following limitations, the slurry viscosity and the rate at which the slurry drains off from the probe affect the measurements and it cannot be used for measuring the load behaviour in dry milling due to the inability of the dry slurry to conduct electrical current. However, the conductivity probe device has been tested on the industrial scale for monitoring the load

behaviour of autogeneous mills but it has not yet been developed and integrated into commercial application mills (Montini and Moys, 1988; Kiangi, 2011). In this work the Sensomag and acoustic sensor have been integrated into a complete measurement system for detecting the toe and shoulder position of the charge for predicting the performance of ball mills and RoM ball mills (Campbell *et al.*, 2000,2005; Clermont *et al.*, 2008,2010; Keshav *et al.*, 2011; Davey *et al.*, 2012).

2.6.2 Strain gauge sensors

The strain gauge sensor measures the strain on an object (Skorupa and Moys, 1993; Dupont and Vien, 2001; Rajamani 2005; Kiangi, 2011). A strain gauge sensor can be made of a round or flat coil fastened to the surface of an object. Strain gauges can be used as load cells, force sensors or torque sensors for monitoring the tumbling mill charge. Tano *et al* (2005, 2008) used a strain gauge sensor with the trade name as Continuous Charge Monitor (CCM) marketed by Metso. The CCM sensor was embedded in a rubber lifter of a 1.414m diameter and 1.22 m length pilot ball mill. Figure 2:7 shows the installation of the sensor in a rubber lifter fitted on a lifter of the pilot ball mill. Figure 2:8 shows the installation of the CCM sensor on the pilot ball mill. The effects of mill filling, mill speed, and percent solids on the toe and shoulder positions were studied. Using the toe and shoulder position the volumetric filling could be calculated.

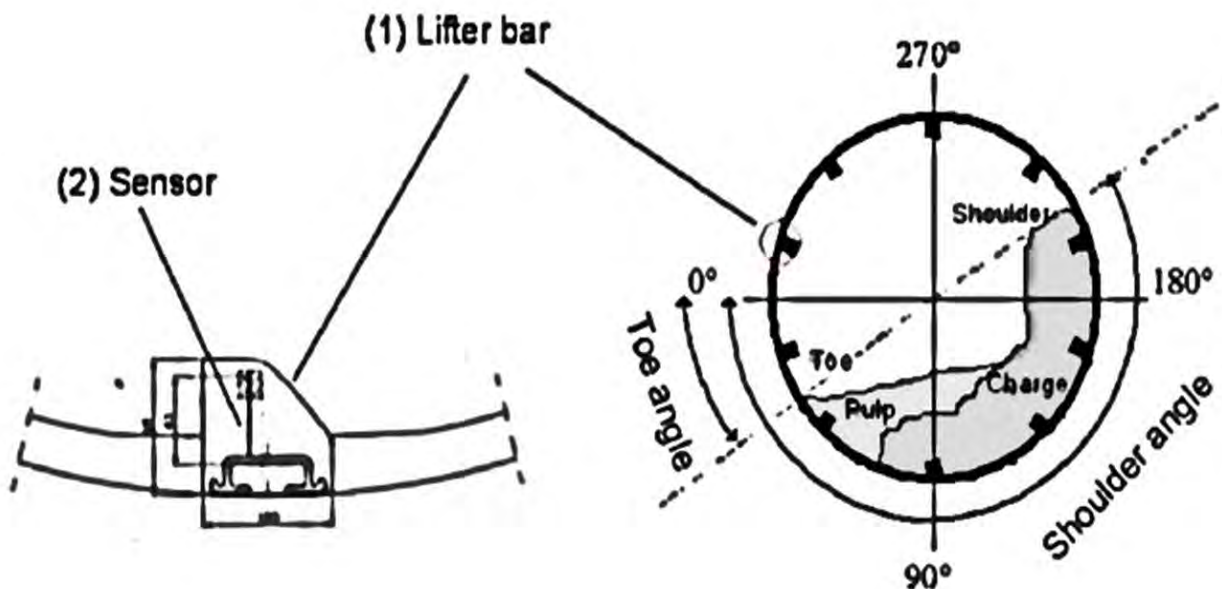


Figure 2:7- the right a cross section of a mill with a horizontal reference line, the left part shows the lifter bar (1) with a strain gauge sensor embedded (2), (Tano, 2005)

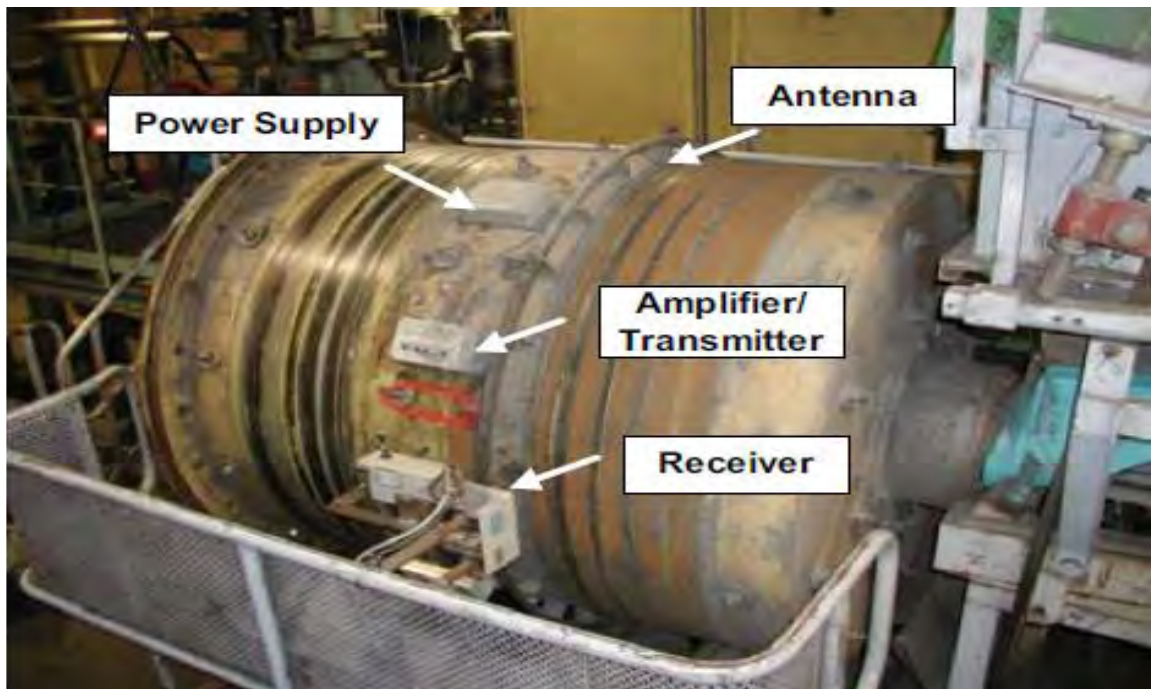


Figure 2:8-Pilot mill equipped with CCM sensor (Tano, 2005)

A series of tests were performed by varying the feed rate and solids content in the mill. Figure 2:9 shows the dynamic events during the transition of the CCM sensor through the mill charge. The toe and shoulder positions are determined from the CCM data.

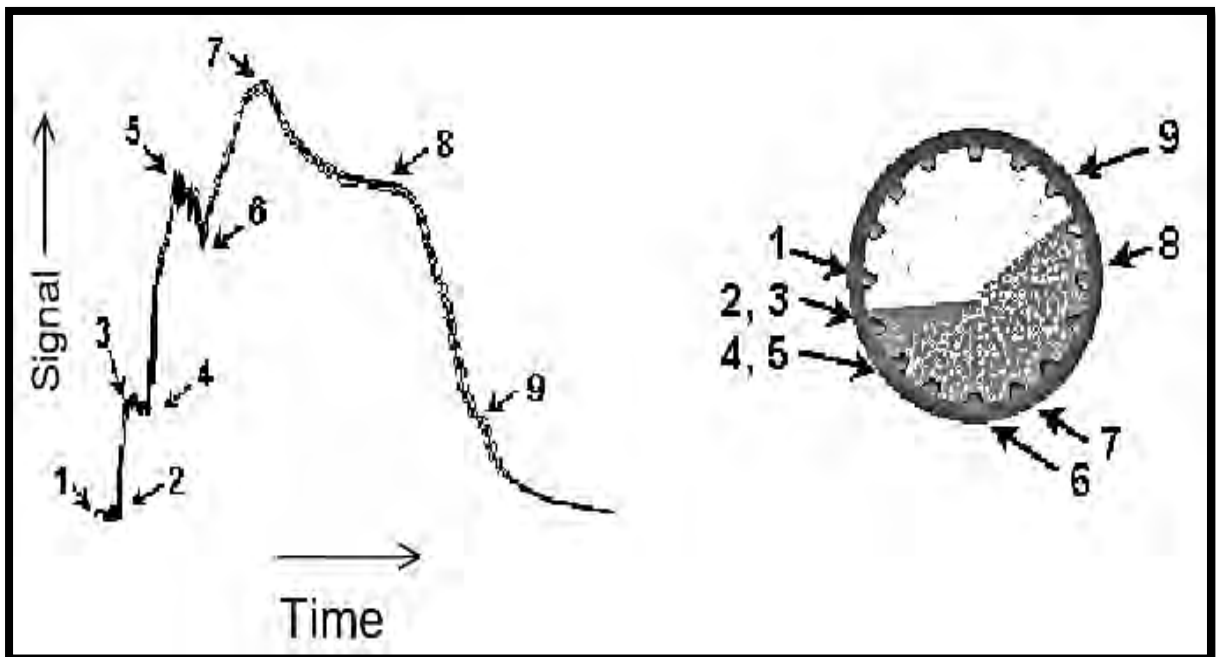


Figure 2:9-The movement of the CCM sensor through mill charge (Tano, 2005)

From Figure 2:9 , the positions of the signal profile are described as follows.

1. The sensor lifter bar (SL) is still in the air
2. The SL hits the surface of the slurry
3. The SL starts to get submerged in the slurry
4. The SL hits the ball charge and starts to get submerged in the charge
5. The SL starts to bend forward due to turbulence in the toe area
6. The SL grips the ball charge again
7. The SL is at peak and begins to bending down
8. The SL has gradually decreased the bending and is at take-off position
9. The SL is leaving the ball charge and starts to slowly rise to an upright position

Tano (2005) estimated the mill filling using the toe and shoulder positions from Equation 2-5.

$$J = \frac{(\theta_S - \theta_T)N - \sin 2\pi(\theta_S - \theta_T)N}{2\pi} \quad (2-5)$$

J- Volumetric filling, (%)

N- Mill speed (revolutions per seconds)

θ_S Shoulder position of the charge

θ_T Toe position of the charge

Figure 2:10 and Figure 2:11 show the relationship between the toe and shoulder angles, as a function of mill filling (Tano, 2005). It was found out that the mill filling has the largest effect on toe and shoulder angles estimated from the sensor signals. The toe position decreases as the mill filling level increases, while the shoulder angles increases with increase in the volumetric filling. Figure 2:12 shows the variation of the toe angle with mill speed. Increasing the mill speed leads to an increase in the toe angle of the charge (Liddell *et al*, 1988; Napier-Munn, 1996; Dupont *et al.*, 2001; Clermont *et al.*, 2010). Due to lift imparted to the charge, as the mill speed increases the charge expands.

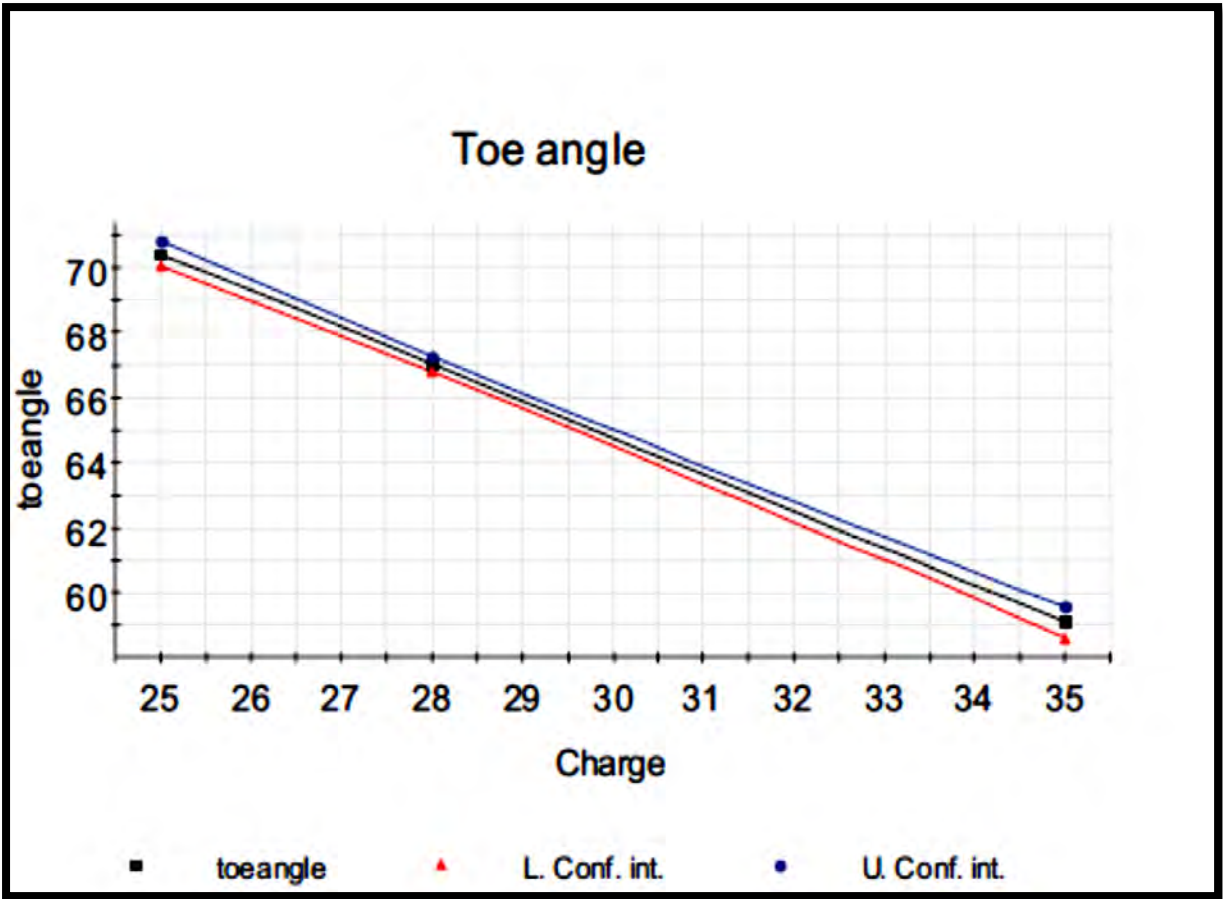


Figure 2:10-The variation of toe angle and charge level (Tano, 2005)

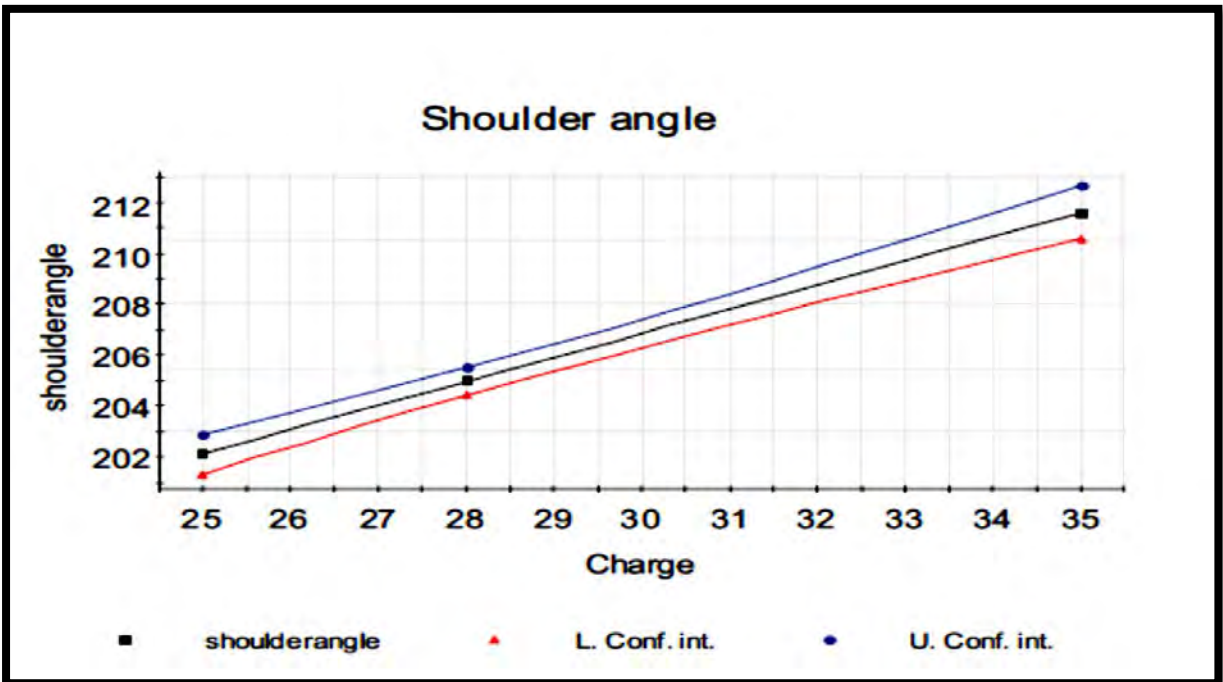


Figure 2:11-The variation of shoulder angle and charge level (Tano, 2005)

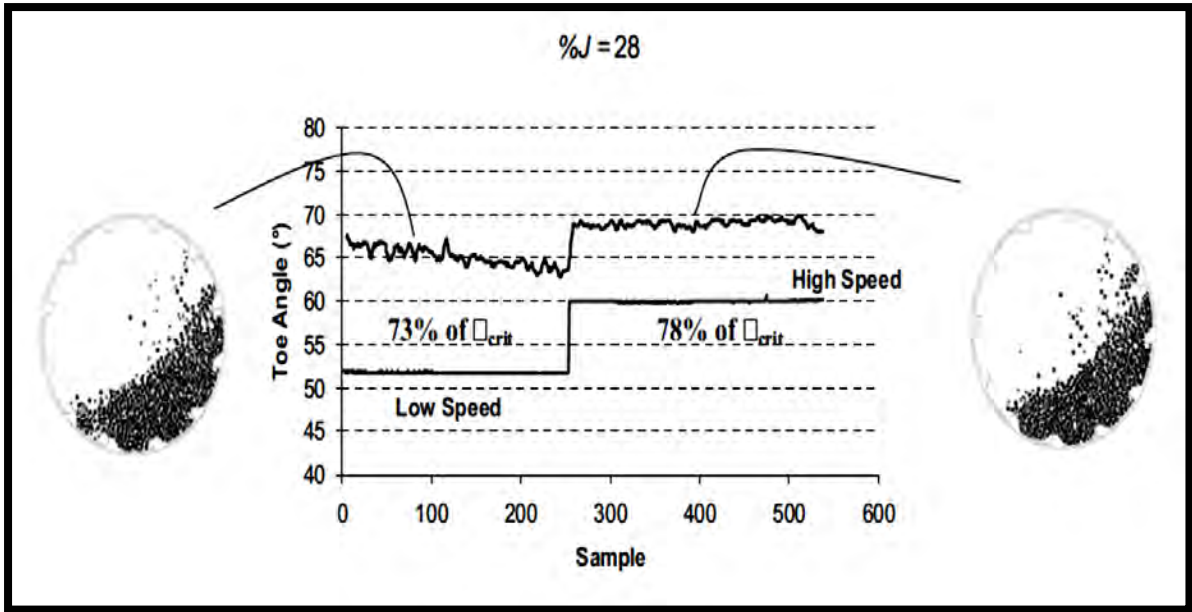


Figure 2:12-The variation of toe angle with mill speed (Tano, 2005)

The CCM sensor reading is affected by thermal expansion due to the variations in the temperature of the strain gauge. The resistance of the gauge will vary as the connecting wires wear out. The rubber lifter should be flexible enough to undergo deformation at the influence of the charge and, robust enough to withstand the impact from the charge. The respective toe and shoulder positions of slurry and media load could not be distinguished which constitutes the main limitations of the CCM sensor. This study was commissioned to overcome this limitation by using a Sensomag device to obtain information about the toe and shoulder position of the media and slurry inside a RoM ball mill.

2.6.3 Inductive proximity probe

The inductive proximity probe is made up of a ferromagnetic coil, which works on the principle of induction. As the mill rotates, the ferromagnetic coil generates a magnetic field within the mill and any steel balls entering the magnetic field cause an amplitude variation in the field. The inductive probe sensor has been used in the mineral processing industry for monitoring conditions within the mill.

Kiangi *et al* (2006, 2011) measured the toe and shoulder positions of the charge in a dry pilot mill using the inductive probe sensor. Figure 2:13 illustrates the installation of an inductive proximity probe on the pilot mill. The effects of mill filling and mill speed on the toe and

shoulder positions as well as the net power were investigated. A series of tests were conducted on the pilot plant using steel balls as the grinding media and dry quartz as the ore. The media toe and shoulder positions were estimated from the inductive probe signal.



Figure 2:13-Photograph of the inductive proximity probe on the pilot mill (Kiangi *et al.*, 2006)

Figure 2:14 shows the variation of angular position and mill power draw with mill filling. They observed that the angular position varies with mill filling and this is due to the cataracting of the charge onto the mill shell resulting in the expansion of the load. Mill power increases gradually as mill filling increases. As mill filling is increased, more power is used as turning moment contributing to the mill rotation (Moys and Montini, 1987; Moys, 1993; Powell *et al.*, 2006; 2011). The main shortfall in the work conducted by Kiangi *et al* (2005, 2011) was that the respective positions of the slurry and media could not be distinguished.

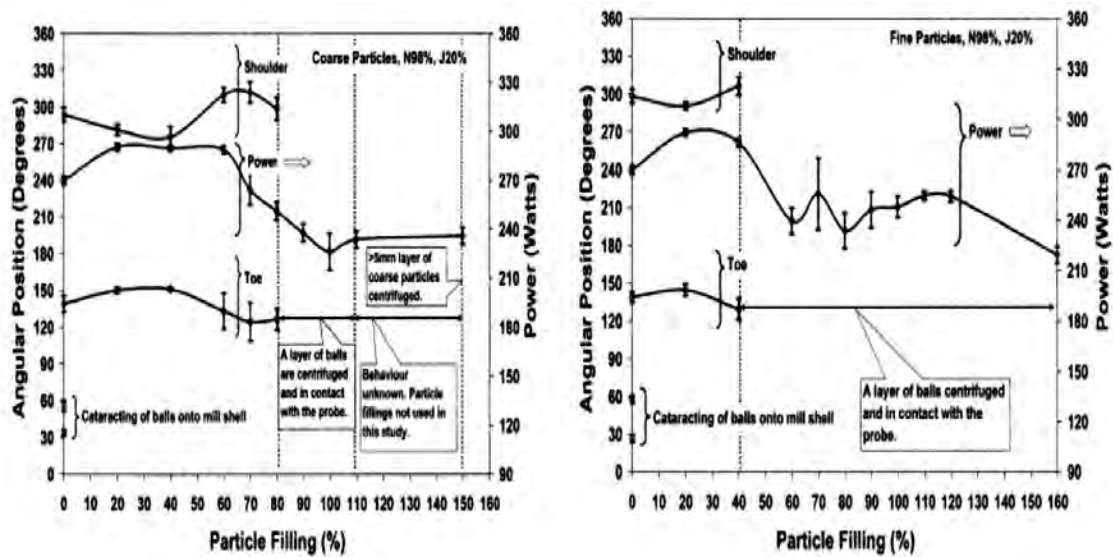


Figure 2:14-Relationship between angular positions and power as a function of mill filling (Kiangi et al 2011)

2.6.4 The Magotteaux Sensomag sensor

The Sensomag device has been developed and integrated into a complete measurement system and is marketed by Magotteaux Pty Ltd (Clermont *et al.*, 2008, 2010; Keshav *et al.*, 2011). The Sensomag sensor is made up of an inductive proximity switch and conductivity probe installed as part of mill liner. They are used for the estimation the toe and shoulder positions of the slurry and ball load in the mill. de Hass *et al* (2008), Clermont *et al* (2010) and Keshav et al, (2011) used the Sensomag sensor to measure the angular positions of the ball media and slurry inside an industrial ball mill. The set up for this study is different from that done by (Clermont *et al.*, 2010; Keshav *et al.*, 2011). Their work was performed on a secondary grinding application on an industrial scale whereas this work is on a RoM ball mill as discussed in section 2.3.4.

2.6.5 Piezo-electric strain transducer

The piezoelectric transducer is made up of a crystal, which measures the strain of an object when subjected to external forces. The electrical current generated is used to attenuate the effect of the external force on the object (Jayant *et al.*, 2001). In the mineral processing industry, piezo-electric strain transducers have been used to monitor the process condition of comminution equipments (Rajamani *et al.*, 2006). In tumbling mills, the liners/lifters are sensitive to impact and collision forces by the charge. Hence, the piezo-electric strain

transducers inserted into the lifters have been used for monitoring the behaviour of the charge in the mill. Figure 2:15 shows a schematic of a piezoelectric strain transducer assembled.

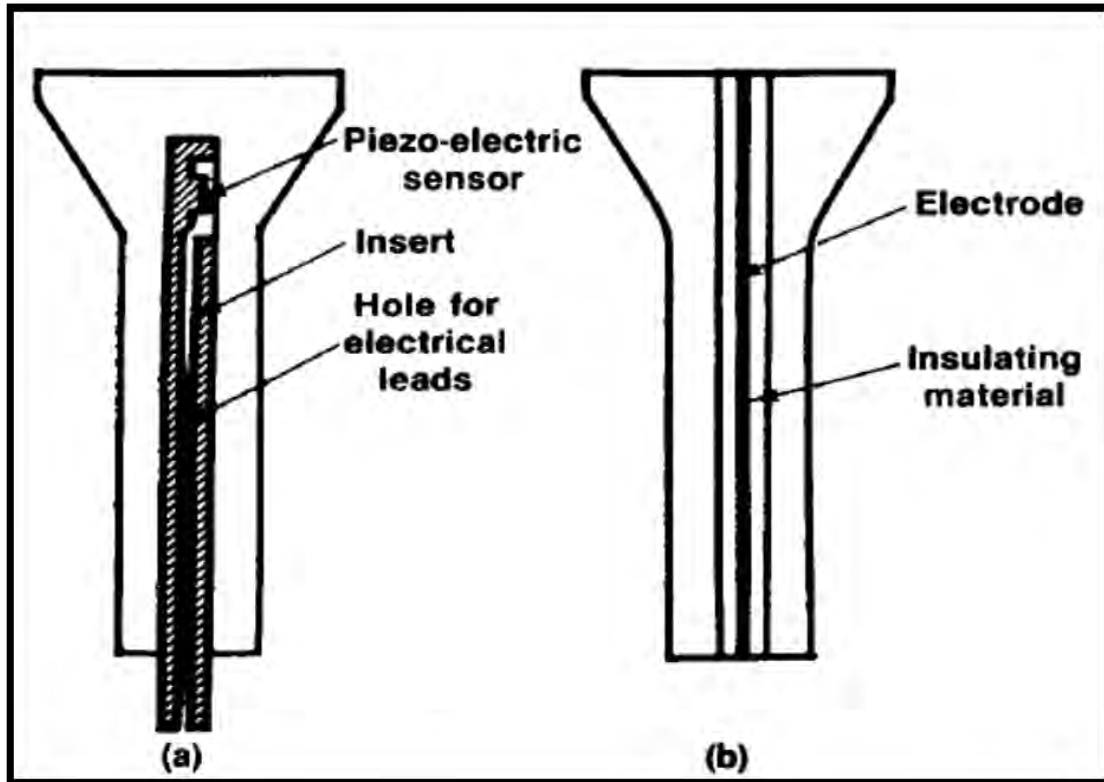


Figure 2:15-Piezoelectric strain transducer (Vermeulen et al., 1985)

Vermeulen *et al* (1984) used the piezoelectric strain transducer on a 16ft by 30ft industrial mill rotated at 85% of the critical speed with a load of 50% by volume. The motion of the charge cataracting and the distribution of angular positions of impacts in the mill were calculated. The relationship between the strain transducer signal and angular position is shown in Figure 2:16. The labels on the profile indicate the impact of the charge on the mill shell. The dynamic volumetric filling was not calculated.

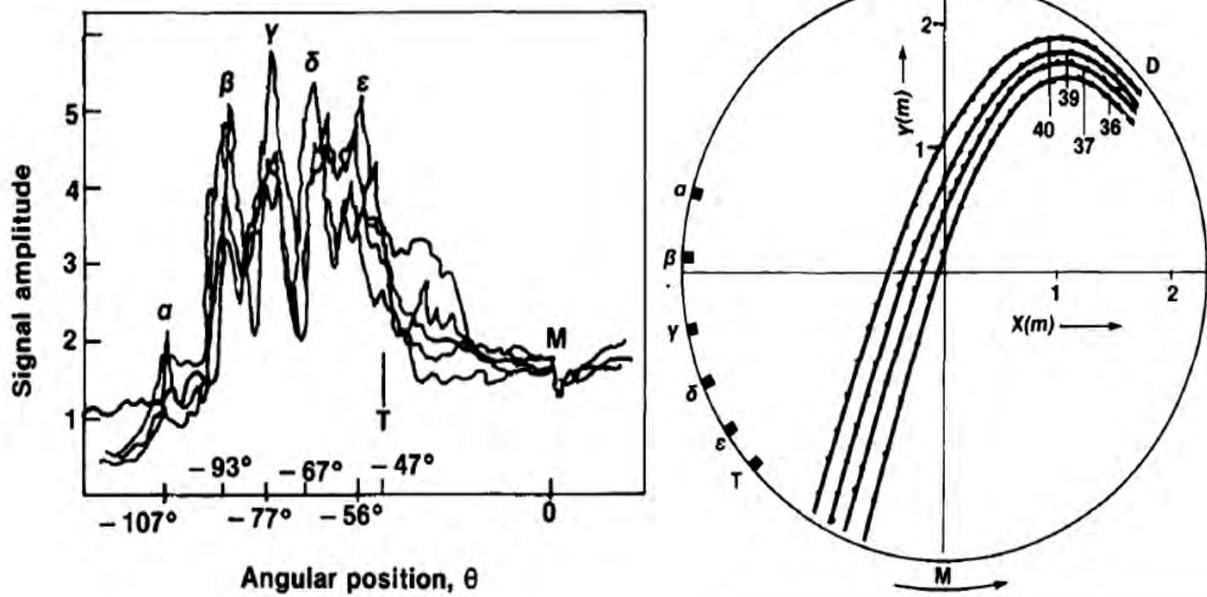


Figure 2:16-To the left are the angular positions calculated from the signal and right part shows the schematic plotted on the mill shell modified after Vermeulen et al., (1985)

Kolacz (1997) used the piezo-electric strain transducer in a pilot ball mill in a dry grinding application for measuring the mill filling. The transducer was installed on the mill shell in order to measure the deformation of the mill shell as a result of the impact of the charge. Figure 2:17 shows the principle of measurement using the piezo-electric transducer. The tension was measured when the transducer was completely buried in the mill load (position 2), while compression was measured when the transducer was out of the mill load. The total strain estimation is the difference between readings, corresponding to compression and tension.

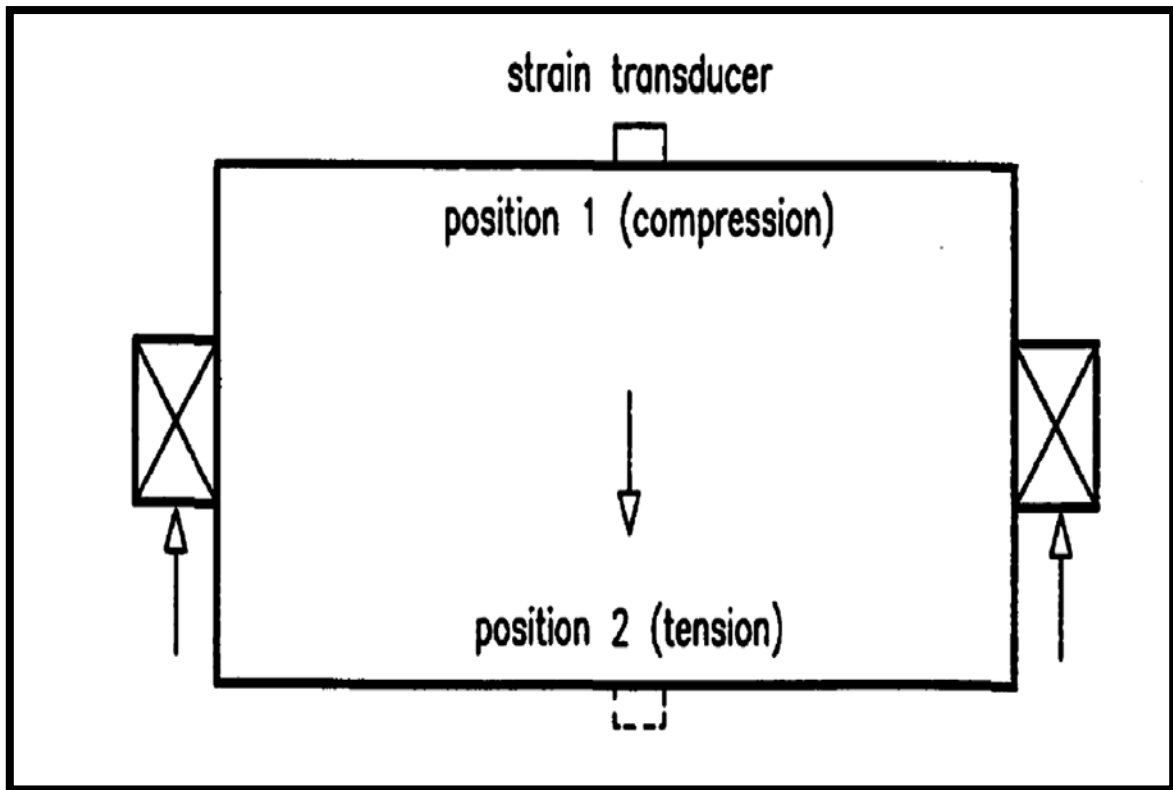


Figure 2:17-Principle of measurement of the mill filling using a strain transducer (Kolacz, 1997)

The total strain is directly proportional to the mill filling. Figure 2:18 shows the strain transducer profile for mill revolution. The high peaks indicate when the strain transducer was completely buried in the mill load. The lower peaks indicate when the strain transducer is out of the mill load. The advantage of using the piezoelectric strain transducer is the ease of installation and replacement within a short period. It can only be used for short-term measurements in a laboratory mill. The strain transducer only gives a measure of the mill load but the toe and shoulder position of the charge cannot be determined.

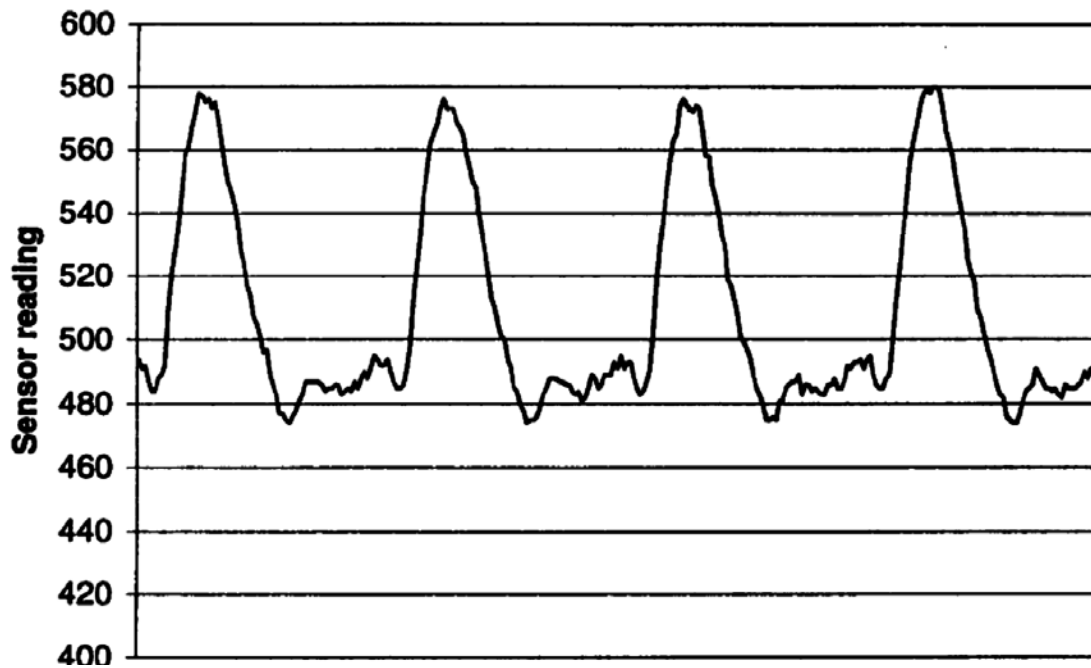


Figure 2:18- The strain transducer reading for each mill revolution (Kolacz, 1997)

2.6.6 Acoustic Emission Measuring Technology (AE)

Acoustic emissions are transient elastic waves generated due to the rapid release of strain energy when the material is subjected to external deformation. The strain is propagated through the surface of the material by a combination of longitudinal and transverse waves (Giordano *et al.*, 1998; Giordano *et al.*, 1999). The tumbling action of the charge within the mill produces an intense vibration signal on the mill shell. The vibration signal represents the process state of the charge within the mill (Su *et al.*, 2008; Campbell *et al.*, 2003). The vibration can be captured by an accelerometer and used for assessing the mill performance (Hou *et al.*, 1998; Dupont *et al.*, 2000; Pax, 2001; Sudarshan, 2006; Huang *et al.*, 2009, 2010). An accelerometer is made up of a piezoelectric crystal used to measure the variation in the vibration produced by an object. An accelerometer can be used to measure the vibration signal emitted from the drive motor, shell, girth gear and the trunnion bearings at the feed and discharge ends of the tumbling mill on laboratory and industrial scale (Zeng and Forsberg 1994).

2.6.7 The CSIRO Acoustic sensor

Commonwealth Scientific and Industrial Research Organisation (CSIRO) developed an acoustic monitor using accelerometers fastened on the mill shell. The acoustic monitor was used to measure the vibration signal on industrial and pilot scale mills (Spencer *et al.*, 1999,

2000; Campbell *et al.*, 2003; Davey *et al.*, 2012). Spencer *et al* (1999, 2000) made use of accelerometers attached to the external shell of an industrial SAG mill to measure the vibration signal. A series of tests were performed to investigate the effects of mill rotational speed, feed rate, ball load and mill discharge density on the vibration signal emitted from the mill shell. It was observed that the vibration signal was sensitive to the operating conditions of the SAG mill. Campbell *et al* (2003, 2005) used the same technology for monitoring the charge motion and estimation of the toe and shoulder position of the mill charge. However, he did not mathematically relate the toe and shoulder position to the volumetric filling. Several experiments have been conducted on both pilot and industrial scale mills to determine the viability of improving the technology. It was observed that an accelerometer can be used to monitor the toe and shoulder positions of the mill charge.

Huang *et al*, (2009, 2010) used similar accelerometers mounted on the external shell of an industrial mill (3.5m diameter by 6m long). The effect of mill filling and ball load on the angular position where the maximum vibration occurs on the mill shell were investigated. Figure 2:19 shows the relationship between angular position and mill filling. It can be observed that the angular position of the maximum vibration point decreased as mill filling increased. This was due to the decrease in vibration events within the mill as mill filling increased.

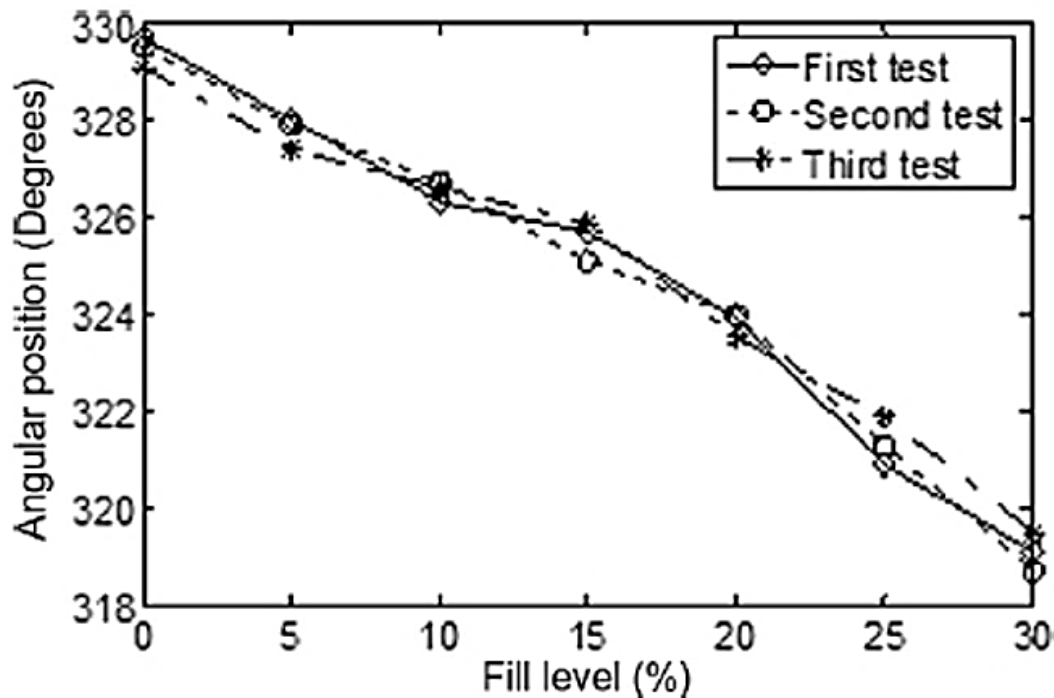


Figure 2:19-Vibration in the angular position of the maximum vibration point on the mill shell with the mill filling (Huang *et al.*, 2009)

The CSIRO acoustic monitor is used as part of this study and the one used has a new telemetry system based around the earlier trial unit (Spencer et al, 1999, 2000; Campbell *et al.*, 2001, 2003) utilizing Sennheiser transmitters and receivers for improving the signal (Davey *et al.*, 2012). All the tests trials were conducted on autogenous (AG) and semi-autogenous (SAG) mills but this work is on the RoM ball mill, which has a ball load between 22-28% and coarse rock in the charge. The value of this work is to estimate the volumetric filling from the toe and shoulder position estimated from the sensor. The volumetric filling estimated from the toe and shoulder position will be compared with mill filling obtained from static measurement as discussed in section 2.7.

2.7 The method of measuring volumetric filling in tumbling mills

The performance of the tumbling mill is sensitive to volumetric filling which affects the power draw, throughput, and quality of ground product (Powell *et al.*, 2006, 2009, and 2012). Each of these performance indicators peaks at different volumetric fillings. Therefore, it is important to obtain regular measurements of volumetric filling on the plant (Keshav *et al.*, 2010). On the industrial scale, the method used for estimating volumetric filling by taking the physical measurements after mill crash stops and grind-out. A crash stop is done by stopping the feed rate into the mill and de-energising the motor (Napier-Munn et al., 1996; Powell et al., 2006; Clermont et al., 2010). The internal dimensions such as the diameter, chord above the charge surface and the height from the roof to the surface of the charge are measured. If the ball load measurement is required, grind-out is performed. To be able to achieve a complete grind-out, the mill is allowed to run without feed until all the rocks are completely ground out and are discharged from the mill. The chord and the height related to the ball load measurements are taken. Figure 2:20 presents the schematic of the important measurements needed in order to calculate the volumetric filling of the charge or the ball load in a tumbling mill. The total mill filling and ball load can be estimated from the internal dimensions measured after the crash stop and grind-out.

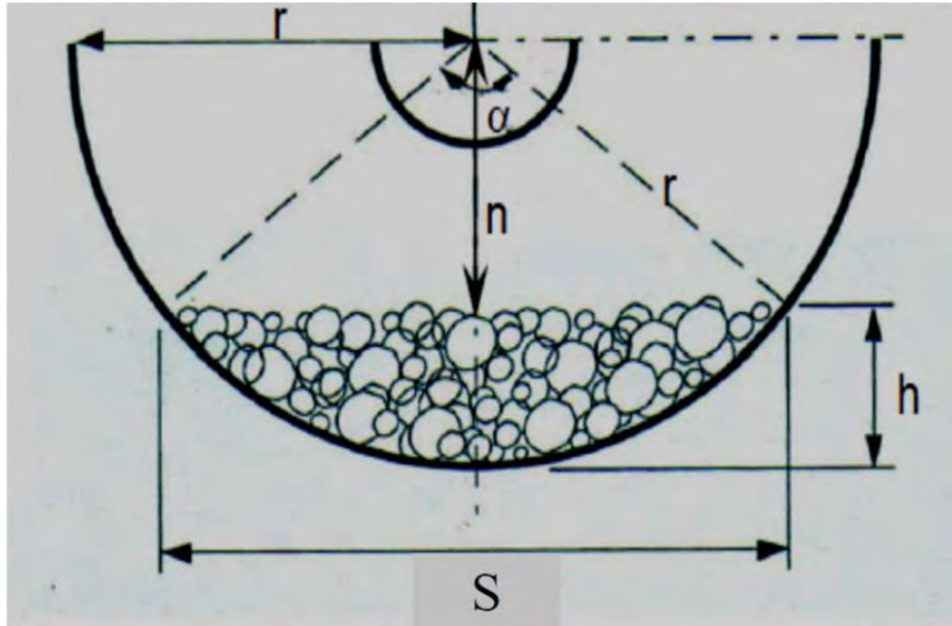


Figure 2:20-A cross –section view of the tumbling mill charge (Napier–Munn *et al.*, 1996)

The derivations of the equations are given as follows (Napier–Munn *et al.* 1996).

$$S = 2r \sin \frac{\alpha}{2} \quad \text{Equation [2-6]}$$

$$h = r \left(1 - \cos \frac{\alpha}{2} \right) \quad \text{Equation [2-7]}$$

$$r = \frac{h}{2} + \frac{S^2}{8h} \quad \text{Equation [2-8]}$$

The cross-section area of the mill charge is given by:

$$A_c = \frac{h}{6S} + (3h^2 + 4S^2) \quad \text{Equation [2-8]}$$

$$V = 100 \times \frac{A_c}{A} \quad \text{Equation [2-10]}$$

$$A = \pi r^2 \quad \text{Equation [2-11]}$$

Allis Chalmers derived a formula, which does not take into account the chord but uses the mill diameter measurement (Napier-Munn *et al.*, 1996)

$$\% \text{ mill load} = 113 - \left(\frac{H \times 126}{D} \right) \quad \text{Equation [2-12]}$$

In equation 2-5 to 2-10,

H = depth of load, m

S = Chord of the charge, m

r = Radius of mill inside liners, m

D= diameter of mill inside liners, m

α = the angle that the chord subtends at mill centre ($^{\circ}$)

A_C = Cross-sectional area of the mill charge (m^2)

A= Cross-sectional area of the mill (m^2)

V= estimate of mill filling (%)

The mill crash stops and grind-outs provide vital information for controlling the tumbling mill, but have the following limitations. It affects production and increase in mill downtime. The mill crash stop cannot be used as an online method for measuring the volumetric filling on the plant.

2.8 Conclusion

The use of online sensors and numerical methods for measuring the charge in the tumbling mill has been reviewed. The studies have been mostly on how to measure the load behaviour in laboratory and pilot-scale RoM ball mill for dry milling applications. Although these sensors have been used to provide information about the behaviour of the mill load there are some challenges associated with their application. The raw data obtained requires complex mathematical interpretation before the information can be meaningful to the plant operator. Some of these sensors do not have the robustness to withstand the severe condition prevailing within an industrial mill.

In view of the above difficulties, this study explored the Sensomag and acoustic sensor for measuring the dynamic behaviour of the charge inside a RoM ball mill at both pilot and industrial scales. On the pilot scale, the Sensomag sensor was used for online measurements of the ball and slurry load at varying mill speed and volumetric filling. The industrial scale employed an acoustic sensor for measuring the vibration signal from the mill shell to estimate toe and shoulder position of the charge at varying feed rates. The volumetric filling was calculated from the toe and shoulder positions, and related to mill performance data.

CHAPTER THREE: THE DESCRIPTION OF EXPERIMENTAL APPARATUS AND METHOD FOR ACOUSTIC SENSOR

3.1 Introduction

The purpose of this chapter is to describe the experimental apparatus used in the industrial scale experimental work. The experimental apparatus used in this study is acoustic sensor. Commonwealth of Scientific and Industrial Research Organisation (CSIRO) of Australia developed the acoustic sensor used in this study as described in Chapter 2 section 2.6.7. The acoustic sensor uses surface vibration signals to locate the toe and shoulder position of the mill charge (Campbell et al., 2001, 2003; Hosseini *et al.*, 2011; Davey *et al.*, 2012). The sensor was installed on a primary mill at Waterval UG2 at the Anglo American Platinum concentrator located in South Africa. The assembling, installation, commissioning and the constant updates of the sensor software was done by the CSIRO team. The role of this study is to use the sensor developed by CSIRO to measure the toe and shoulder positions of the mill charge and to estimate the volumetric filling. The experimental equipment and test methodology are discussed in this chapter. The results and analysis are reported in chapter four.

3.2 Flowsheet of UG2 primary grinding circuit

The flowsheet for the primary grinding section at UG2 Waterval Concentrator is shown in Figure 3:1. The set-up consists of two feed silos, run-of-mine ball mill (primary mill), trommel screen, and vibratory screens. Table 3:1 shows the RoM ball mill specifications whereas Table 3:2 shows the operating conditions. The feed to the mill is drawn from the feed silos by chute feeders onto the feed belt. Water is added to the mill to make up 85% solids slurry in the mill. The mill product discharges onto the trommel screen and wash water is added to ensure that no carry over fines report to the pebbles stream. The undersize material from the trommel is pumped from a sump onto the vibratory screens for classification. Water is sprayed on the screen to ensure that the screen is operated efficiently. The oversize material from the vibratory screen is recirculated to the mill for further grinding. The undersize material from the vibratory screen is pumped to the primary rougher flotation section for separation to obtain a concentrate and tailings streams. The concentrate is then sent to a cleaning stage, while the tailings are sent to the secondary section of the plant for grinding in a secondary mill and then floated again. Sections 3.3 and 3.4 discuss the experimental apparatus and methodology applied in obtaining data from the milling circuit.

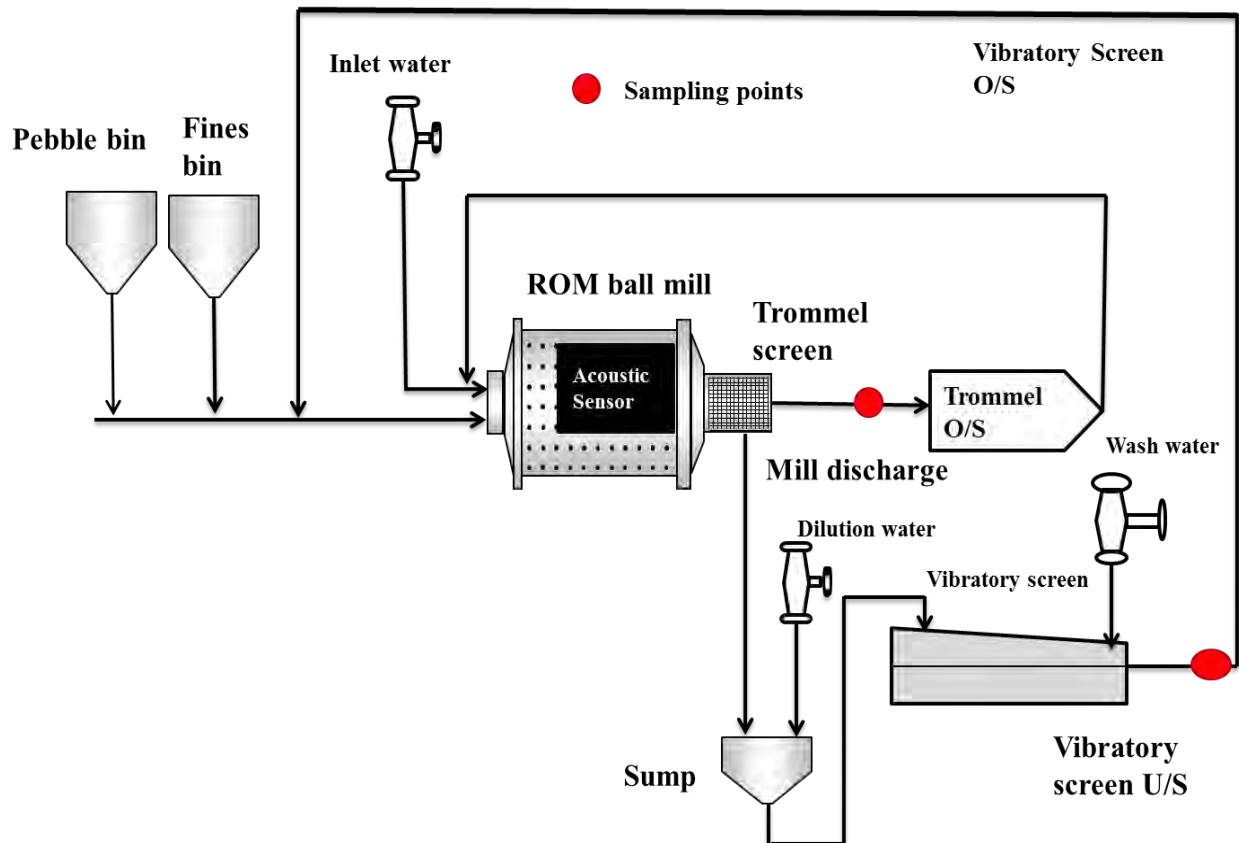


Figure 3:1-A schematic of the Primary grinding circuit at Angloplatinum UG2 Waterval concentrator

Table 3:1-Primary mill specifications

Mill diameter inside liners, m	7.13
Mill length, m	8.5
Mill speed, (% critical speed)	75
Mill type	Grate discharge
Mill motor ,MW	11
Mill rotation	Anticlockwise

Table 3:2-Primary mill operating conditions

Bulk ore density ,t/m ³	3.8
Steel density ,tm ³	7.9
Top size of steel ball, mm	70
Ball load ,%	22-29
% Solids	70- 80
Mill capacity, tph	400-750

3.3 Experimental Apparatus (Acoustic sensor)

The objective of this study was to determine the dynamic positions of the toe and shoulder of the mill charge using the acoustic vibration technology in order to estimate volumetric filling from these measurements. The key features of this sensor are accelerometers, transmitter box, radio frequency antennae, proximity switch, trigger bolt, and inertial power supply. The acoustic monitor detects vibration signal due to the tumbling action of the charge in the mill. The vibration signal is in the form of an electrical voltage. This information is collected by the data acquisition system at a sampling rate of 100 000 data samples per second. At the end of 12 revolutions, the raw data signal is transmitted to a computer via wireless telemetry for storage. The raw data is then processed using MATLAB software to extract the total band power signal as well as the toe and shoulder angles of the mill charge. The functions of the key features of the CSIRO acoustic sensor used in this study are discussed in sections 3.3.1 to 3.3.3.

3.3.1 Transmitter Box/Receiver

The transmitter box consists of a multi-channel transmitter, trigger bolt, and receiver onto which all four accelerometers are connected. The transmitter box powers the accelerometer modules and transmits the signals from the accelerometer. This was mounted at the girth of the mill shell as depicted in Figure 3:2 (Davey *et al.*, 2012).

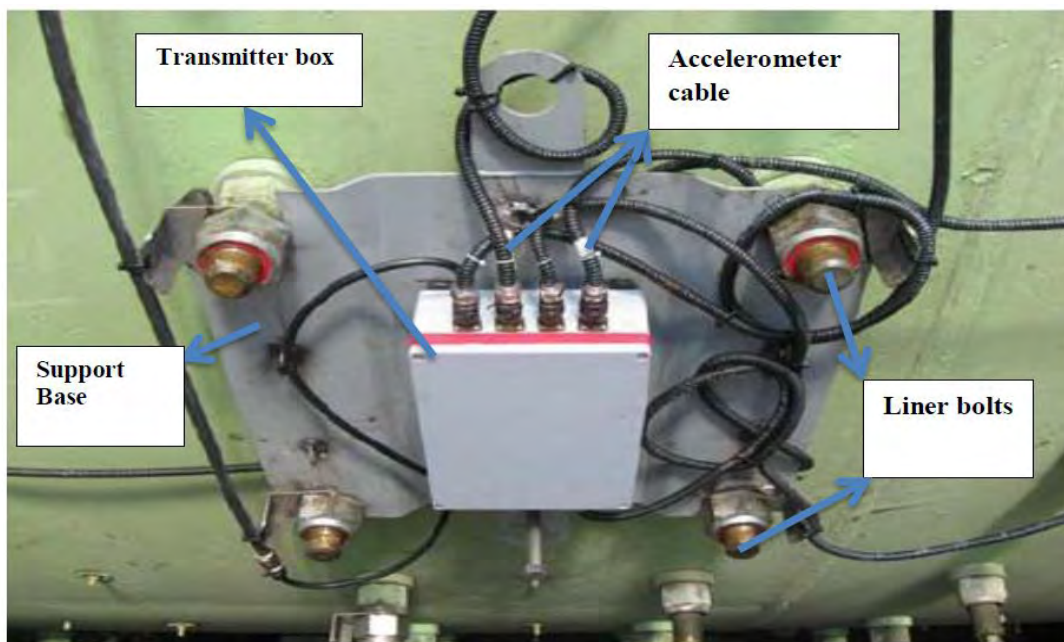


Figure 3:2-The location of Transmitter box on the mill (Davey *et al.*, 2012)

3.3.2 Accelerometer module

The accelerometer module consists of anti-shocking rate sensors, connected to charge converters. These are used for transmitting the vibration signals from the mill shell. The accelerometers have been designed for easy installation and replacement (Davey *et al.*, 2012). The accelerometer modules are attached to the end of the mill lifter bolts as shown in Figure 3:3. The inertial power supply was mounted at the feed end on the mill shell. Its function was to provide a continuous power supply to the on-mill monitor by the pendulum-driven generator as the mill rotates. Section 3.3.3 explains the reference point used for obtaining the angular positions of the charge on the mill shell.

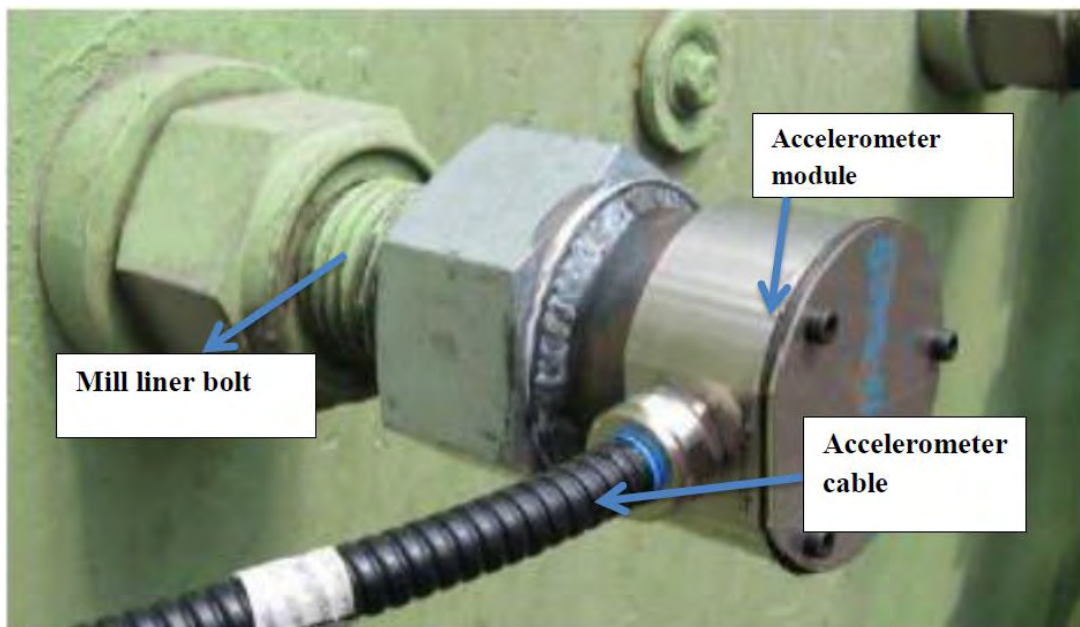


Figure 3:3-A photograph of the accelerometer mounted on the mill lifter

3.3.3 Angular position for each accelerometer

The mill rotates in an anti-clockwise direction looking from the discharge end. The convention used by the software to specify the angular position of the accelerometers at any given time is to designate the 0° (or 360°) position at 3 o'clock position on a clock, with the angles increasing in an anti-clockwise direction around the mill. Figure 3:4 illustrates the conversion chart for the location of the proximity switch. Each of the four accelerometers has been assigned to a channel (Ch) via the user interface programme for receiving the signal from the accelerometers. The accelerometer located at the lifter bolt close to the feed end was assigned to Ch1, followed by Ch2, and then Ch3 and finally Ch4 at the discharge end of the mill.

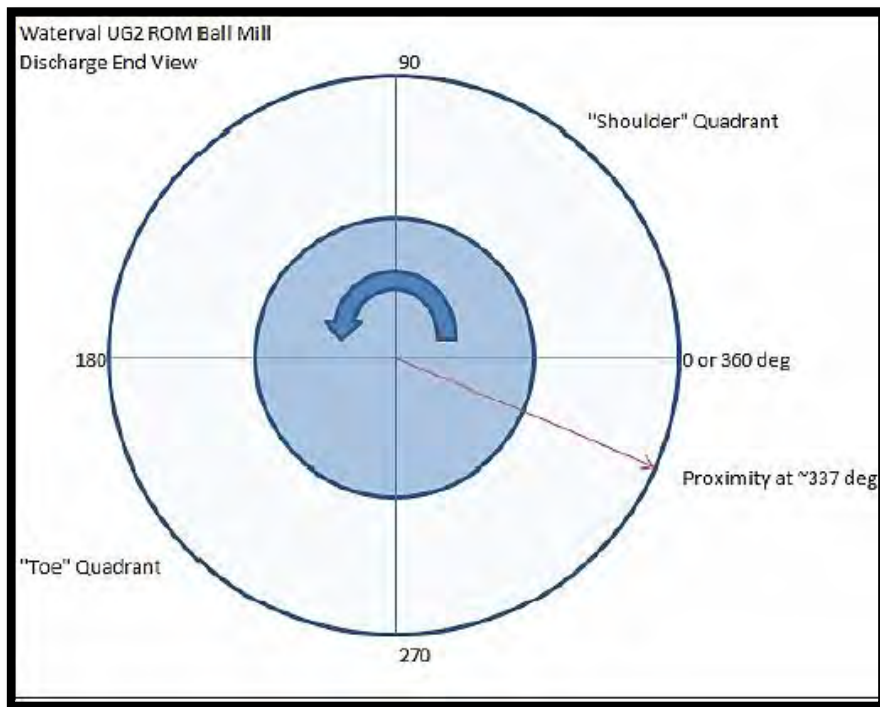


Figure 3:4-Specification location of each accelerometer on the mill

3.4 Experimental methodology

This section gives the description of the experimental methodology employed in obtaining the toe and shoulder angles of the charge used in estimating the dynamic volumetric filling. A series of mill surveys were conducted around the milling circuit. The first objective of this test work was to estimate the dynamic volumetric filling using the toe and shoulder positions obtained from the acoustic monitor for an industrial RoM ball mill. Table 3:3 summarises the conditions for the tests performed.

Table 3:3-The conditions of the experiment at the Waterval UG2 Concentrator

Feed rate (tph)	Water addition (m3/hr)	Media addition (tph)	Solids concentration (%)
400	107	70	79
500	77	71	87
675	149	71	82
700	121	75	85
750	120	71	86
760	130	73	85

The second objective of this study was to relate the dynamic volumetric filling calculated from the toe and shoulder position of the charge to mill performance. The experimental work involved making changes in the feed rate and water addition to the mill to the levels shown in **Table 3:3**. The feed rate was adjusted to the required level and then the mill was allowed to run until steady state was reached. During this period, the mill operating variables such as power draw, inlet water addition, and feed rate trends were monitored on the plant's System Control and Data Acquisition (SCADA) in the control room. At the steady state when the power draw, mill weight and product size trends remain unchanged for an hour. Samples were collected from the key streams identify on the primary grinding circuit (Refer to Figure 3:1). Samples were cut at fifteen-minute intervals for the test period of one hour. For each stream, a dummy sample was cut first followed by the main sample for analysis. The main sample was called the 'A sample' and the backup sample for storage called the 'B sample'. The details of the sampling procedure for each stream are discussed in sections 3.4.1 to 3.4.3.

3.4.1 Sampling the vibratory screen oversize

The vibratory screen oversize samples were manually collected by moving a 5-litre tray along width of the entire screen. The samples obtained were placed in a bucket during the test period. The time taken for each sample along the screen was recorded for the flow rate calculation. Figure 3:5 shows the sampling point for the vibratory screen oversize.



This is where the sample was collected

Figure 3:5- A picture showing the sampling point for the vibratory screen oversize

3.4.2 Vibratory screen undersize

The vibratory screen undersize sample is pumped into sump. The sample from the vibratory undersize screen was cut using the automatic sample cutter fitted to the sump. Samples were cut by pressing the automatic cutter switch intermittently. Figure 3:6 shows the sampling point for the vibratory screen undersize.



Figure 3:6-An auto-sampler for cutting vibratory screen undersize

3.4.3 Trommel oversize stream

The trommel oversize stream sample was collected from the trommel outlet. A 20-litre bucket was placed at the outlet, which was timed to help calculate the flow rate. The sample was collected for a period of 30 second due to the heavy flow of material from the trommel screen.

3.4.4 Mill grind-out

The original plan was to performed mill crash stops after each survey but due to the productions constraints only one grind-out was perform. The grind-out was done on a day before the survey during the general plant shutdown to measure the ball load. During the grind-out all the feed streams to the mill were stopped simultaneously and allowed to run for 25 minutes. The mill discharge pumps and screens continued to run uninterrupted. Grind-out was completed when the mill discharge on the screens showed no slurry on it. The mill was

stopped by de-energising the mill motor. Mill lock-out was performed. The feed hopper was open for air to enter and to cool the mill. The mill internal dimensions were taken, which included the charge height from the surface of the ball charge to the shell at the top (roof). The mill internal diameter and the chord across the surface of ball charge. The ball charge was calculated from these measurements. Figure 3:7 shows a photograph of the ball charge after grind-out. The ball load calculated from the physical measurements was 28%, which was consistent throughout the test.



Figure 3:7-A photograph of the ball charge after grind-out

3.4.5 Sample processing

The samples obtained from each sampling point after each survey were immediately weighed wet to determine the wet mass. The slurry samples were then filtered and dried in an oven at a temperature of 125°C. Non-slurry samples, the vibratory screen over size samples were placed on trays after weighing. The dried samples were weighed to obtain the dry mass and de-lumped while the non-slurry samples did not require de-lumping. All the samples were screened on a 1mm screen to obtain the plus 1mm and sub 1 mm portions. The sub 1mm samples were split using a rotary splitter to obtain test samples of about 300g. One sub-sample from each sample was wet screened to obtain the particle size distributions as

described in section 3.4.6. The trommel and vibratory screen oversize samples were screened on standard test sieves from 45mm to 1mm.

3.4.6 Wet screening of sub -1mm samples

Wet screening was conducted to obtain the particle size distributions of the vibratory screen undersize and oversize sub 1mm samples. Table 3:4 indicates the size fractions, which were used in the wet screening procedures. The screen stack was vibrated by a vibratory sieve shaker, as shown in Figure 3:8.

Table 3:4-The screen size used for the dry and wet screening procedure

Wet screening size	Dry screening size
-212 μm +150 μm	-1000 μm +850 μm
-150 μm +106 μm	-850 μm +600 μm
-106 μm +53 μm	-600 μm +425 μm
-53 μm +38 μm	-425 μm +300 μm
-38 μm +25 μm	-300 μm +212 μm
	-212 μm +150 μm

The sub-sample is initially weighed and wet screened on the finest screen (25 μm). The screen is firmly placed onto a vibratory sieve shaker. An empty 20-litre bucket was placed beneath the clamped screen. The sub sample to be screened is then placed on the screen and water introduced on it to dampen the sample to avoid dust when the sieve shaker is turned on. The sieve shaker is then turned on while a stream of water via a hosepipe ran onto the sieve continuously.

The screening process is stopped when clear water discharges from the undersize. The undersize is labelled and kept aside. The oversize is placed on a 150 μm sieve, which is firmly clamped onto the vibratory sieve shaker. An empty 20-litre bucket is placed underneath the sieve and wet screening proceeded as described for the 25 μm sieve. When only clear water is discharged at the bottom of the screen, the 150 μm oversize is placed on a pan and dried at 80°C. The dry material is then weighed and packed in clearly labelled plastic bags awaiting dry screening with screen sizes above 150 μm . The undersize is screened on a 106 μm sieve using the same procedure described for the 150 μm sieve. The undersize from the 106 μm sieve is screened on 75 μm and the procedure repeated on all the fractions in the root two

series down to 25 μ m. The oversize from these screens is dried in an oven at 80°C. The dried samples are weighed and stored safely awaiting the dry screening masses to complete the particles size distribution. The undersize from the 25 μ m sieve is combined with the original minus 25 μ m, filtered and dried.



Figure 3:8-Wet screening of sub 1mm

The resulting fractions from both wet and dry screening are weighed and the masses recorded. The integrity of the screening and weighing process are verified by immediately adding up all the screen fraction masses and the total sub 25 μ m fraction, and checking whether it is close to the total sub-sample mass recorded at the beginning of the screening. The dried oversize from 90 μ m is weighed and dry-screened on a stack consisting of screen series 850 μ m, 600 μ m, 425 μ m, 300 μ m, 212 μ m, and 150 μ m, thereafter, entered in a spreadsheet. The resulting masses of each size fraction from both wet and dry screening were added up to check whether they are close to the starting mass of the sample recorded at the beginning of the screening process.

CHAPTER FOUR: INDUSTRIAL SCALE EXPERIMENTAL RESULTS AND ANALYSIS OF THE ACOUSTIC SENSOR

4.1 Introduction

The experimental apparatus used for this study is the CSIRO acoustic sensor described in Chapter 3 section 3.3. The methodology used to obtain the experimental results is described in section 3.4. The purpose of this chapter presents the results obtained from the experimental campaigns performed using the acoustic monitor installed on a RoM ball mill at Anglo Platinum UG2 Waterval Concentrator. The variable tested was mill feed rate. The experiments were performed to evaluate the CSIRO acoustic sensor's response to changes in the mill operating conditions. The operational variables from the experimental data are mill power draw and mill load measurements were obtained from the plant's System Control and Data Acquisition (SCADA) system in the control room. The data extracted from the acoustic sensor includes the total vibration power as well as the toe and shoulder angles of the mill charge during the survey period. Table 4: 1 shows the mill performance data as well as the toe and shoulder angles from the acoustic sensor. The relationship between the data obtained from the acoustic sensor, and mill operating variables are discussed in this chapter.

Table 4: 1-The average toe, shoulder angles from the acoustic sensor and the mill performance data from the

Feed rate (tph)	Power (MW)	Mill mass (Tons)	% - 75 μ m	kWh/t	Shoulder angle (°)	Toe angle (°)	Band power (volts)
400	8.5	819.4	54.9	21.25	51.9	222.9	0.109
500	9.1	840.3	46.6	18.20	52.6	221.5	0.107
675	9.3	850.5	40.9	13.78	53.8	220.2	0.096
700	9.5	860.3	38.6	13.57	54.2	218	0.091
750	9.8	870.9	36.4	13.07	55.2	216.2	0.081
760	10.1	890.2	32.1	13.29	56.3	215.2	0.06

4.2 The total vibration power

The total vibration power is a measure of the vibration caused by the motion of the mill charge on the mill shell and it represents the different charge profiles within the mill. The toe and shoulder positions are calculated from the vibration signal. Therefore, the analysis of the total vibration power would be a very useful tool in establishing the charge profile of

tumbling mills since the operating variables and charge motion are related (Rolf *et al.*, 1982). In this study, the mill mass was changed by varying the feed rate to the mill at constant ball load of 28% which was consistent throughout the experiment. Figure 4:1 shows the variation of total vibration power and mill mass. It can be seen that the total vibration power decreased as mill mass increased. An increase in the mill mass meant an increase in the total charge level, which resulted in a decrease in the impact height. A low mill mass gives a high total vibration power because of an increased in the charge to shell collisions. A high mill mass produces a low total vibration power signal due to the decrease in collision of charge to shell impact. Furthermore, the amount of fines material in the mill also prevents the impacts of the steel balls on the mill shell by acting as a cushion absorbing some of the impact from the balls.

Huang *et al* (2010, 2011) used accelerometers attached to the external shell of an industrial mill for measuring the vibration signal. In their interpretation, the band power (vibration signal) decreased as the load in the mill increased due to the dampening of the impact by the charge material in the mill. Behera *et al* (2006) measured the vibration signal from the shaft of a laboratory ball mill of size 900 mm diameter and 150 mm long using an accelerometer. The vibration signals were measured under dry as well as wet grinding conditions for different operating conditions of mill speed, volumetric filling, powder loading, and time of grinding. They observed that the charge mass influences the vibration signals emitted due to the impact on the mill shell. Behera *et al* (2006) concluded that the vibration signal is a function of the mill rotation speed, volumetric filling, powder loading, and time of grinding. This is similar to what was found in this study.

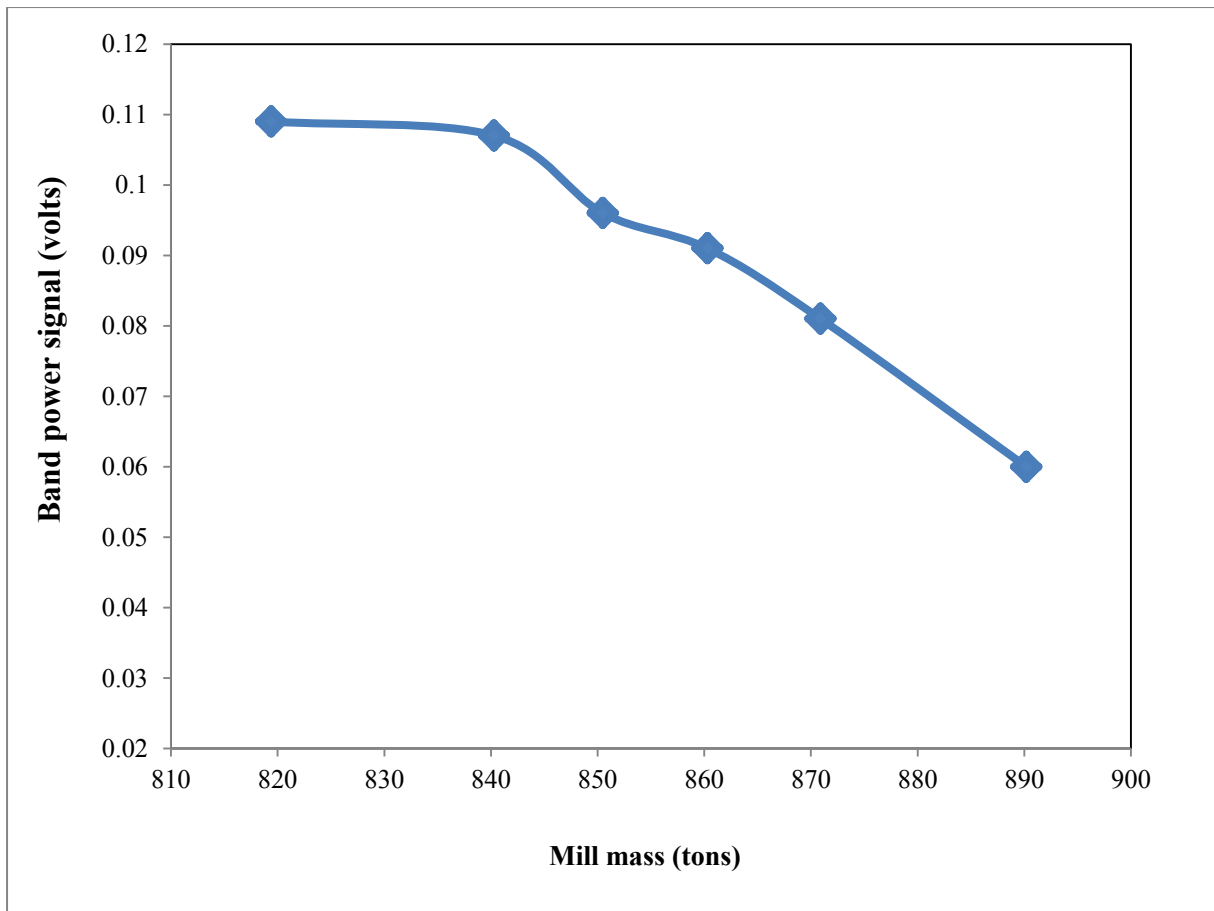


Figure 4:1-The variation of total vibration power with mill mass

4.3 The profile of the toe and shoulder angle

The toe and shoulder angles were extracted from the acoustic sensor. These are standard outputs from the sensor and are presented as angles. The shoulder position is defined as the angle around the mill shell where the minimum vibration occurs while the toe angle is defined as the position on the mill shell where the maximum vibration occurs on the mill shell. The measurements of the toe and shoulder angles are based on the direction of the movement of mill's rotation. The toe and shoulder angles are key parameters for describing the shape of the charge because these are the boundaries of contact of the charge on the shell. Most of the power draw equations make use of the toe and shoulder position of the mill charge for estimating the theoretical power draw of the tumbling mill (Bond, 1961; Austin *et al.*, 1984; Morrell, 1993, 1996; Moys 1993; Dong *et al.*, 2002). The toe and shoulder positions are the inputs for calculating the dynamic volumetric filling.

Figure 4:2 shows the variation of the toe and shoulder angles during the test period. It can be seen that the toe and shoulder angles varies together (Tano, 2005; Kiangi *et al.*, 2005, 2011). The peaks in the toe angles suggest variation in the shape of the charge along the mill axis of rotation (Davey *et al.*, 2012).

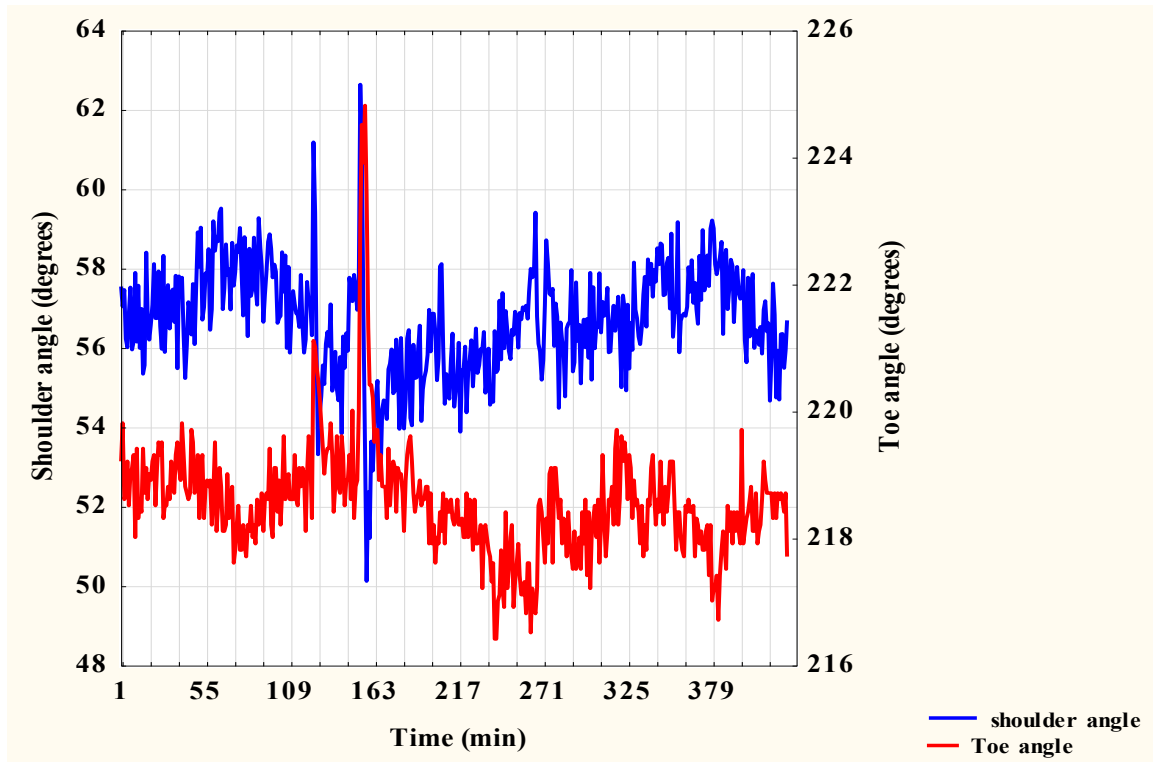


Figure 4:2-The variation of toe and shoulder position with time

Figure 4:3 shows variation of the toe angle and mill power draw with time. It is noticeable that the toe angle and the mill power draw moves together. When there is a peak in the toe angle, the power also peaks immediately thereafter. This also shows that the acoustic sensor is sensitive to changes in the mill operating conditions.

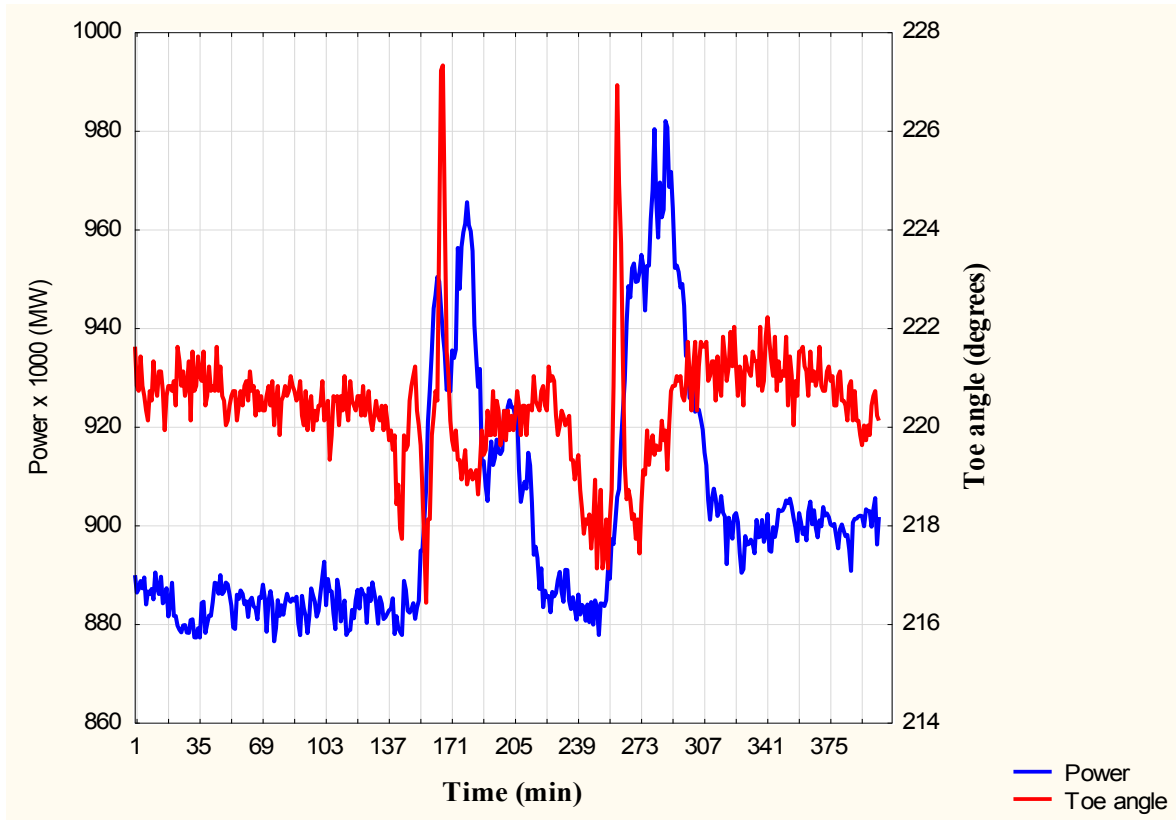


Figure 4:3-Variation of toe position and mill power draw

4.4 The results for calculation of the dynamic volumetric filling

Volumetric filling is one of the operating variables in the grinding process. The objective of this section show how the dynamic volumetric filling was calculated from the toe and shoulder position estimated from the acoustic monitor. The toe and shoulder positions were substituted into Equation 4-1 developed by Morrell (1993) to calculate the volumetric filling. The calculation procedure is presented in Appendix 1. From equation 4-1, θ_S is the shoulder angle, θ_T the toe angle, and J_t represents the volumetric filling.

$$\theta_S = \frac{\pi}{2} - \left(\theta_T - \frac{\pi}{2} \right) \left((0.3386 + 0.1041\phi c) + (1.54 - 2.5673\phi c)J_t \right) \quad \text{Equation 4-1}$$

In order to verify that the dynamic volumetric filling estimated from the toe and shoulder position is accurate, the Morrell power predictor model was used to simulate the power draw by manipulating the mill filling to obtain the power for each test. The parameters for the Morrell power draw model are given in Table 4:2.

Table 4:2- The mill parameters for calculating the volumetric filling B

Mill Data	
Diameter (m)	7.13
Belly length inside liners (m)	8
Feed Cone Angle (degrees)	22.5
Discharge Cone Angle (degrees)	22.5
Trunion diameter (m)	1.5
Fraction of crit. speed	0.75
Ball volume (%)	28
Total filling of cylindrical section (%)	35
Void Filling Fraction (slurry fills load)	1
Ore specific gravity	3.8
Liquid specific gravity	1
Discharge slurry % solids	86

The volumetric fillings obtained are given in Table 4:3. It should be noted that the dynamic volumetric filling, A, was obtained using the filling models from the toe and shoulder positions. The dynamic volumetric filling, B, was obtained from the Morrell power model. The relative error of between A and B is 4-8%. It can be seen from Table 4:3 that the volumetric fillings estimated using the sensor toe and shoulder angles is higher than those obtained from the static measurements. This is because the toe and shoulder angles used for calculating the dynamic volumetric filling are estimated from the motion of the charge in the mill. This shows that the volumetric filling can be estimated from the toe and shoulder angle estimated from the acoustic sensor.

Table 4:3-Calculated mill filling using Morrell mill filling and power equation

Feed rate (tph)	Shoulder position (radians)	Toe position (radians)	critical speed (% critical)	Power (MW)	Dynamic volumetric filling (%)		
					A	B	Relative error (%)
400	0.91	3.89	0.75	8.50	33.2	30.5	8.1
500	0.92	3.87	0.75	9.10	34.5	33.1	4.1
675	0.94	3.84	0.75	9.30	36.5	34.5	5.5
700	0.95	3.80	0.75	9.48	37.5	35.8	4.5
750	0.96	3.77	0.75	9.80	39.5	37.6	4.8
760	0.98	3.76	0.75	10.10	40.0	38.2	4.5

4.4.1 Relationship between the dynamic volumetric filling and mill mass

The variations in the volumetric filling have shown to have an influence on the mass of the charge in the mill (Morrell, 1993). Figure 4:4 illustrates the relationship between the dynamic volumetric filling and mill mass was measured by the load cell sensor when the mill running. The dynamic volumetric filling calculated from the toe and shoulder angles obtained from the acoustic sensor. The mill mas were measured from the load cell sensor installed under the mill. It can be seen that the relationship between mill filling and the mill load is linear. This is very important because most of the plants measure mill mass either from load cell or pressure sensor. The dynamic volumetric filling and mill mass provides useful information to the plant operator for the control of the mill. This can be used as a proxy for online measurements of volumetric filling on the plant.

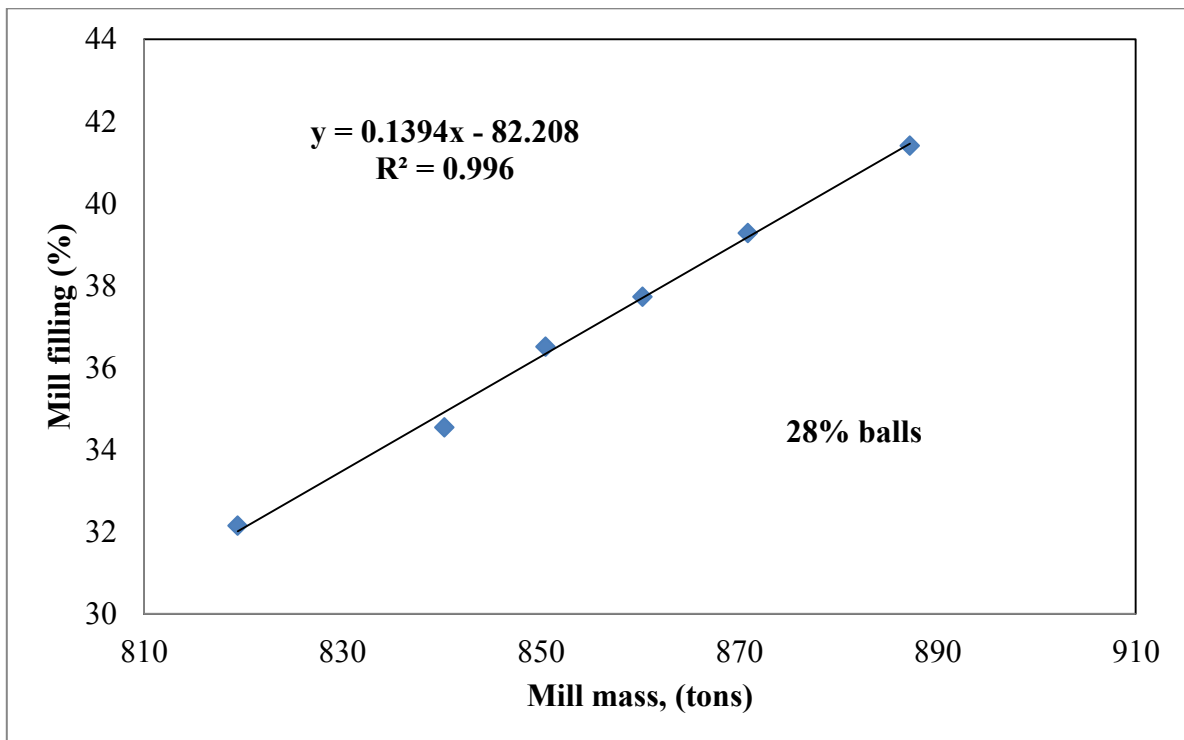


Figure 4:4-The relationship between calculated mill filling and mill load

The trend obtained from Figure 4:4 is similar to Figure 4:5 obtained by Powell et al (2006). They used mill crash stop method to obtain the volumetric filling which is different from this work. Getting the trend obtained from graph, using the established grind curves methodology, but with added advantage the volumetric filling can be measured on-line.

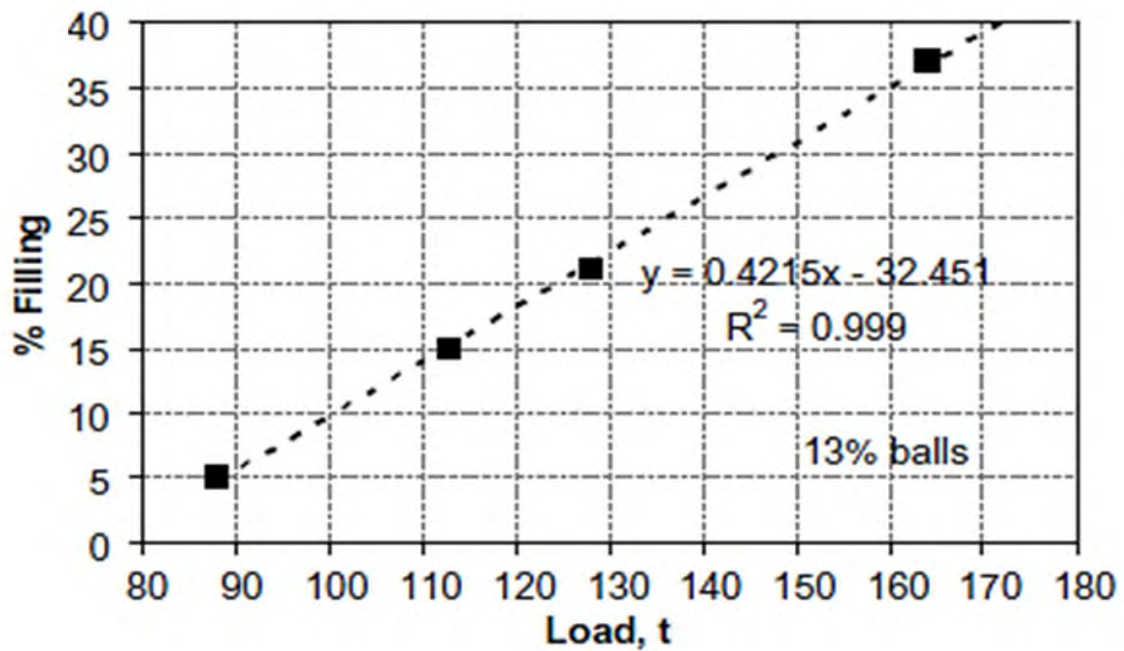


Figure 4:5- The filling and mill load relationship (Powell *et al.*, 2006)

4.4.2 The results of the dynamic ball filling calculations

The measurement of the ball filling degree is critical to this study because this is another method to compare the dynamic volumetric filling estimated from the toe and shoulder positions. The ball loads were measured during general plant shutdown. The height of the charge was measured from the ball surface to the roof of mill. The ball loads were calculated using the Allis Chalmers formula (Equation 4-1). The toe and shoulder positions estimated from the sensor during the grind-out period were used to estimate the dynamic ball filling. Table 4:4 shows the calculated ball load and dynamic ball filling degree from the toe and shoulder position just before the stop. From Table 4:4 it can be seen that the dynamic ball filling estimated from the toe and shoulder angles are slightly higher than the static ball filling. The reason is that the toe and shoulder angles were estimated from the dynamic behaviour of the charge within the mill. The relative error between the dynamic and static mill filling is between 3-8%.

Table 4:4-Comparison between the static and dynamic ball filling degree

Grind-out	Static ball load (%)	Dynamic ball load (%)	Relative error (%)
1	26.4	27.3	3.4
2	29.7	31.2	5.1
3	27.9	29.8	6.8
4	26.9	29.3	8.9
5	28.2	30.2	7.1

4.5 Relationship between grind and the toe and shoulder angle

This section analysed the influence of the dynamic positions of the charge on the fineness of grind that can be achieved by the RoM ball mill. The dynamic volumetric filling was calculated from the toe and shoulder angles estimated by the acoustic sensor. Figure 4:6 shows a schematic of the conceptualised toe and shoulder angles of the charge and the corresponding volumetric filling. A decrease in the toe angle indicates an increase in the volumetric filling while an increase the toe angle represents a decrease in the volumetric filling. However, an increase in the shoulder angle indicates a rise in the volumetric filling.

Figure 4:7 shows the relationship between the shoulder angles and grind. It can be seen that the grind decreased as the shoulder position of the charge increased. A high shoulder position imparts more lift to the charge, which increases void spaces between the steel balls (Austin *et al.*, 1984). Charge fills the void spaces between the steel balls and the effective collision zone. The reason could be due to the drop in the impact height from the shoulder region, which decreased the impact force on the charge. Figure 4:8 shows the variation of the grind and toe angles. Increasing the toe position increases the grind. An increase in the toe position indicates a reduction in volumetric filling. Increasing the toe angle increases the void spaces between the steel balls and the collision increases and there is increased contact of steel balls with the charge (Shoji, 1982).

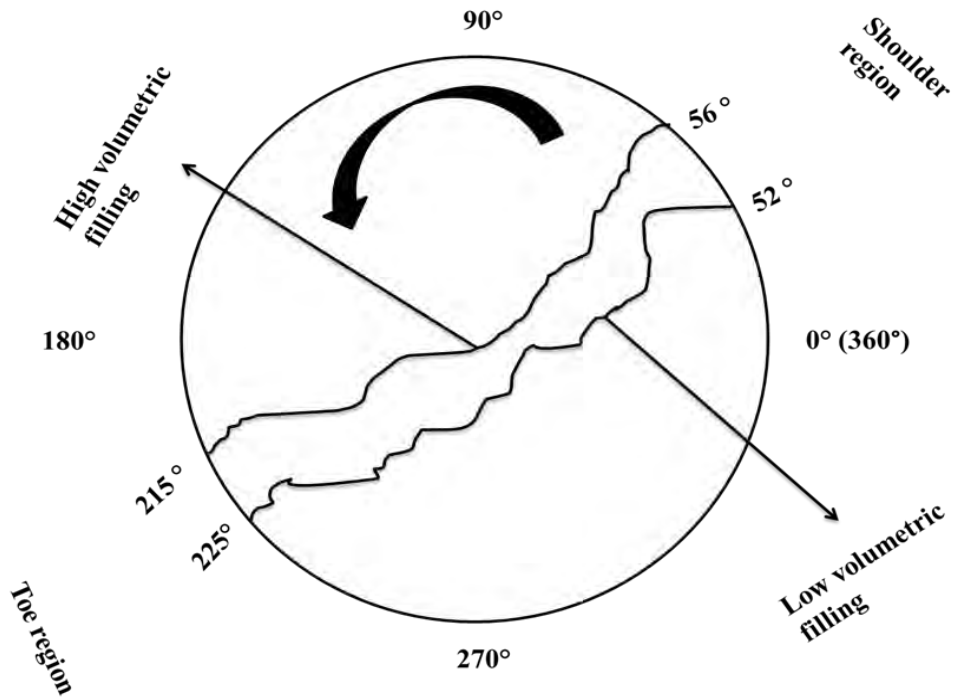


Figure 4:6-A schematic of the mill cross-section showing the toe and shoulder angles and the corresponding volumetric filling

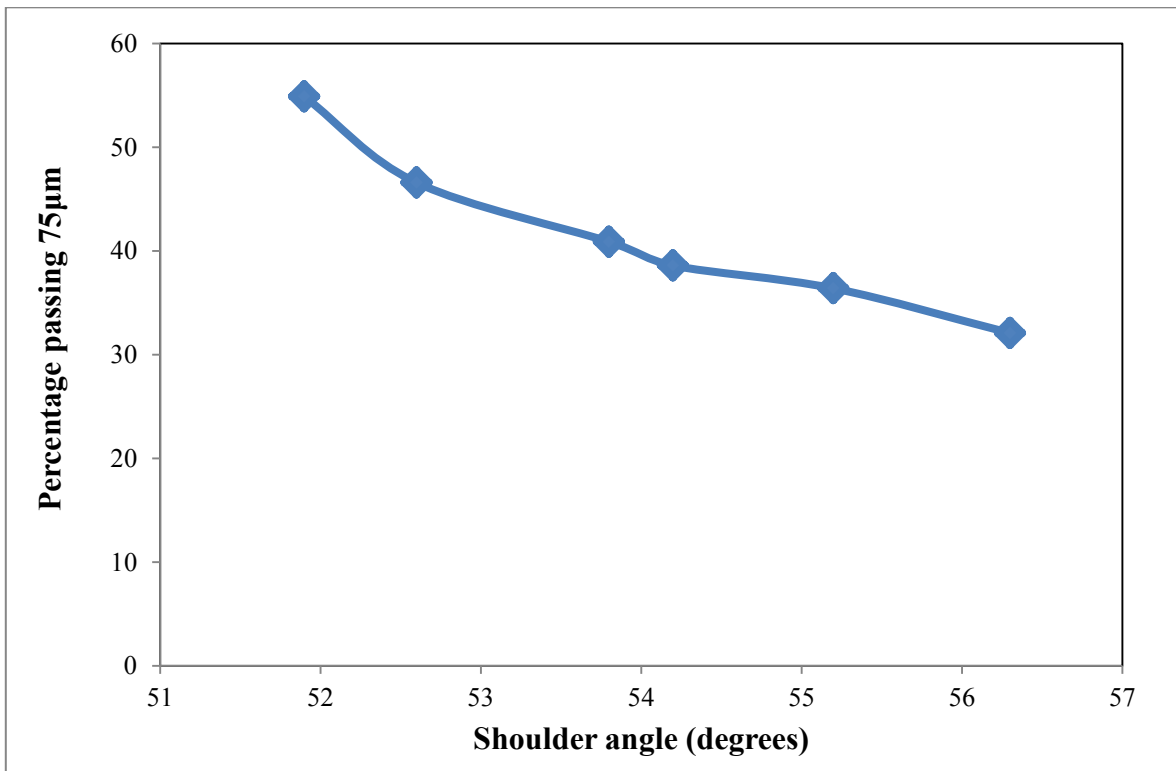


Figure 4:7-The variation of grind and shoulder angle

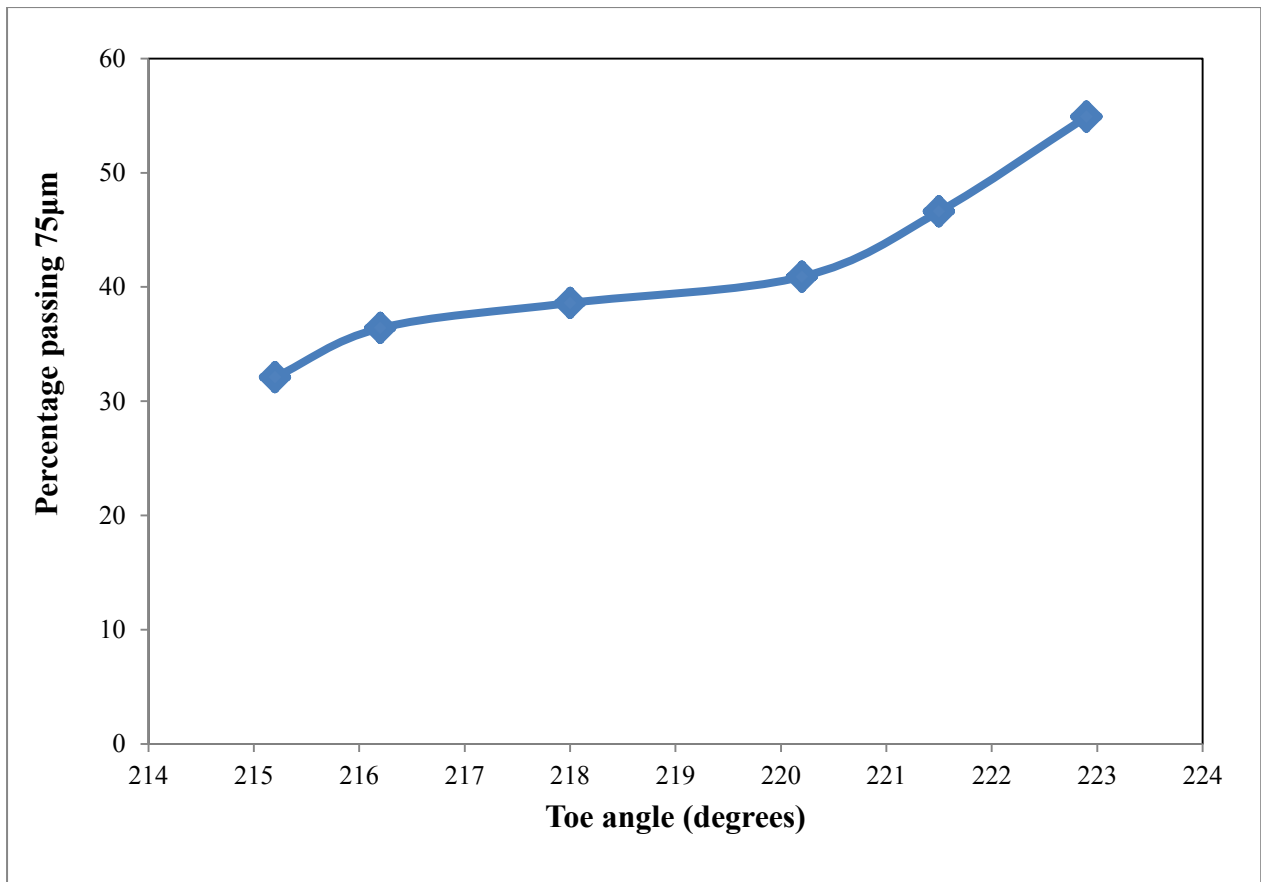


Figure 4:8- The variation of grind with toe angle

4.6 Relationship between dynamic mill filling and dynamic positions

The focus of this section is to assess the influence of toe and shoulder position of the mill charge on the dynamic volumetric filling. The importance of using the toe and shoulder angles in calculating dynamic volumetric filling because they are the boundary contact of the charge on the mill shell (Moys *et al*, 1988; Morrell, 1993; Kiangi *et al*, 2005, 2011). The changes in the toe and shoulder positions influence the dynamic volumetric filling of the tumbling mill.

Figure 4:9 show the relationship between dynamic volumetric filling and shoulder position of the mill charge. It can be seen that the shoulder angles increased with an increase in the volumetric filling. This was due to the rise in the level of the charge in the mill. Figure 4:10 shows the variation of the toe angle and volumetric filling. The toe angles decreased as the volumetric filling increased, due to the increase in the load level in the mill (Refer to Figure 4:6).

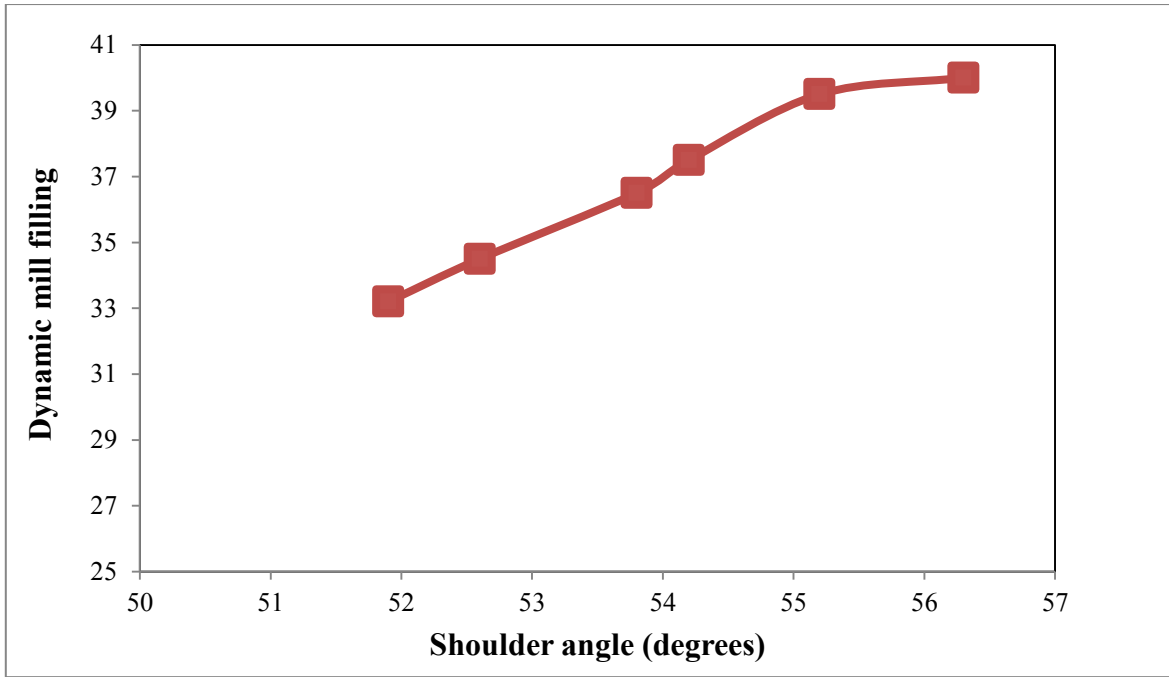


Figure 4:9-Variation of calculated dynamic filling with shoulder angle

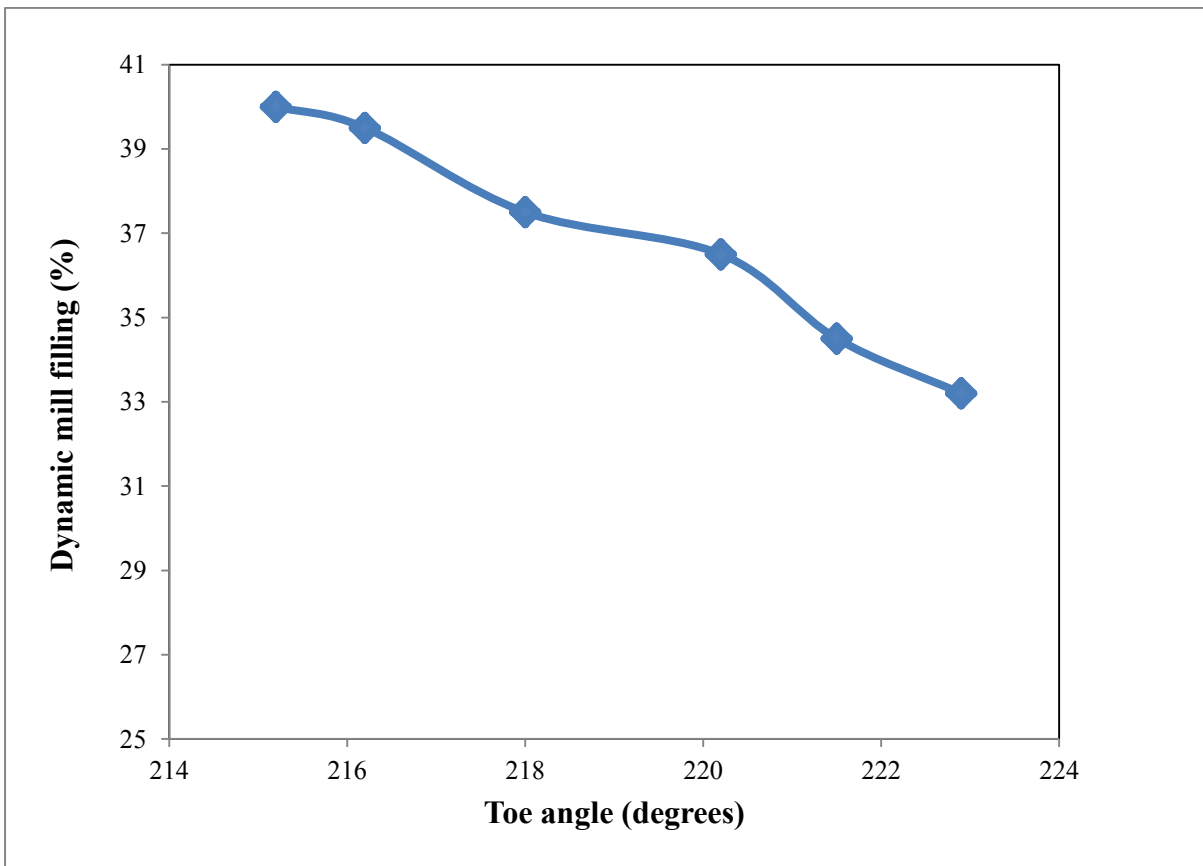


Figure 4:10-Variation of calculated dynamic filling with toe angle

The observations made regarding the influence of the shoulder and toe position on the dynamic volumetric filling are in agreement with the findings in the study reported by Van Nierop *et al* (1996). They used conductivity probes for measuring the conductivity of the slurry in pilot and industrial mills. The toe and shoulder positions of the media and slurry were estimated from the conductivity probes signals. In their investigation, they analysed the effect of mill fillings on the dynamic positions at varying operating conditions. They observed that the shoulder position varies with increasing mill filling while the toe increases with decreases.

4.7 Relationship between mill power and grind

A grind curve methodology was applied to the data obtained from the CSIRO acoustic sensor for assessing the performance of the RoM ball mill used in this study. At the start of the experimental work, the total ball load measured was 28%, which was consistent throughout. The dynamic volumetric filling was calculated from the toe and shoulder positions of the charge estimated by the CSIRO acoustic sensor. The grindcurve methodology developed for the RoM ball mill is presented in Figure 4:11.

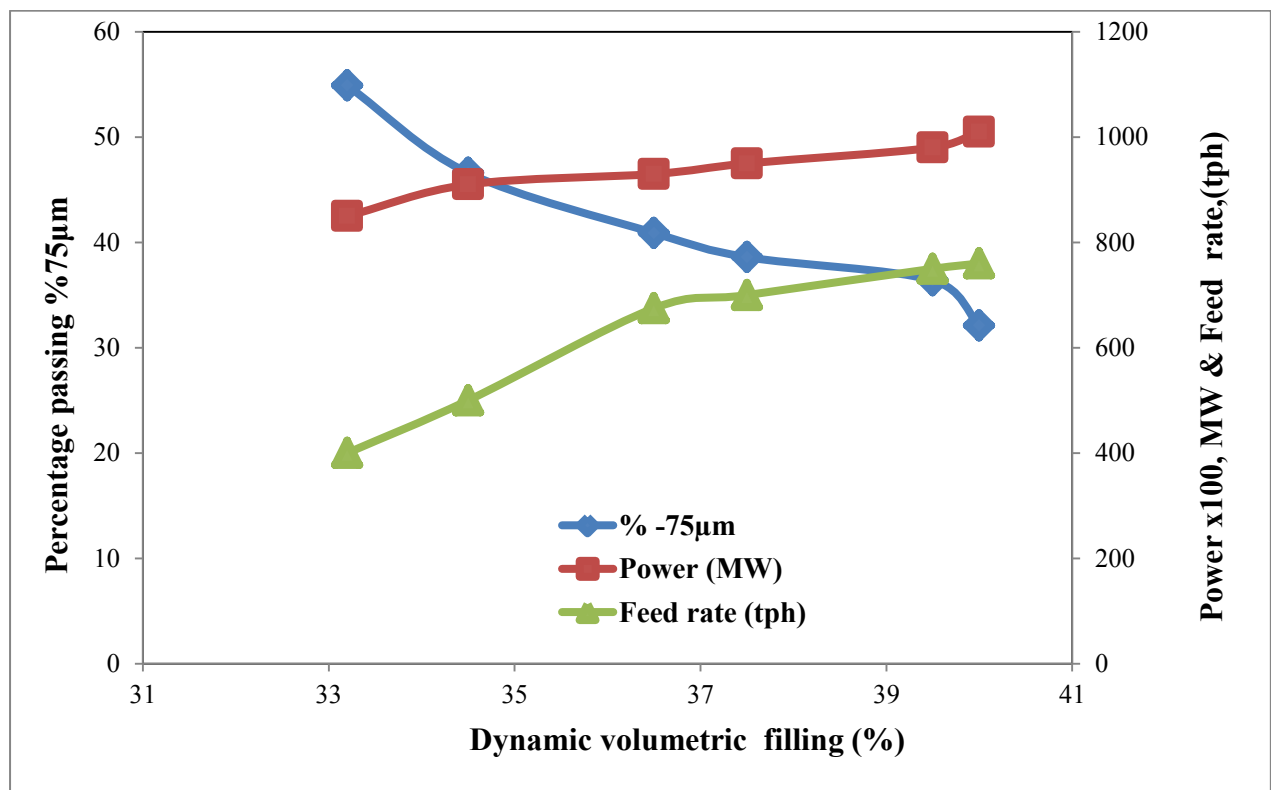


Figure 4:11-Variation in power, feed rate, grind with dynamic volumetric filling

Figure 4:11 show how the variation of feed rate, power draw and the materials passing $75\mu\text{m}$ vary with the dynamic volumetric filling. It can be seen that the lowest mill filling (33%) gave the coarsest grind (54%). The grind was found to be finer at higher volumetric filling which could also be attributed to attrition breakage due to cascading of the charge. As compared to the work of Powell et al (2012), it seems that in this test work, the RoM ball mill was operated in the region before the power peak and lower than the maximum throughput as the RoM ball mill was running with lower throughput. Increasing the volumetric filling from 33% to 40% gave the coarsest grind. The reason is that at the lowest volumetric filling the void space between the steel balls are not completely filled with the slurry and the effective collision is high. There is an increased contact of steel balls with the charge. Increasing the volumetric filling dropped the effective collision zones of the charge (Austin *et al.*, 1984). The decrease in the grind can also be attribute to the residence time of the materials in the mill. Since the RoM ball mill is a mixture of coarse rock and steel balls and the residence time in the mill is very short for the material to undergo effective breakage. The power draw increases steadily with the volumetric filling. The reason is that more momentum energy is required to lift the charge for it to rotate.

The grind curve obtained from this study is different from the SAG mill presented by Powell *et al* (2006, 2009, 2010) shown in Figure 4:12. The ball load was 7% and the volumetric filling was varying between 19% and 40%. They found that the grind and power draw peaks at 33% mill filling and began to decrease afterwards.

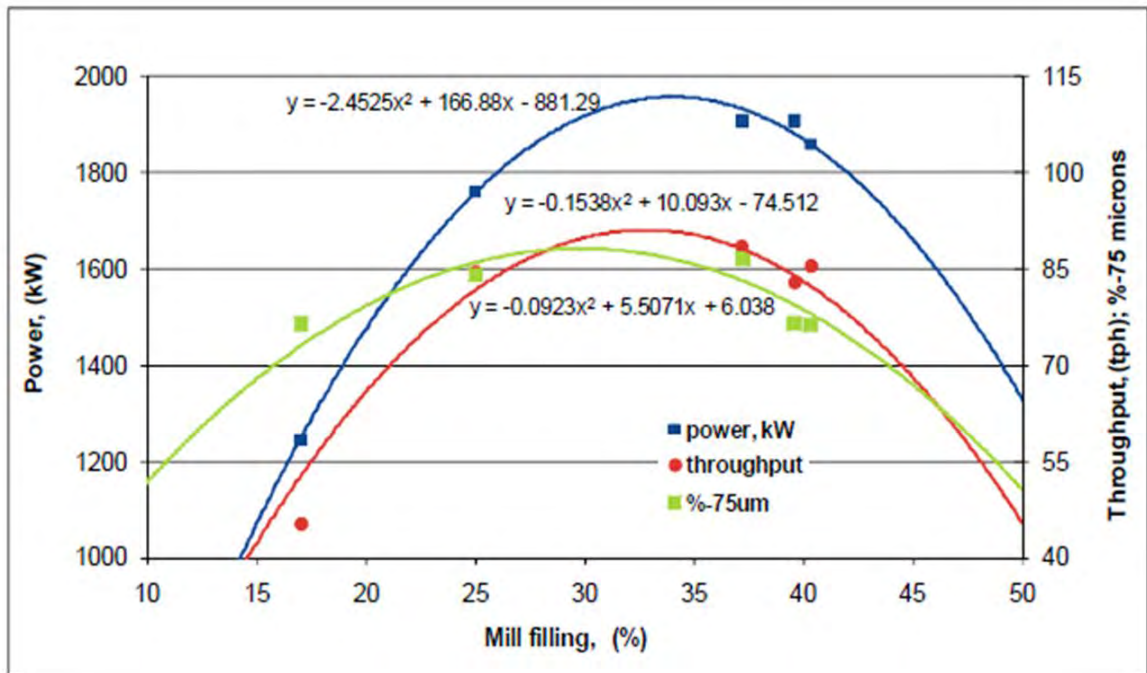


Figure 4:12- The grind curve methodology developed for a SAG mill (Powell *et al.*, 2012)

4.8 Conclusions

The acoustic monitor was used in this study to estimate the band power, toe and shoulder position of the mill charge. The dynamic volumetric filling was estimated from the averaged toe and shoulder position. A strong relationship was observed between the band power and the mill performance variables. In addition, it was seen that the dynamic volumetric filling affects the toe and shoulder position as well as the grind. It can be concluded that for RoM ball mill with high ball load the grind is finer at low volumetric filling.

CHAPTER FIVE: THE DESCRIPTION OF EXPERIMENTAL APPARATUS AND METHODOLOGY FOR PILOT SCALE USING THE SENSOMAG SENSOR

5.1 Introduction

The purpose of this chapter is to describe the experimental apparatus and methodology using the Magotteaux pilot plant station located at Frank Concentrator in Rustenburg, South Africa. The Magotteaux pilot plant has capacity for speed and ball load adjustment over a wide range of operating conditions. The Magotteaux pilot plant station is equipped with a mill that can be configured to operate as an AG/SAG mill, RoM ball mill, or Conventional ball mill. In this test, it was configured to operate as RoM ball mill. The mill is equipped with a device called the Sensomag. The Sensomag can be used for measuring the toe and shoulder angles of the mill charge (de Hass *et al.*, 2008; Clermont *et al.*, 2010; Keshav *et al.*, 2011). The experimental work reported in this study involved varying the mill speed and ball filling degree. This was done to assess the relationship between the Sensomag output measurements namely; toe and shoulder angles and these were then used for calculating the dynamic volumetric filling of the charge. The influence of the dynamic volumetric filling of the charge on the mill performance was then analysed.

5.2 The description of the Magotteaux pilot plant

A schematic of the Magotteaux pilot plant used in this study is shown in Figure 5:1. The setup consists of a stockpile and two feeders, one for coarse and the other for fine material. The inlet water supply is regulated to achieve the required density of the mill discharge. The Table 5:1 and Table 5: 2 shows the specifications and operating conditions of the Magotteaux Pilot RoM ball mill, respectively.

Table 5:1-The Specifications of the Magotteaux Pilot RoM ball mill

Mill diameter (m)	1.25
Mill length (m)	2.2
Speed ,% critical	65-90
Lifter height ,mm	50
No of rows of lifters	10
Discharges grate open area (%)	4
Grate size (mm)	18

Table 5: 2- The operating conditions of the Magotteaux Pilot RoM ball mill

Ore solids density (Merensky)	3.1
Steel density ,tm3	7.9
Top size of steel ball, mm	70
Ball load ,%	15-26
% Solids	70- 80
Feed rate, kg/hr	1200-5000

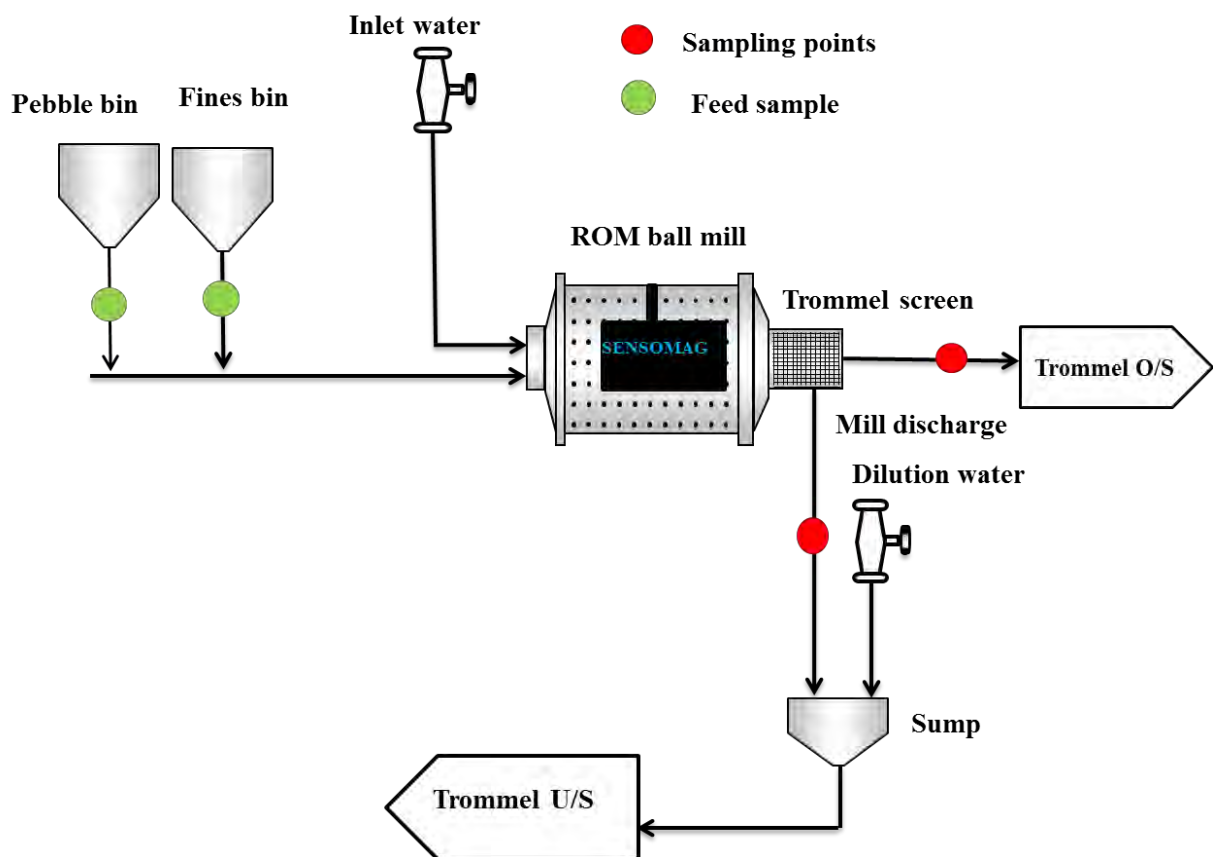


Figure 5:1-Flow sheet of the Magotteaux RoM Ball mill pilot plant

The pilot mill is equipped with a variable speed drive. At the discharge end of the mill, there is a trommel screen having an aperture size of approximately 5.6mm. The screen separates the mill discharge pebbles from the slurry. A sump is positioned at the discharge end of the mill to collect the trommel screen undersize, which is then pumped, to the downstream circuit of the plant. The trommel screen oversize discharges into a bin where it is either collected for sizing or recycled to back the mill. During operations, wash water is sprayed onto the

trommel screen to wash off the fines from the pebbles to reduce losses of fines. The Sensomag device performs online measurements of the toe and shoulder positions, which can be used to calculate the dynamic volumetric filling. The key features and operation of the Sensomag device are discussed in section 5.3.

5.3 The experimental device (Sensomag sensor)

The main experimental device in this study is the Sensomag sensor developed by Magotteaux Pty Ltd (Clermont *et al.*, 2010). In this study, the Sensomag device was used for the estimation of the dynamic positions of the toe and shoulder positions of the mill charge. The set up for this work is different from the work done by Clermont *et al* (2010) and Keshav *et al* (2011). Their work was on a secondary grinding application on an industrial scale but this work is on a RoM ball mill, which is a primary grinding application with coarse rocks in the charge.

The principal element of the Sensomag sensor is a wear-resistant polyurethane beam, installed inside the mill as part of the mill liner. The beam contains proximity inductive and conductive sensors for direct measurements of ball and slurry in the mill. Figure 5:2 shows the internal section of the Sensomag unit installed inside the mill. The external set-up for the pilot plant grinding mill is shown in Figure 5:3. As the mill rotates, a magnetic field is generated within the mill and the presence of ferromagnetic balls entering the magnetic field causes an amplitude variation. The variation in the magnetic field is detected by the electronic components within the sensor (Clermont *et al.*, 2008, 2010; Keshav *et al.*, 2011). The presence of slurry is estimated when the double metallic electrode meets the slurry. The raw signals are transmitted to a central processing unit via a wireless link where they are processed to estimate the toe and shoulder angles of the ball and slurry. Figure 5:4 shows the reference point for the Sensomag and the angular position of the ball and slurry load. The experimental methodology performed using the Sensomag is described in section 5.4.

**POLYURETHANE
BEAM**

MILL LINER



Figure 5:2-Polyurethane sensor beams for the Sensomag (Keshav *et al.*, 2011)

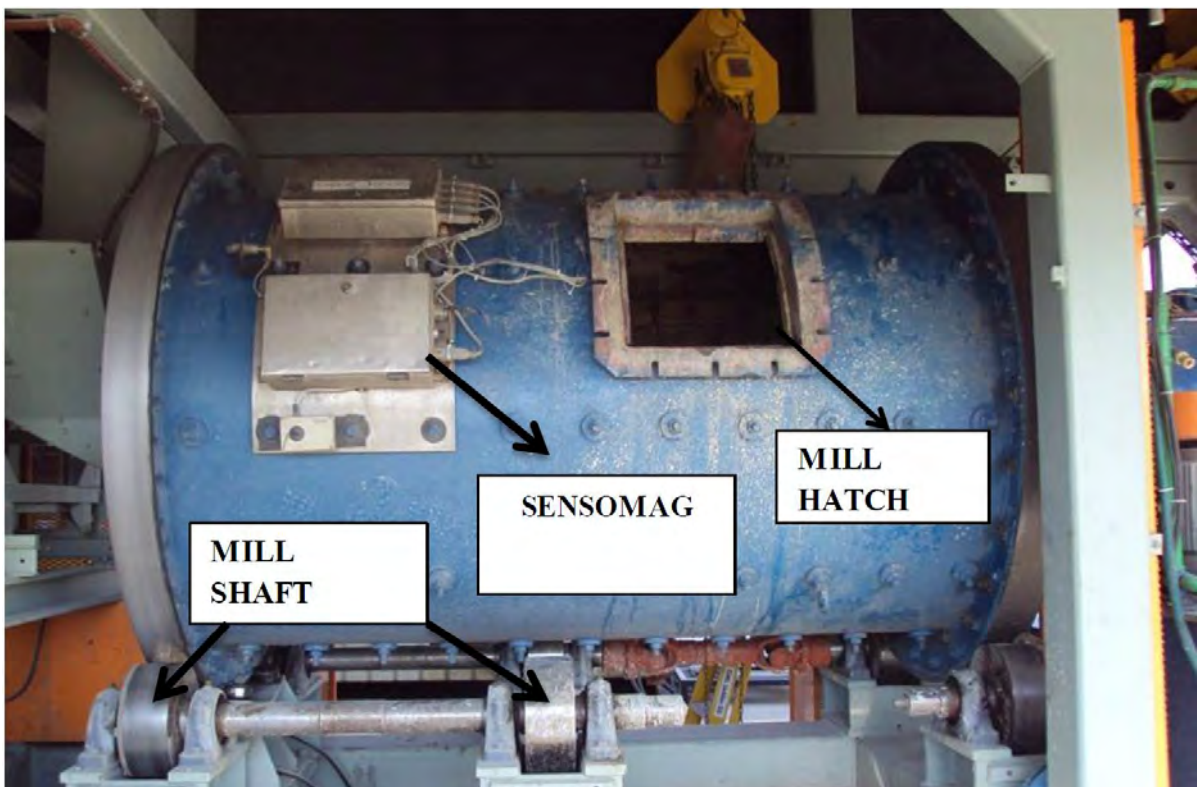


Figure 5:3-The external installation of Sensomag on the pilot mill

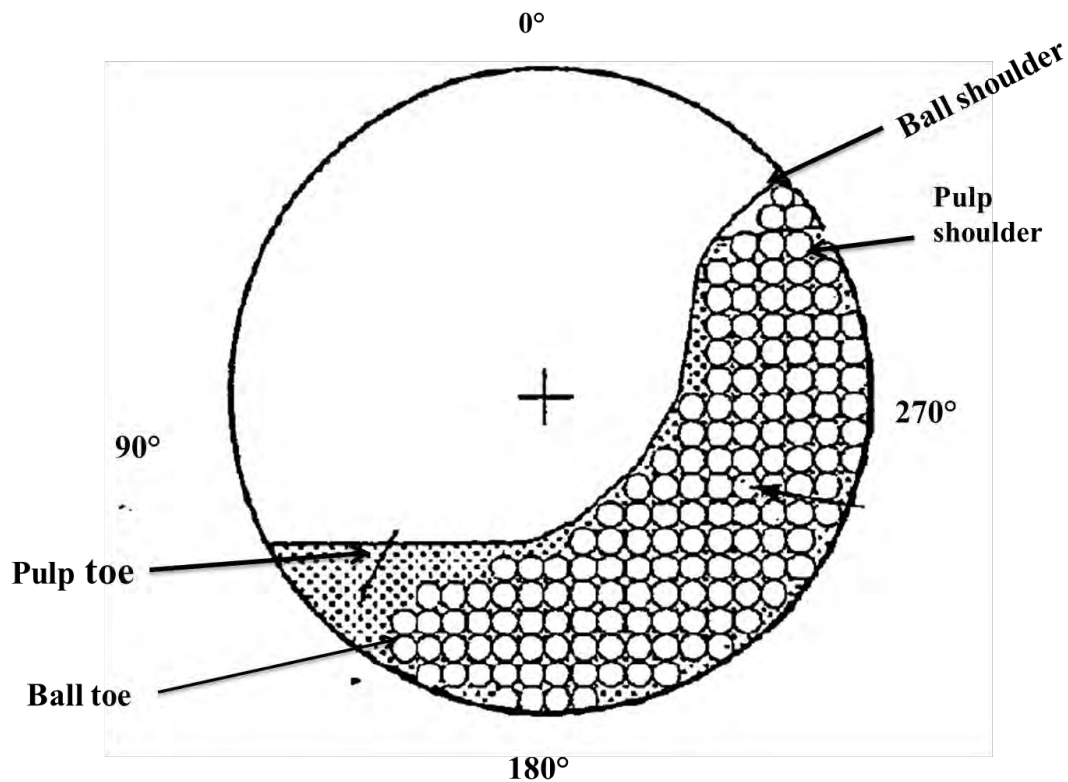


Figure 5:4- The reference point for the Sensomag and the angular positions of the slurry and ball load

5.4 Experimental programme

This section describes the experimental programme for the work conducted using the Magotteaux pilot station to generate the data for analysis. The Sensomag device was employed in this study for measuring the toe and shoulder position of the charge in degrees. The experiments were performed at varying mill speeds and ball filling degrees. The dynamic volumetric filling estimated from the toe and shoulder positions of the charge were compared with the mill filling calculated from the crash stop measurements. Sections 5.4.1 and 5.4.2 explain the sample preparations and test conditions for the experimental work.

5.4.1 The feed sample preparation

The ore used for the test was Merensky (total of 80 tons). The sample was prepared at Mintek and delivered in bags of 500kg. Onsite, the material was screened on a 50 mm screen, where the oversize material constituted the coarse feed (+50 mm) and the undersize (-50 mm) material constituted the fines feed. This was done to vary the ratio of fines to coarse fed to the mill. Figure 5:5 shows the stockpile of the fines and coarse feed for the test work. The fines

and the coarse material were transferred into the fine and coarse feed bins using front-end-loader. The dry feed sample was scooped from a stockpile using the front-end loader (Bobcat). The size distributions for the feed were obtained by screening the sample on a deck of screens from 90.0mm down to 1.0mm.



Figure 5:5-A picture showing the fine feed (a) and coarse (b) feed stockpile

5.4.2 Experimental conditions

At the pilot plant two different experiments were performed. The first set of tests were conducted to investigate the effect of mill speed on the toe and shoulder positions and hence dynamic filling in order to assess the mill performance. The mill speeds considered in this study were 75%, 80%, and 85% of the critical speed. The steel ball filling degree was 24% by volume and the in-mill percent solids was 75%. Table 5:3 shows the detailed test schedule with the range of feed rates and mill speed. The second set of experiments focussed on the influence of ball filling degree on the toe and shoulder positions hence dynamic volumetric filling. For these tests, the mill was operated at 75% of the critical speed and the percent solids in the mill were maintained around 75%. Table 5:4 summarises the test conditions for the second experiment. The sampling procedure is discussed in section 5.5.

Table 5:3-Experimental conditions for the mill speed and feed test

Survey No.	Speed (% critical speed)	Feed rate (kg/hr)
1	75	1200
2	75	1800
3	75	2400
4	80	2400
5	85	1800
6	85	2100
7	85	2400
8	85	2800

Table 5:4-Experimental conditions for the ball load and feed test

Ball load (%)	Feed rate (kg/hr)
15.0	2000-3000
20.0	2500-3500
23.5	2000-3000
26.0	2000-3500

5.5 Sampling procedure

The test methodology discussed in section 3.4 was followed for all the tests at the pilot plant. This has been repeated here because the set-up is different and some aspects have been introduced which are not covered under the industrial test work. The RoM ball mill was operated under open circuit conditions.

The mill was started up and feed allowed in at a low feed rate in each experiment. The feed rate was then adjusted upwards slowly until the set point was reached. The mill was allowed to stabilise. Steady state was reached when there was no change in the feed rate, mill load water addition, and power trend lines. The operation of the mill was assessed by monitoring the power draw, load, mill inlet water, and feed rate trends on the plant's System Control and Data Acquisition (SCADA) in the control room to ensure the mill was operating at steady

state conditions. The Sensomag sensor measured the toe and shoulder positions of the charge which were stored in a computer every minute via a telemetry system.

A full survey was conducted after the mill had stabilised. Prior to sampling of the mill discharge, two buckets labelled 'A' and 'B' were weighed to obtain the mass when empty and were then placed at the trommel screen oversize and undersize sampling points on the plant. These were used during the sampling. During the survey, samples were cut from the trommel oversize and undersize at every 15-minute intervals for a one hour period. The procedures followed at each sampling point are discussed in sections 5.5.1 to 5.5.3.

5.5.1 Trommel screen undersize

Sampling of the trommel undersize was done by cutting multiple samples from the discharge stream using a 5-litre tray. However, before sampling, the wash water tap was closed to avoid excess water being collected with the sample. The samples were cut by moving the tray across the flow. For the flow rate measurements samples were taken and the time for cutting the whole stream recorded for flow rate calculations.

5.5.2 Trommel screen oversize

During the test period, the sample from the trommel oversize stream was collected using a bin as shown Figure 5:6. A bucket was used to collect the whole stream for each sampling interval. The sample collected was used for both particles size distribution and flow rate of the pebbles.

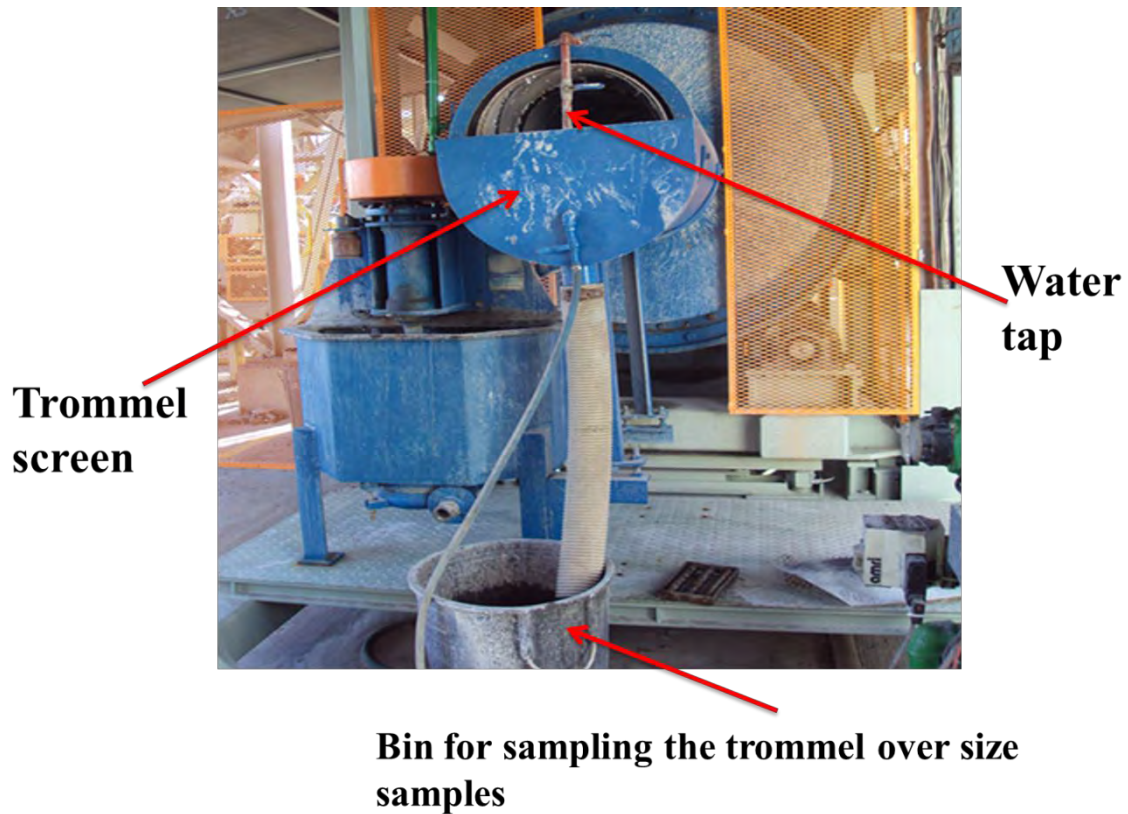


Figure 5:6-Sampling of trommel undersize discharge

5.5.3 The mill crash stop

The mill was crash-stopped after each survey was completed. This was done by stopping the feed and water streams into the mill and de-energising the mill motor simultaneously. The mill was allowed to cool down by opening the hatch for air to enter. The height measurement from the roof of the mill to the charge surface was taken and the chord across the charge was measured at three different positions. After taking the measurements, the charge was emptied out. The balls were separated from the rocks and the rock charge was screened to obtain the particle size distribution.

All the samples collected were prepared and processed according to the sample processing procedure described in sections 3.4.5 and 3.4.6.

CHAPTER SIX: PILOT PLANT TEST RESULTS FROM THE SENSOMAG SENSOR

6.1 Introduction

This chapter presents the results showing the influence of mill speed and ball load on the toe and shoulder positions of the charge and the performance of the RoM ball mill at the pilot scale. The toe and shoulder angles were extracted from the Sensomag device. The key variables tested were mill speed and ball filling degree. The dynamic volumetric fillings were calculated using the toe and shoulder positions and these were compared with volumetric filling values obtained from the physical measurements after the mill crash stop. This chapter presents some findings, which are beneficial to the mineral processing industry when using the Sensomag sensor to monitor the grinding circuit.

6.2 Effect of mill speed on the toe, shoulder angle and mill performance

The results presented in this section indicate the effects of mill speed on the toe and shoulder position of the charge and mill performance. In this study, the tests were performed at three different speeds 75%, 80%, and 85% of the critical speed. A total of eight pilot tests were performed. Table 6:1 shows the toe and shoulder angles of the slurry and ball load estimated from the Sensomag sensor. The tests performed showed that the toe and shoulder positions of the charge varied with mill speed. The ball toe and shoulder angles represent the bottom and the top of the grinding media load in the mill. The slurry toe and shoulder angles represent the top and bottom of the slurry load. The trend observed here are in agreement with the behaviour of the toe and shoulder positions with variation in mill speed observed by Morrell (1993), Moys *et al* (1988) and Tano, (2005). The mill performance data obtained from each test speed includes power draw, percentage passing 75 μ m and static volumetric filling as given in Table 6:2.

Table 6:1-Average values for the mill filling toe and shoulder positions from the Sensomag power and grind for varying speed and feed test

Test No.	Speed (% critical)	Slurry shoulder (°)	Slurry toe (°)	Ball shoulder (°)	Ball toe (°)
1	75	318.4	141.5	317.2	147.6
2	75	324.1	136.9	322.7	145.3
3	75	328.5	134.0	328.2	140.2
4	80	334.4	136.8	334.1	140.7
5	85	333.1	142.2	333.3	145.8
6	85	335.4	139.8	336.1	140.1
7	85	342.8	138.6	344.2	139.2
8	85	345.8	136.2	346.9	135.0

Table 6:2-The mill performance data from the varying speed and feed test

Test NO.	speed (% η critical)	% Mill filling (Static)	Mill weight (kg)	% -75 μ m	Power (kw)
1	75	29.7	10830.0	66.0	28.2
2	75	38.9	11458.8	55.0	29.2
3	75	44.7	11755.0	50.2	30.1
4	80	42.9	11516.0	48.3	31.3
5	85	33.8	11016.9	56.9	33.2
6	85	35.5	11266.8	50.6	33.4
7	85	45.6	11759.0	47.7	33.6
8	85	47.3	11865.0	45.8	34.0

6.2.1 The results for the calculations dynamic volumetric filling

The objective of this section is to calculate the dynamic volumetric filling from the toe and shoulder angles estimated from the Sensomag. The reference point for the Sensomag is at the 12 o'clock position while the CSIRO acoustic sensor is at 3 o'clock. The reference point for the Sensomag was changed to 3 o'clock position for consistency in this study. The dynamic filling was calculated from the toe and shoulder positions of the charge and the key variable was mill speed.

Equation 2-1 for volumetric filling in section 2.5.1 was used to calculate the dynamic volumetric filling from the average of the toe and shoulder angles of the mill charge. The static volumetric filling was calculated from the physical measurements taken at stationary after mill crash stop. Table 6:3 shows the calculated dynamic volumetric filling for three different mill speed settings. The toe and shoulder angles are in radians. Table 6:4 shows a comparison between static volumetric filling estimated from the physical measurements from the crash stop and dynamic volumetric filling calculated for the toe and shoulder angles from the slurry and ball load.

Table 6:3-Calculated volumetric filling for the slurry load from the toe and shoulder positions from the Sensomag for the varying speed test

Mill speed (ϕc)	Feed Rate (kg/hr)	Shoulder angle (radians)	Toe angle (radians)	Dynamic volumetric filling (%)
75	1200	0.8456	4.0408	31.9
75	1800	0.9439	3.9600	40.0
75	2400	1.0203	3.9096	47.0
80	2400	1.1243	3.9589	45.7
85	1800	1.1007	4.0530	37.0
85	2100	1.1416	4.0108	39.1
85	2400	1.2711	3.9906	47.2
85	2800	1.3236	3.9483	50.3

Table 6:4-Comparison between volumetric fillings estimated from the crash stop measurements and the sensor toe and shoulder angles.

Speed (% critical)	Static mill filling (%)	Dynamic volumetric filling (%)	Relative difference (%)
75	29.7	31.9	7.4
75	38.9	40.0	2.8
75	44.7	47.0	5.1
80	42.9	45.7	6.5
85	33.8	37.0	9.5
85	35.5	39.1	10.1
85	45.6	47.2	3.5
85	47.3	50.3	6.3

It can be seen from Table 6:4 that the volumetric fillings estimated using the sensor toe and shoulder angles is higher than those obtained from the static measurements. This is because the toe and shoulder angles used for calculating the dynamic volumetric filling are estimated from the motion of the charge in the mill. The average relative difference between the static and the dynamic volumetric filling is between 2-10%. This shows that the toe and shoulder angles are good estimates of volumetric filling, because these are the boundaries of contact of the mill charge on the liners/lifters.

6.2.2 Effect of mill speed on the toe and shoulder position

The effect of mill speed on the toe and shoulder positions of the mill charge was investigated on the RoM ball mill. The essence of mill speed is to raise the charge higher and increase the amount of lift imparted to the charge, which leads to expansion of the mill load. Mill speed has a significant influence on the dynamic positions of toe and shoulder angles of the mill charge (Morrell, 1993).

The profile of the slurry and ball shoulder angles for the test performed at the same feed rate (2400kg/hr) when the mill was operated at 75%, 80%, and 85% of the critical speed are shown in Figure 6:1 and Figure 6:2, respectively. It can be seen that the shoulder angle increased with an increase in the mill speeds. The reason was that as mill speed increased, the charge was lifted to a higher height along the rising side of the mill shell before departing to the toe region. The lift imparted to the charge was more pronounced at higher mill speeds which resulted in higher shoulder angles. Figure 6:3 and Figure 6:4 show the variation of the

toe angles for the slurry and ball as mill speed increased. It can be observed that the mill speed appears to have an influence on the toe angle of the charge. The decrease in the toe angle is due to cataracting balls and slurry landing on the mill shell above the toe region. It is noticeable that variations in the toe angle with the mill speed were more pronounced at 85% critical speed. Figure 6:5, Figure 6:6 and Figure 6:7 show the schematic of the toe and shoulder angles at 75%, 80%, and 85% critical speed.

Others authors (Vermeulen *et al.*, 1986; Moys *et al.*, 1988; Napier-Munn *et al.*, 1996; Agrawala, 1997; Dupont *et al.*, 2001; Spencer *et al.*, 2000 and 2005) have reported these similar trends. Morrell (1993) reported that the toe and shoulder angle of the mill charge is affected by varying the mill speed. Kiangi *et al* (2006, 2011) measured the toe and shoulder angles of the mill charge in a dry pilot mill as a function of mill speed (varied between 63-98% critical) using an inductive proximity probe. They observed that the shoulder position increases while the toe position decreases when the mill speed is increased. Tano *et al* (2005,2008) used a strain gauge sensor fitted on a pilot ball mill in wet grinding. The mill speeds tested were 73% and 78% of the critical speed. The toe and shoulder angles of the mill charge were measured using the strain gauge sensor. The results showed that the shoulder position increases with increasing mill filling. The toe angle decreases with increasing mill filling.

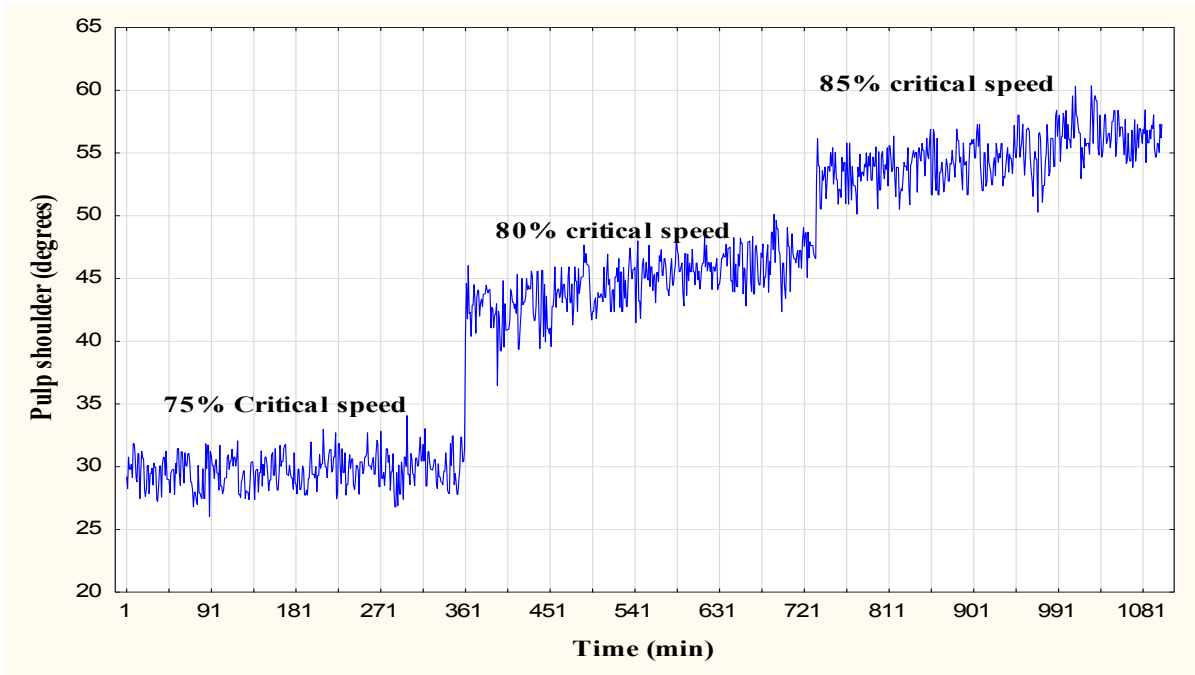


Figure 6:1-The variation of slurry shoulder angles with mill speed at feed rate of 2400kg/hr

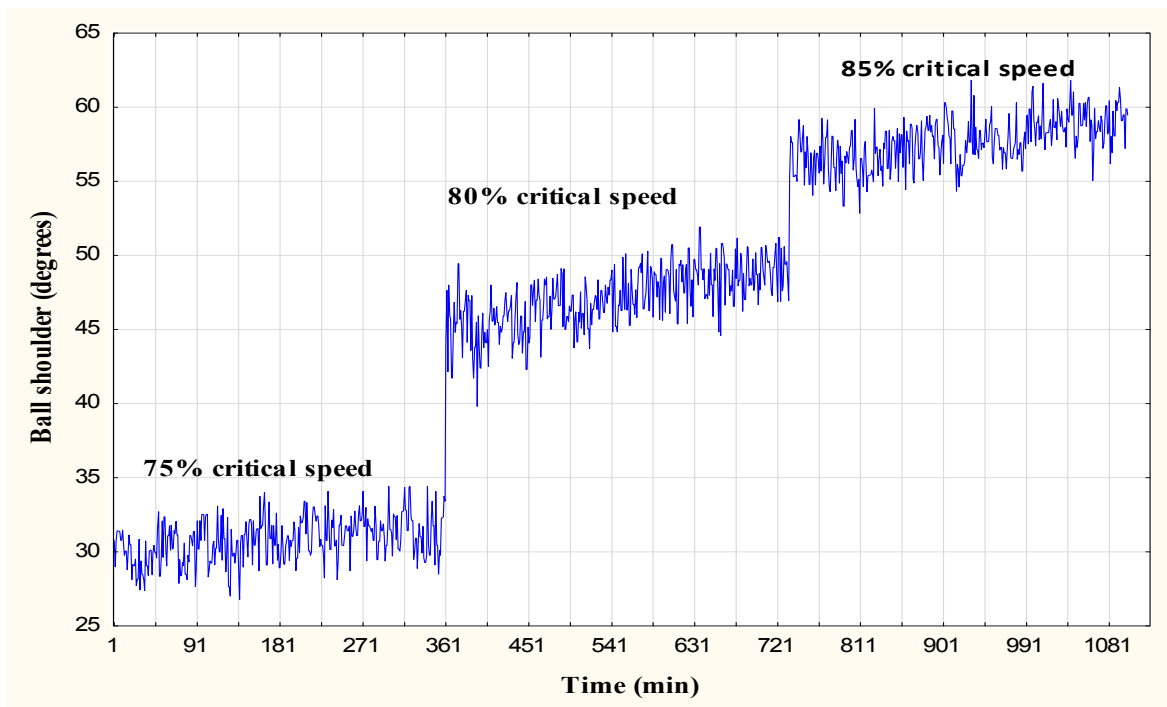


Figure 6:2-The variation of ball shoulder angles with mill speed at feed rate of 2400kg/hr

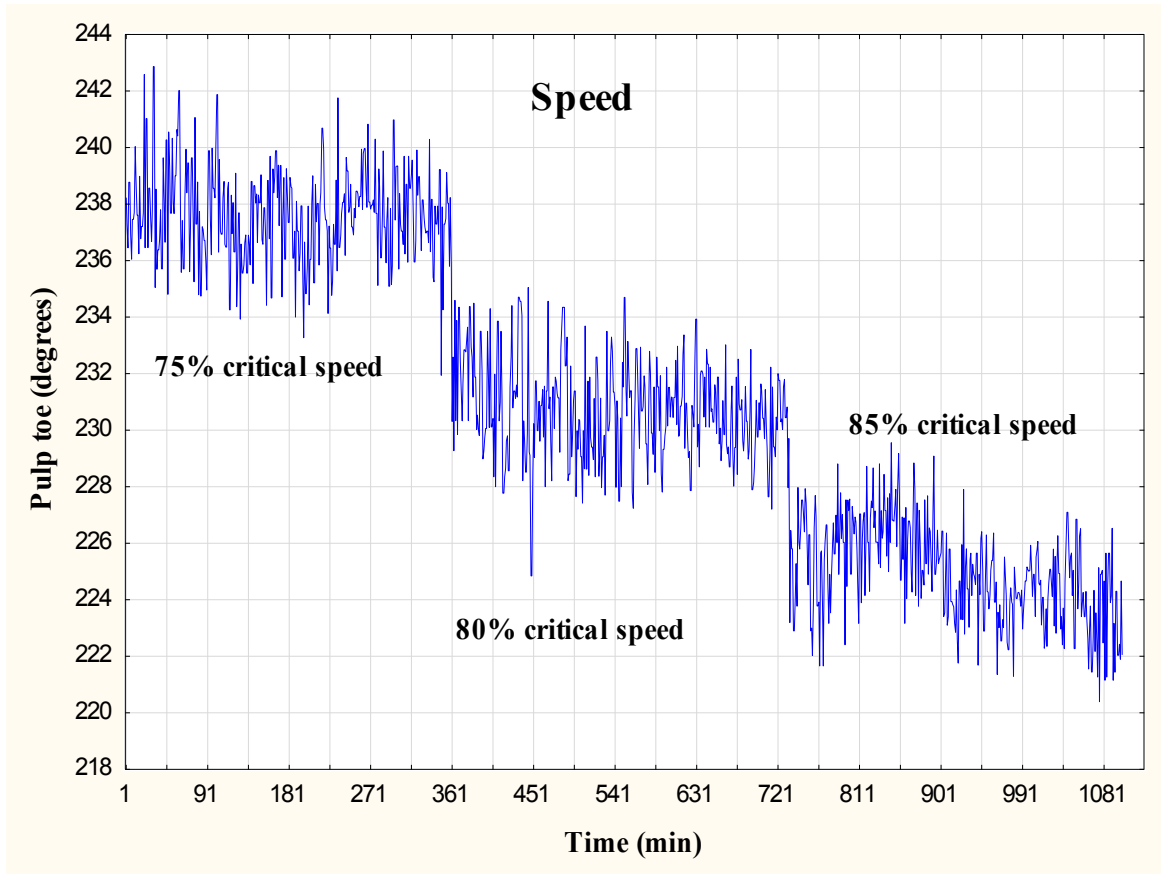


Figure 6:3-The variation of slurry toe angles with mill speed at feed rate of 2400kg/hr

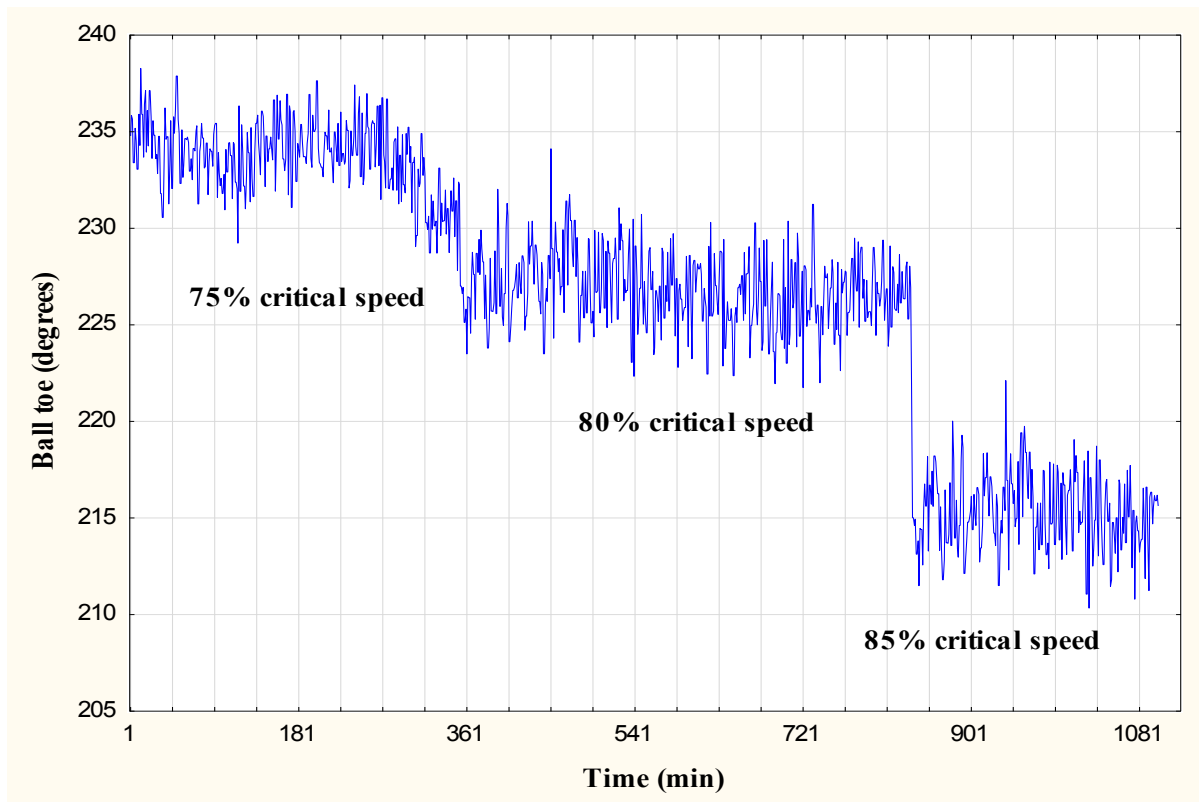


Figure 6:4-The variation of ball toe angles with mill speed at feed rate of 2400kg/hr

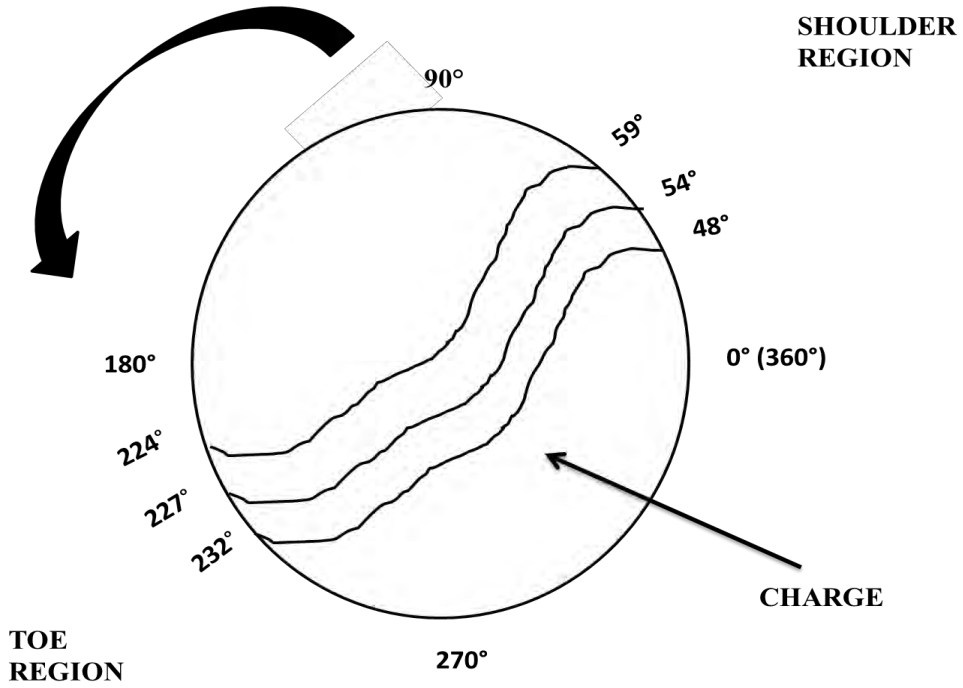


Figure 6:5-Schematic showing the toe and shoulder angles at 75% critical speed

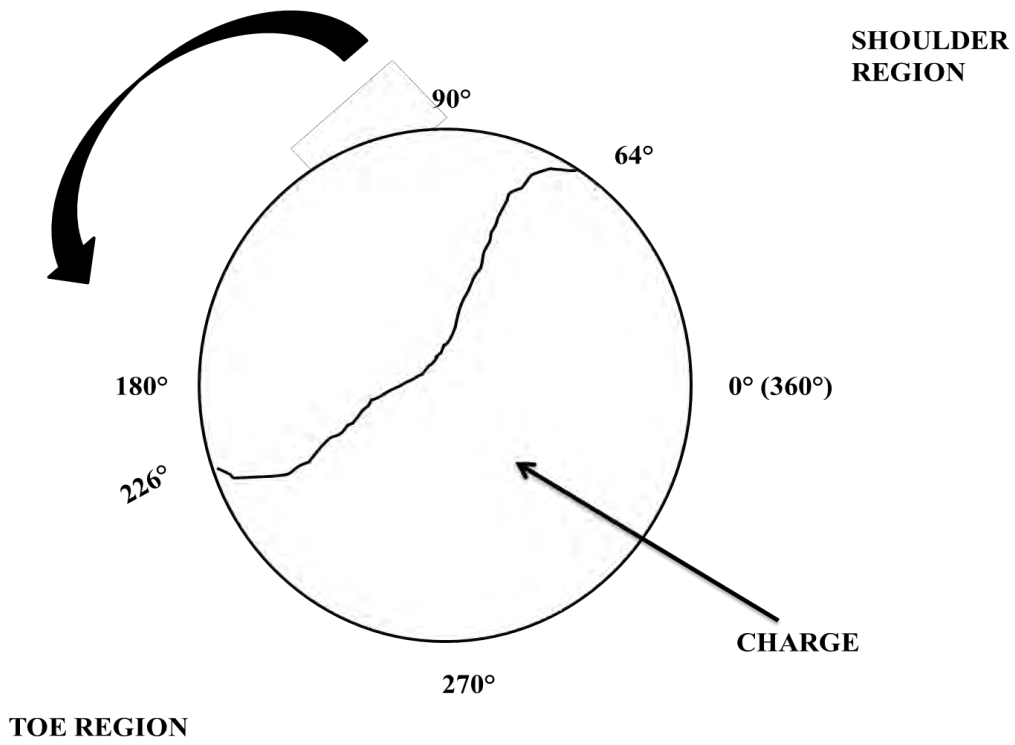


Figure 6:6-Schematic showing the toe and shoulder angle at 80% critical speed

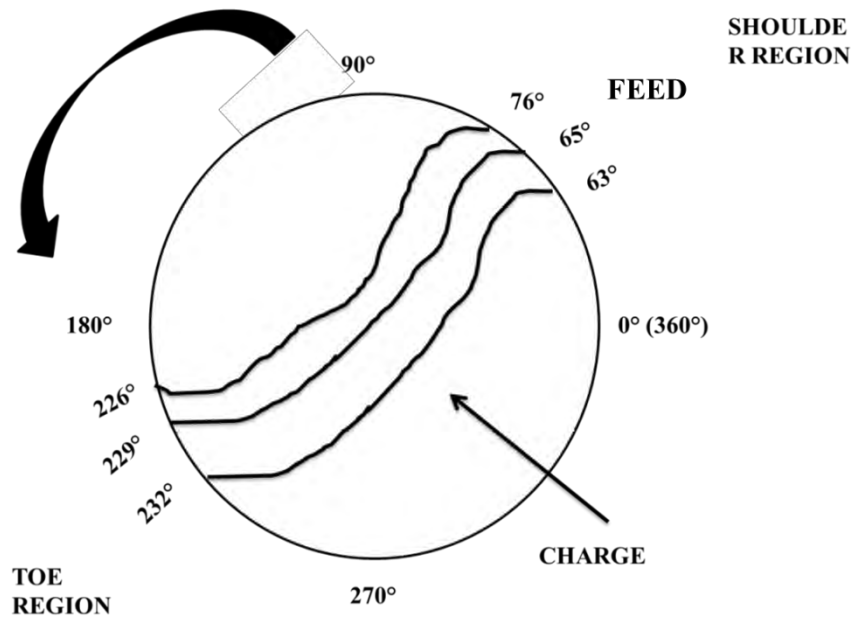


Figure 6:7-Schematic showing the toe and shoulder positions at 85% critical speed

6.2.3 The relationship between volumetric filling and toe and shoulder angle

This section discusses the effect of volumetric filling on the toe and shoulder angles of the mill charge, when the mill was operated at three different speeds. Figure 6:8 and Figure 6:9 show the variation of the dynamic volumetric filling and shoulder angles for the ball and slurry load at mill speeds of 75 % and 85% of the critical, respectively. It can be seen that there is a direct relationship between the dynamic volumetric filling and the shoulder angles. The reason is that as volumetric filling increases the level of the charge the load exerts force on the mill liners, which reduces the frictional force between the charge and the liners. The rock at the lower bottom of the charge pushes material further up along the mill shell (Morrell, 1993; Napier-Munn *et al.*, 1996; François *et al.*, 2013). It is noticeable that the trends for the slurry and ball are identical but the slurry shoulder is slightly higher than that of the steel balls. The reason is that at the shoulder region, the trajectory of the slurry is different from that of the ball as the slurry is lifted higher than the steel balls. This is due to the pulp adherence on the liners and the difference in the specific gravity of the slurry and the steel ball (3.1 and 7.9, respectively).

The trend observed in this study is different from the studies conducted on secondary ball mills using the Sensomag. It was reported that the ball shoulder angle was higher than that of

the slurry. The reason was that the slurry drains through the steel ball (De Haas *et al.*, 2008; Clermont *et al.*, 2010; Keshav *et al.*, 2011).

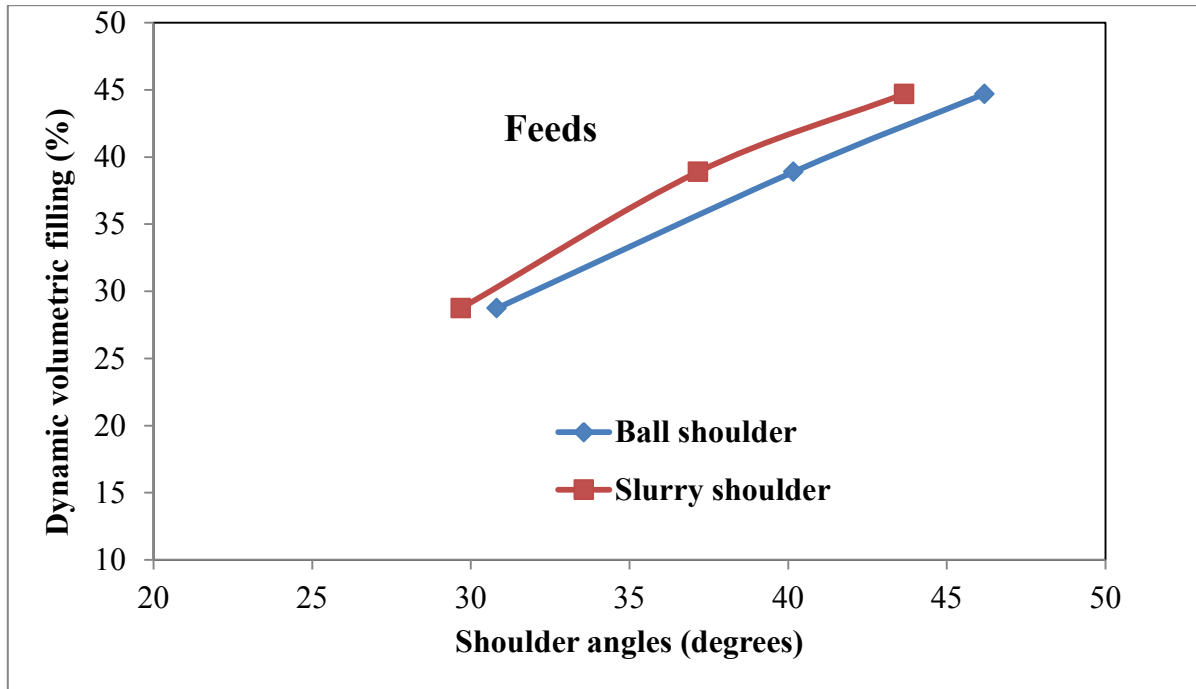


Figure 6:8-The variation of dynamic volumetric filling with shoulder angles at 75% critical speed

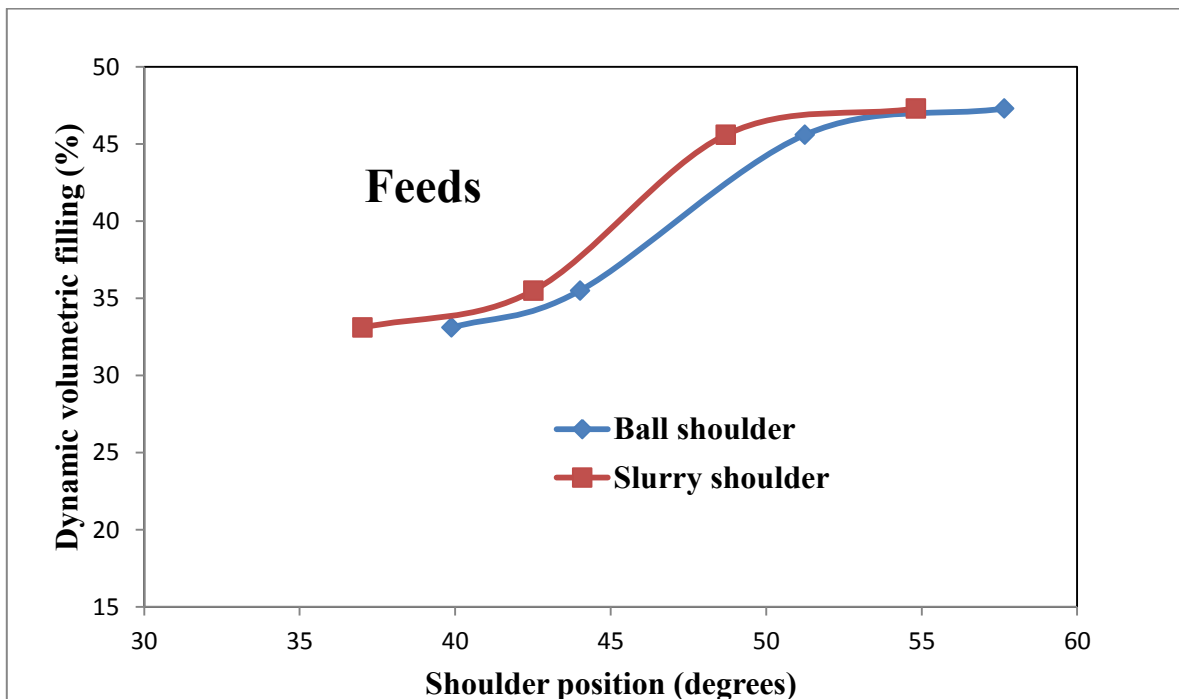


Figure 6:9- The variation of dynamic volumetric filling with shoulder angles at 85% critical speed

Figure 6:10 and Figure 6:11 show the variation of volumetric filling and toe angles for the ball and slurry load at 75% and 85% critical speed, respectively. It can be observed that the toe angle decreased as the dynamic volumetric filling increased. The reason was that the trajectory of the charge at the toe angle was different. The charge at the rising side of the mill shell impact directly onto the liners rather than onto the charge at the toe region. It can be seen that the profiles of the slurry and steel ball are higher at 75% critical speed than at 85% critical speed. The reason is that for mill speed above 80% critical speed, the toe position is a weak function of the mill speed which is linearly dependent on the volumetric filling (Moys *et al.*, 1988).

These trends are in agreement with findings by Morrell (1993), Tano *et al* (2005, 2008), Moys *et al* (2010) and Keshav *et al* (2010). Tano (2005) used a strain gauge mounted in a lifter to determine the effect of mill filling on the toe and shoulder angle in a pilot ball mill. He concluded that the charge level has the largest effect on the calculated toe and shoulder angles from the strain gauge sensor (See Figure 2:10 and Figure 2:11). Morrell (1993) also concluded that mill speed and volumetric filling mainly affect the load profile.

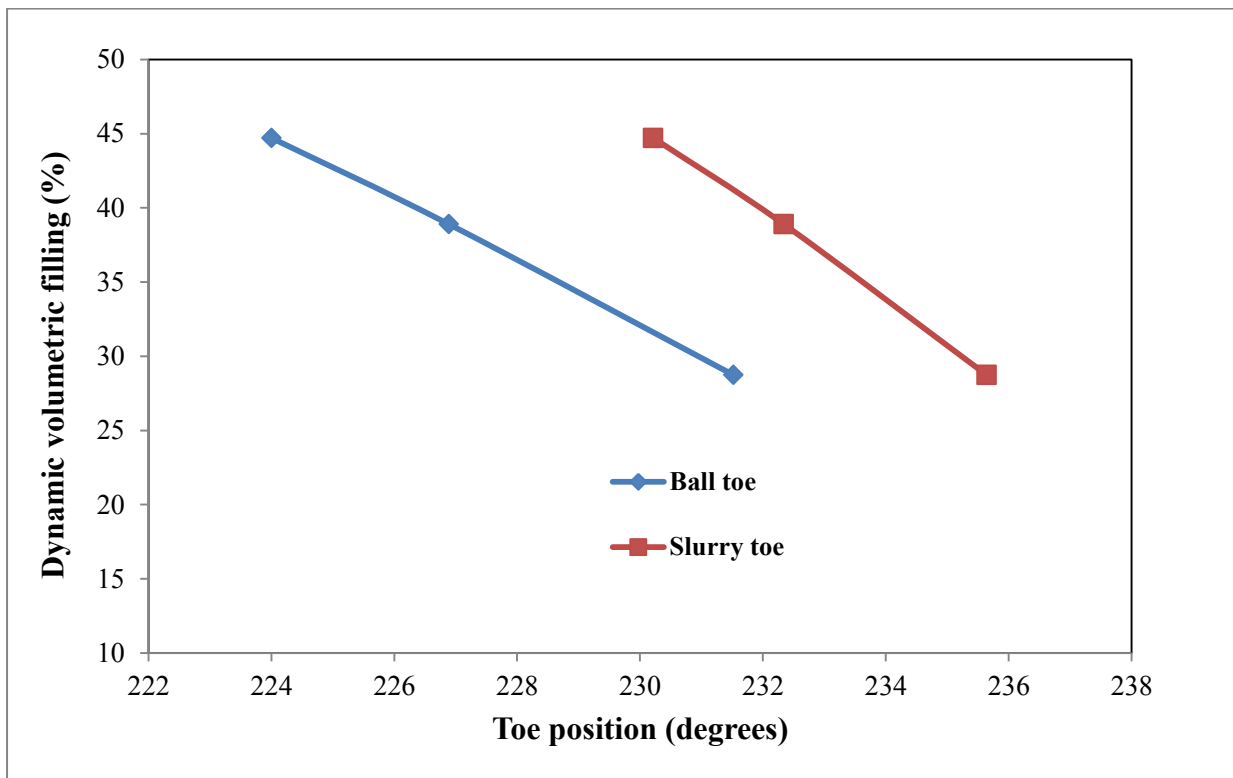


Figure 6:10-The dynamic volumetric filling with the toe angle at 75%

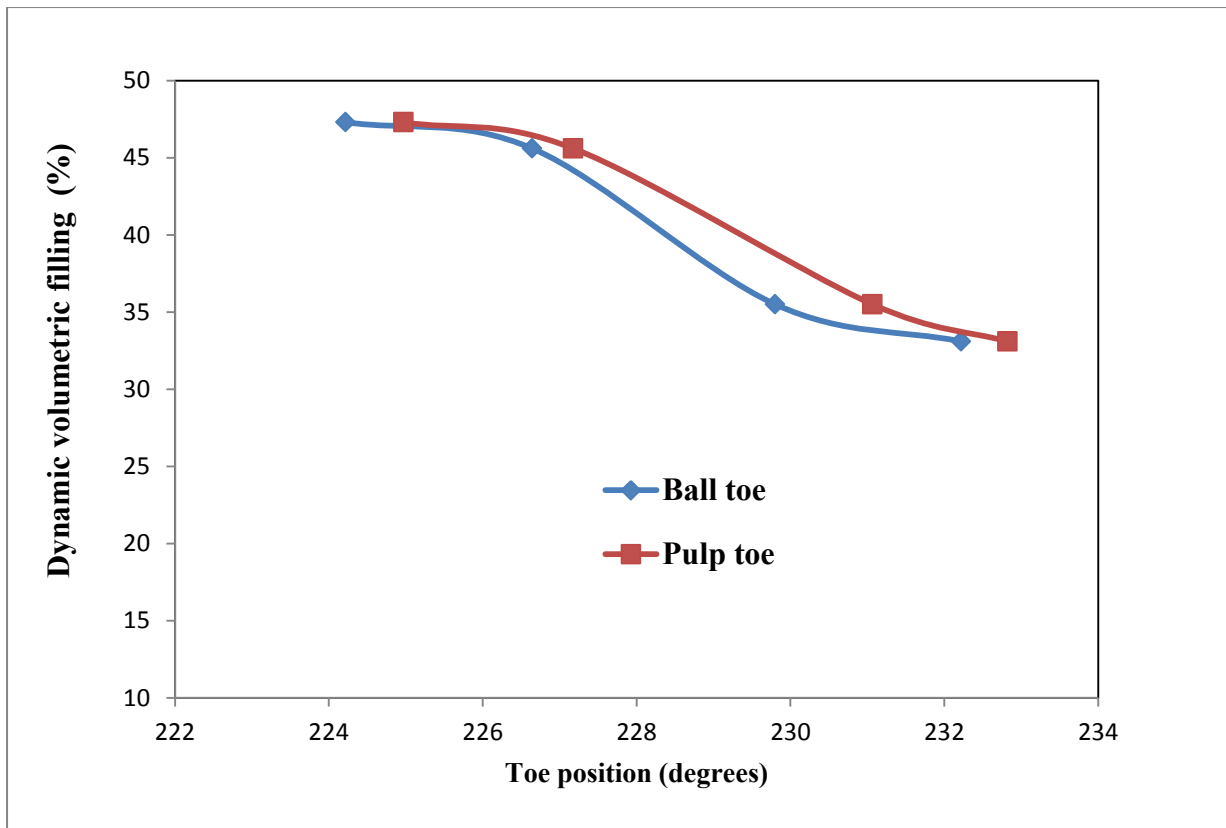


Figure 6:11- The dynamic volumetric filling with the toe angle at 85% critical speed

6.2.4 The relationship between toe and shoulder angles and mill power draw

The relationships between the toe and shoulder positions of the slurry and ball load on the power draw were investigated. The toe and shoulder angles reported here were measured using the Sensomag device on the Magotteaux Pilot Plant mill. Figure 6:12 and Figure 6:13 show the variation of mill power draw with the shoulder angles of both the slurry and ball load at 75% and 85% critical speed, respectively. Figure 6:14 and Figure 6:15 show the variation of mill power draw and toe angles for the ball and slurry load at 75 and 85% of the critical speed. It can be observed that the toe and shoulder angle for the media and slurry load influences the net mill power. Conversely, the power draw increased as the shoulder angles for both the ball and slurry increased. The increase in the shoulder angle indicated the rise in the load level in the mill and hence more power was needed to lift the charge along the rising side. The trend at the toe angle for the ball and slurry is different. The power draw decreased with an increase in the toe angle for the ball and slurry load. It has been assumed that the charge cataracts onto the mill shell which does not contribute to the power draw by the mill (Moys *et al.*, 1985; Kiangi *et al.*, 2005, 2011).

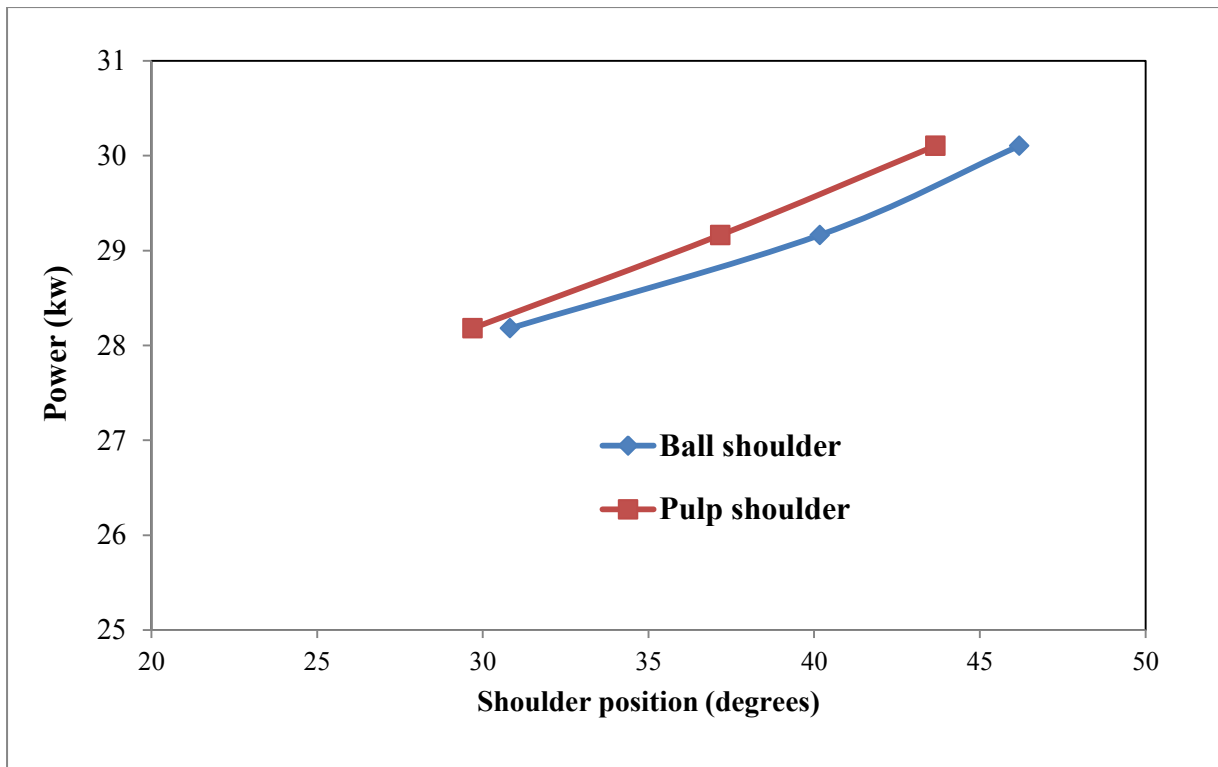


Figure 6:12-The relationship between power draw and shoulder positions for the ball and slurry at 75% critical speed

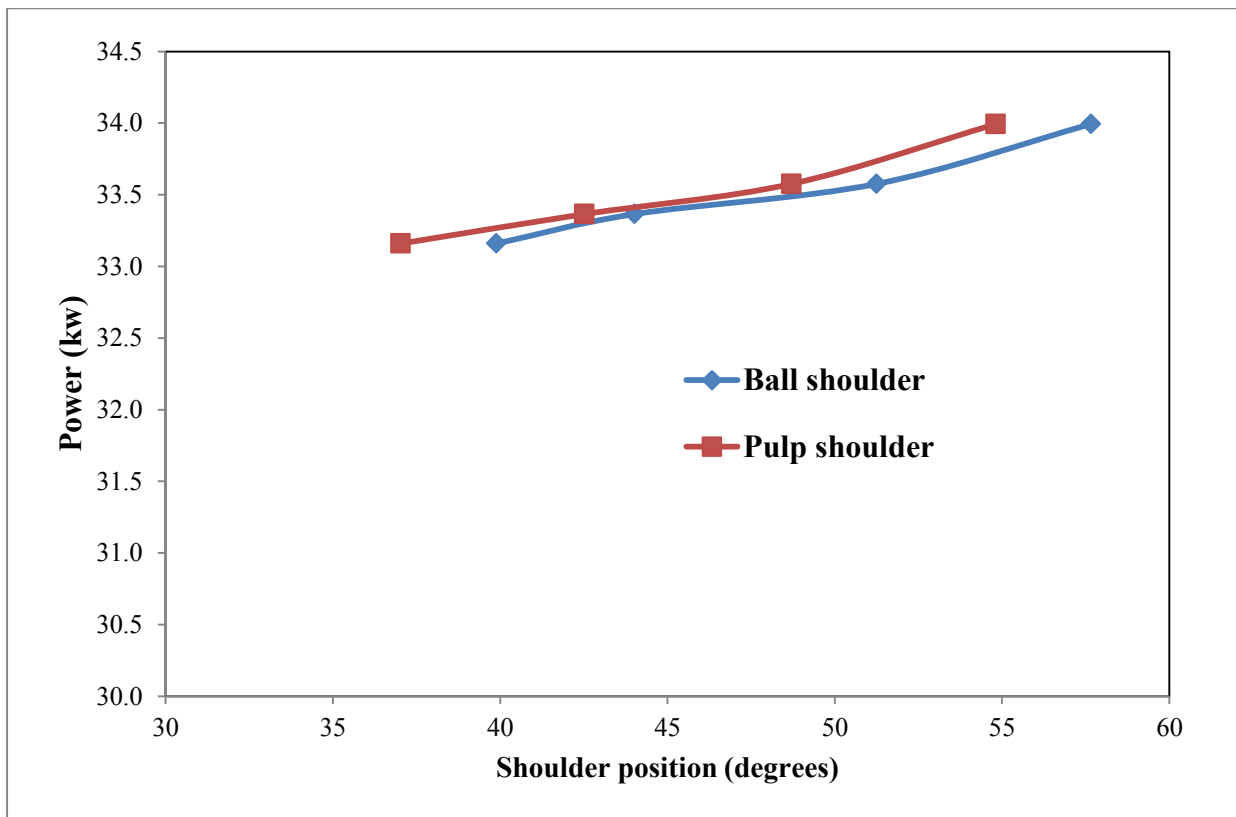


Figure 6:13-The relationship between power draw and shoulder positions for the ball and slurry at 85% critical speed

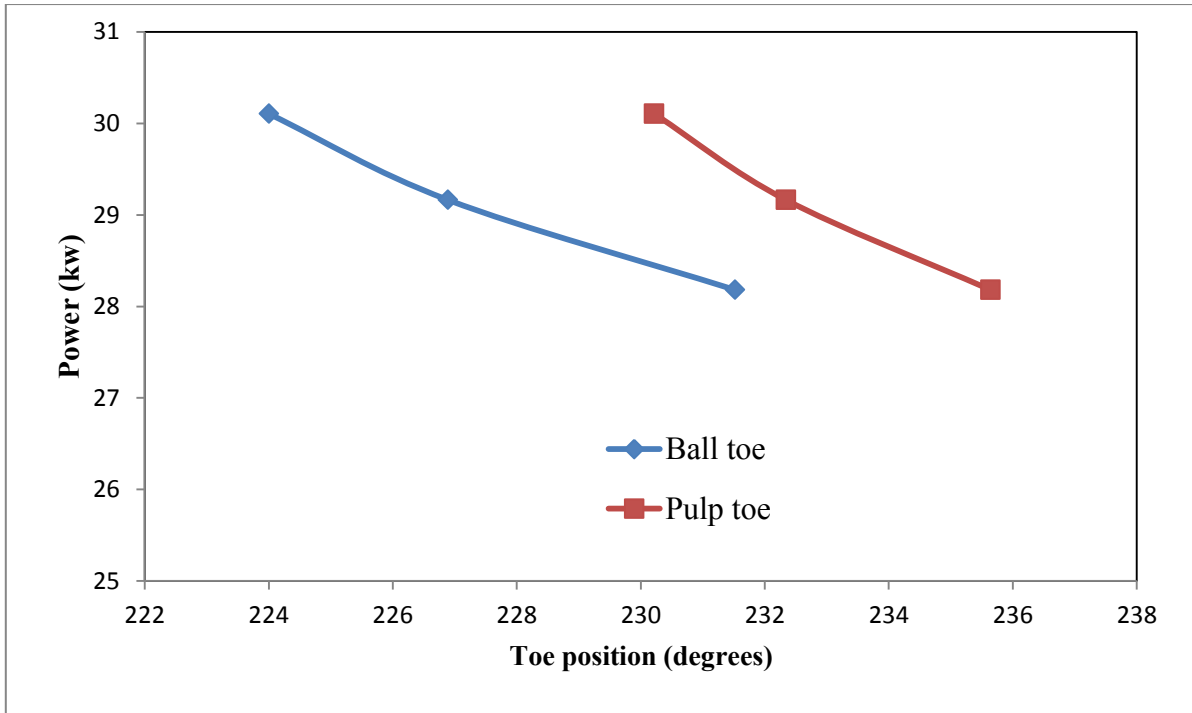


Figure 6:14-The relationship between power draw and toe positions for the ball and slurry at 75% critical speed

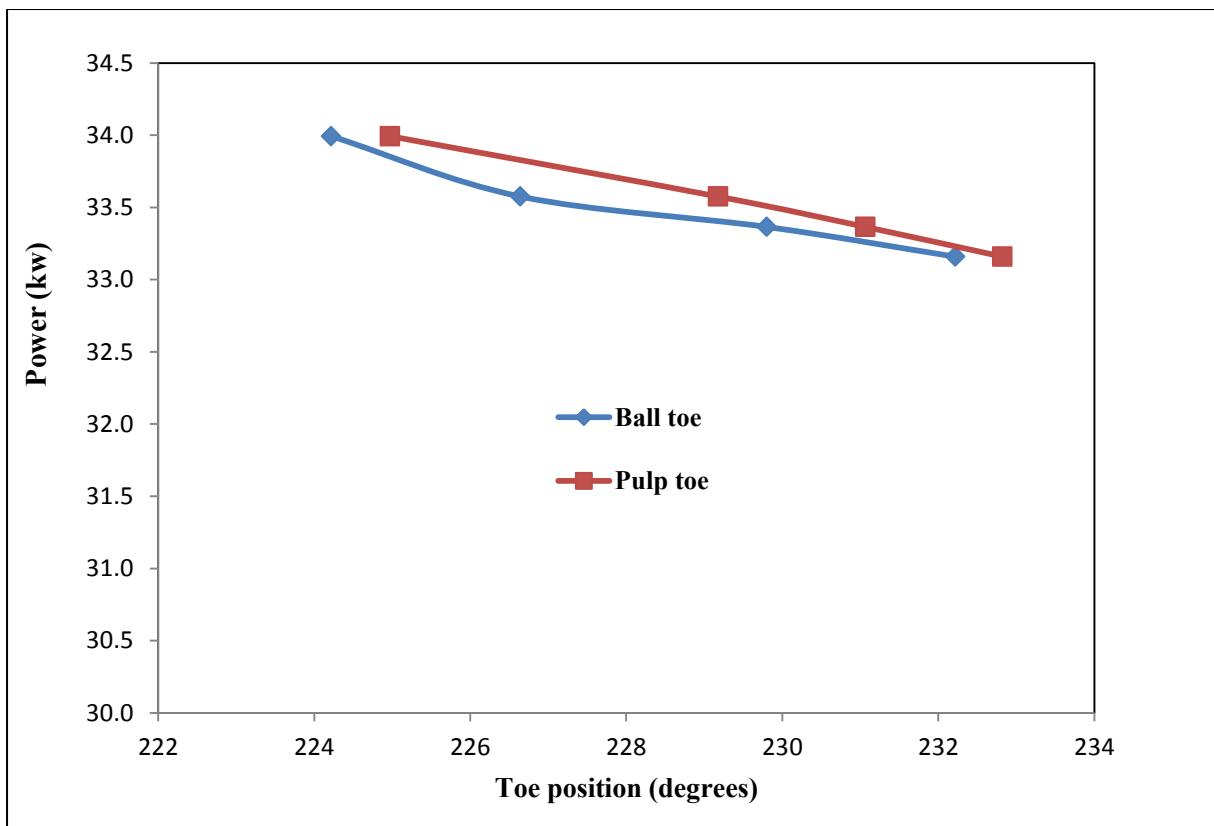


Figure 6:15-The relationship between power draw and toe positions for the ball and slurry at 85% critical speed

6.2.5 The relationship between percentage passing 75 μ m, toe and shoulder angle

This section discusses the grind curve methodology for the data obtained from the experiment conducted at the pilot plant. The variation of the material passing percentage 75 μ m with the slurry shoulder angle for the ball and slurry for 75 and 85% critical speed are shown in Figure 6:16 and Figure 6:17 and, respectively. It can be seen that the grind increased with an increase in the shoulder angle. The reason is that the coarse material in the charge is broken by impact breakage. As the shoulder angle increases, the drop height for the charge from the shoulder region decreases. This reduces the impact force of the grinding medium, which decreases the amount of fines materials in the product (Wills, 2006).

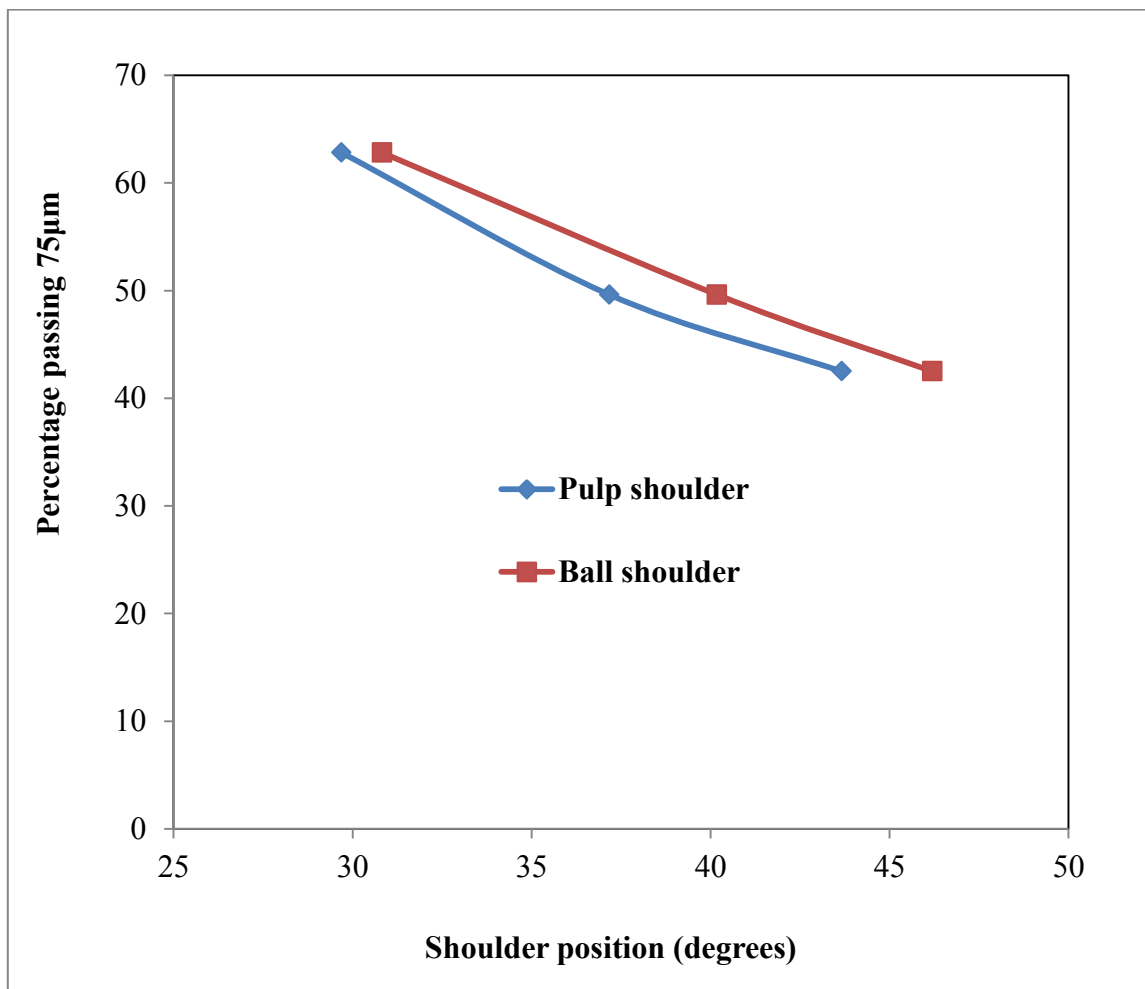


Figure 6:16-The relationship between 75 μ m and shoulder position for the ball and slurry load at 75% critical speed

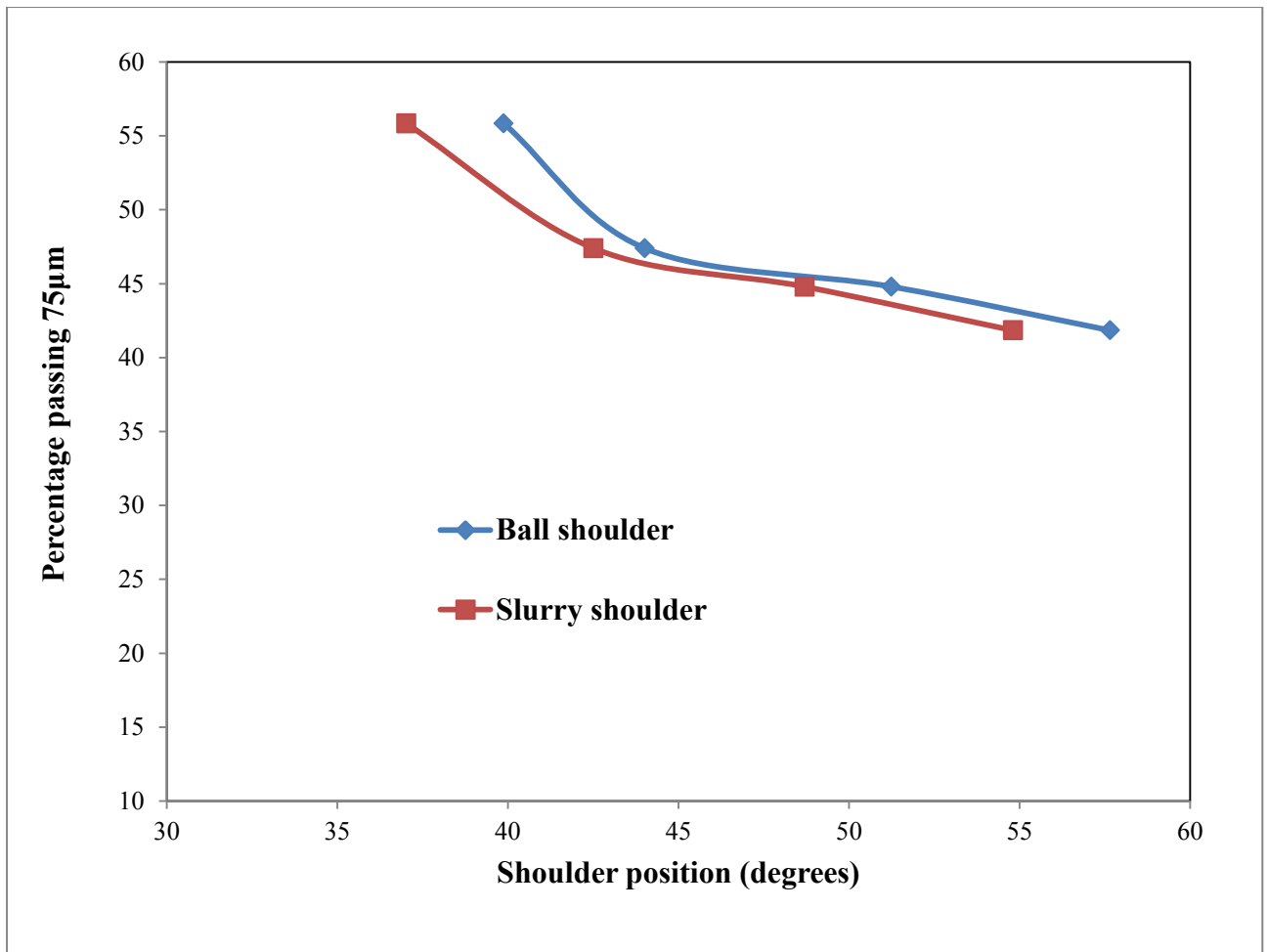


Figure 6:17-The relationship between 75µm and shoulder position for the ball and slurry load at 85% critical speed

Figure 6:18 and Figure 6:19 show the variation of material passing percentage 75µm with toe angle for the 75 and 85% critical speed, respectively. It can be seen that increasing the toe position made the grind coarser. The reason is that the coarse material in the charge is mainly broken by impact breakage, which reduces due to the decreased in the drop height from the shoulder position to the toe position as the volumetric filling increases and therefore reducing the breakage rate (Powell *et al.*, 2006, 2009, and 2012). As a result, the impact force on the charge increases. Figure 6:20 shows the particle size distribution of the mill discharge products and the feed when the mill was operated at 85% of the critical speed. It can be seen that the grind coarsened as feed rate increased. As the feed rate increased, the collision energy drops due to a decrease in the free space for particle collisions (Austin *et al.*, 1987; Spencer *et al.*, 1999). The toe and shoulder positions obtained from the Sensomag are very important information that can facilitate better understanding and control of the milling

process. The toe and shoulder positions can be used to calculate the volumetric filling of the mill charge.

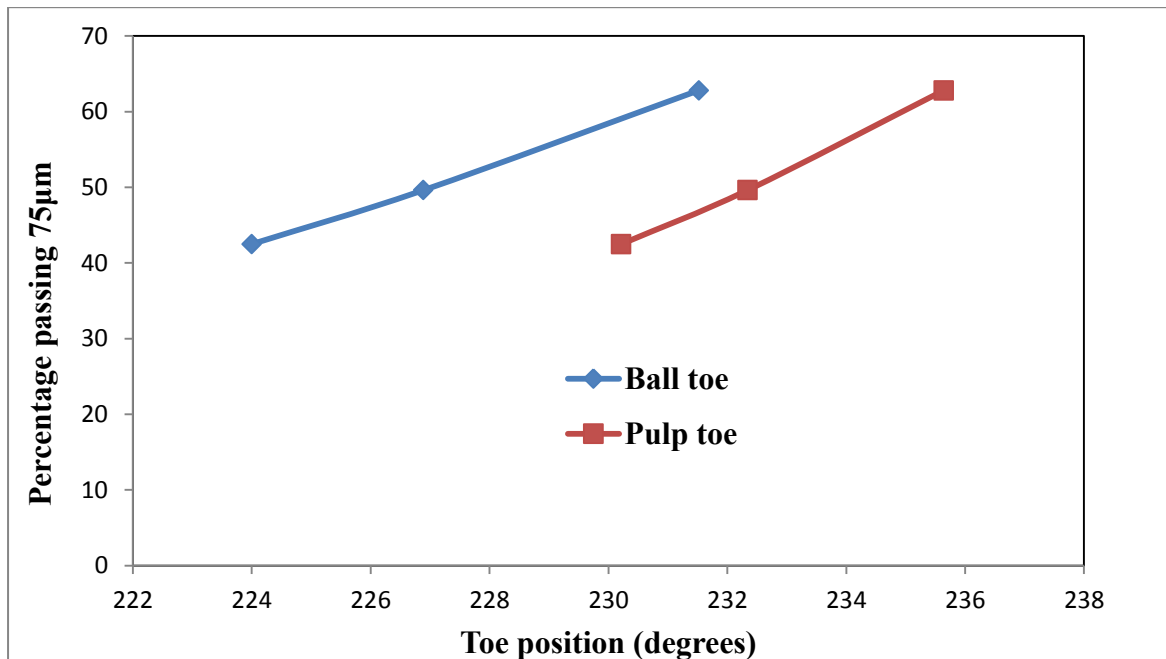


Figure 6:18-The relationship between 75µm and toe position for the ball and slurry load at 85% critical speed

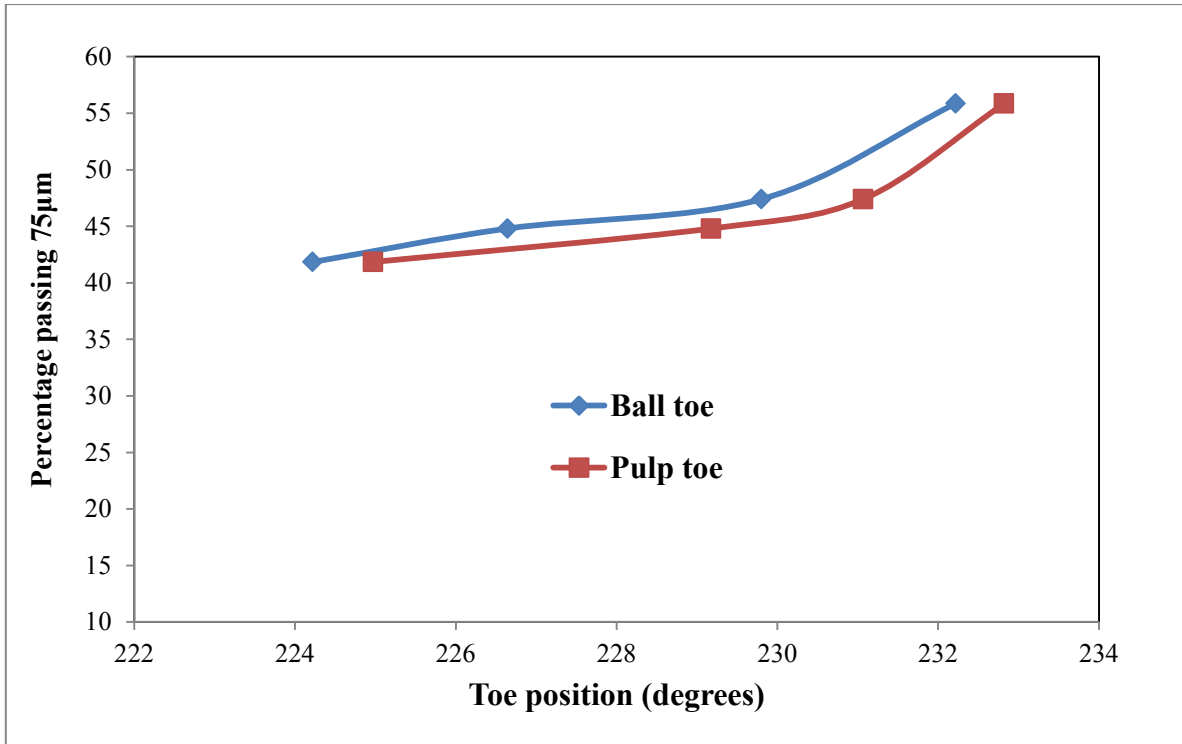


Figure 6:19- The relationship between 75µm and toe position for the ball and slurry load at 85% critical speed

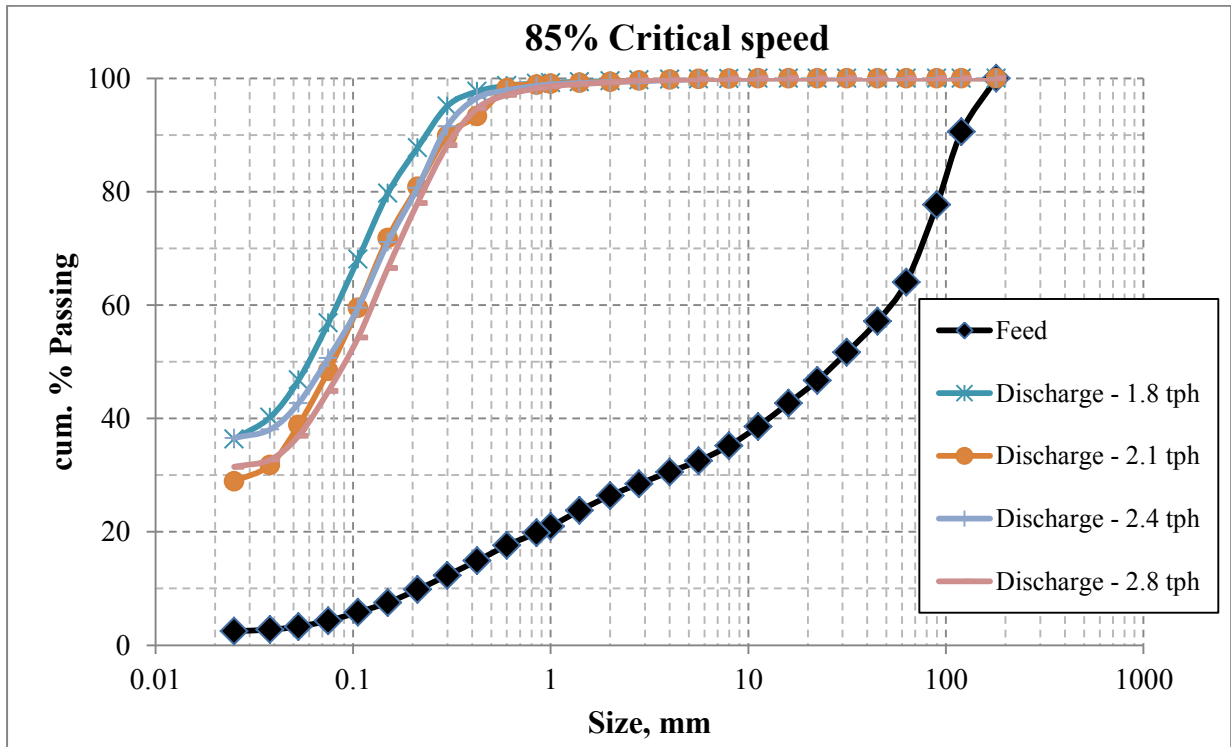


Figure 6:20- Particle size distribution of the feed and the mill discharge product at varying feed rate

6.3 The effect of ball filling on the toe, shoulder angle and mill performance

This section presents the results obtained from test performed by varying the ball filling degree. The objective was to investigate the effect of ball load on the toe and shoulder position of the mill charge. The experiments were conducted at 75% critical speed and 75% solids, which was constant throughout. Table shows the toe and shoulder positions estimated from the charge by the Sensomag. The calculated dynamic volumetric filling was estimated from the toe and shoulder angles of the mill charge using Equation 2-1. It can be seen that the toe angles for the ball and slurry increased with an increase in the feed rate for each ball filling degree. The shoulder positions for the slurry and the ball load increased with varying feed rate.

Table 6:5-Results obtained from second experimental campaign

Ball load (%)	Feed rate (kg/hr)	Ball toe (°)	Ball shoulder (°)	Slurry toe (°)	Slurry Shoulder (°)	Dynamic volumetric filling (%)
15	1500	149.7	274.8	160.4	270.6	21.4
15	2000	146.4	280.4	156.8	295.7	23.4
15	2500	148.9	287.1	148.2	285.5	27.5
15	2750	146.6	290.8	145.7	288.1	28.5
15	3000	146.1	293.7	143.7	290.0	30.4
20	2000	142.5	290.3	144.8	285.6	27.6
20	2500	144.8	295.6	142.7	291.2	30.3
20	3000	139.4	297.4	142.0	292.9	33.0
20	3500	138.7	316.4	138.0	312.7	44.3
20	3250	142.0	303.9	144.8	298.6	33.9
23.3	2000	137.2	292.2	140.6	272.9	29.2
23.3	2500	135.7	297.4	138.1	283.0	31.0
23.3	3000	133.4	301.3	136.3	294.7	33.3
23.3	3400	131.1	303.9	133.1	299.5	37.3
26	2000	140.8	305.8	144.1	299.3	33.2
26	2500	138.4	308.6	141.2	305.6	35.3
26	3000	136.1	311.7	138.3	310.3	37.5
26	3300	134.8	314.3	137.0	317.9	39.6

6.3.1 Relationship between dynamic volumetric filling, toe and shoulder angle

This section discusses the effect of dynamic volumetric filling on the toe and shoulder angles for different ball load tests. Figure 6:21 and Figure 6:22 show the relationship between the

dynamic volumetric filling and the shoulder angle at 23.3% and 26% ball load, respectively. It can be seen that the shoulder angle varied with dynamic volumetric filling. As the mill filled up the shoulder angles increased for the ball and slurry due to the rise in the charge level in the mill.

Figure 6:23 and Figure 6:24 show the relationship between the dynamic volumetric filling and the toe position of the ball and slurry load, respectively. The toe position for the ball and slurry load decreased as volumetric filling increased since the charge occupies higher volume in the mill. It can be seen that the toe position for a 26% ball load was higher than that for a 23.3% ball load. For a 23.3% ball load the charge is thrown off at a greater distance from the bulk load and impact on the mill shell at a lower angular displacement than the 26% ball load.

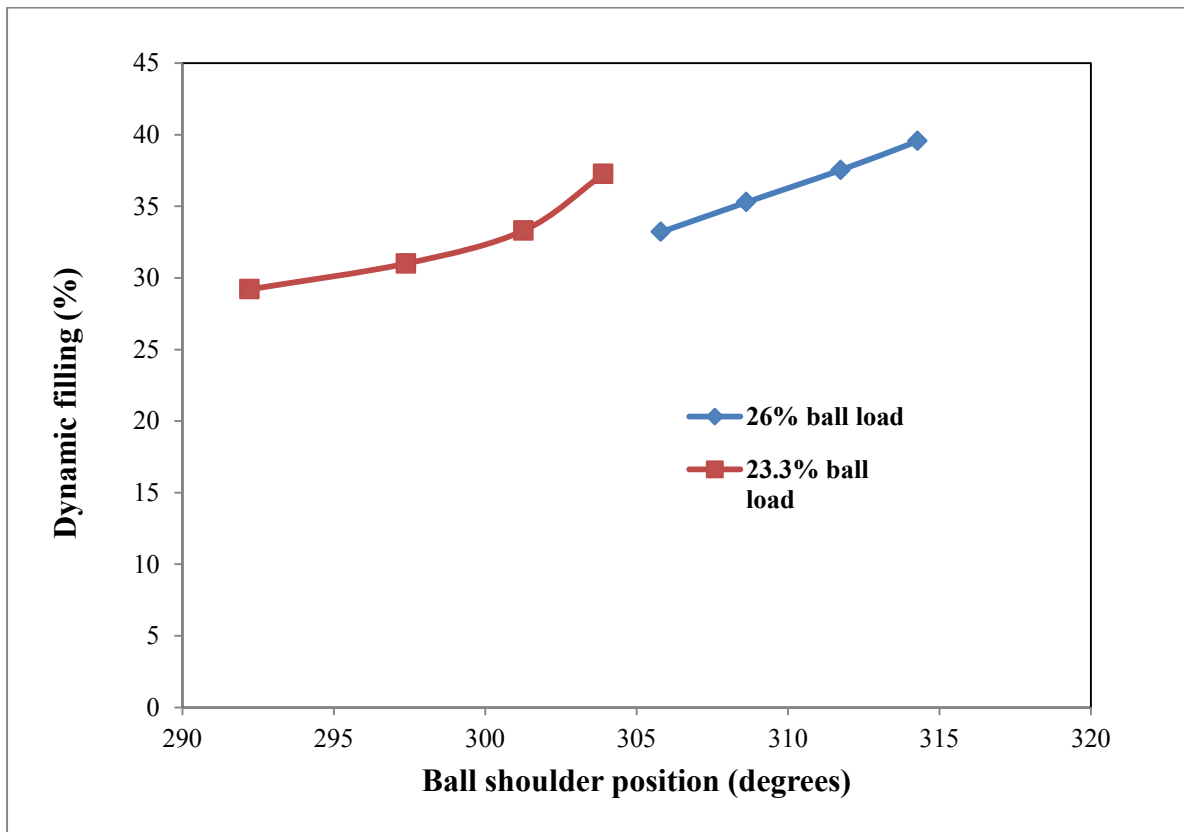


Figure 6:21-Dynamic mill filling and ball shoulder position at varying ball load

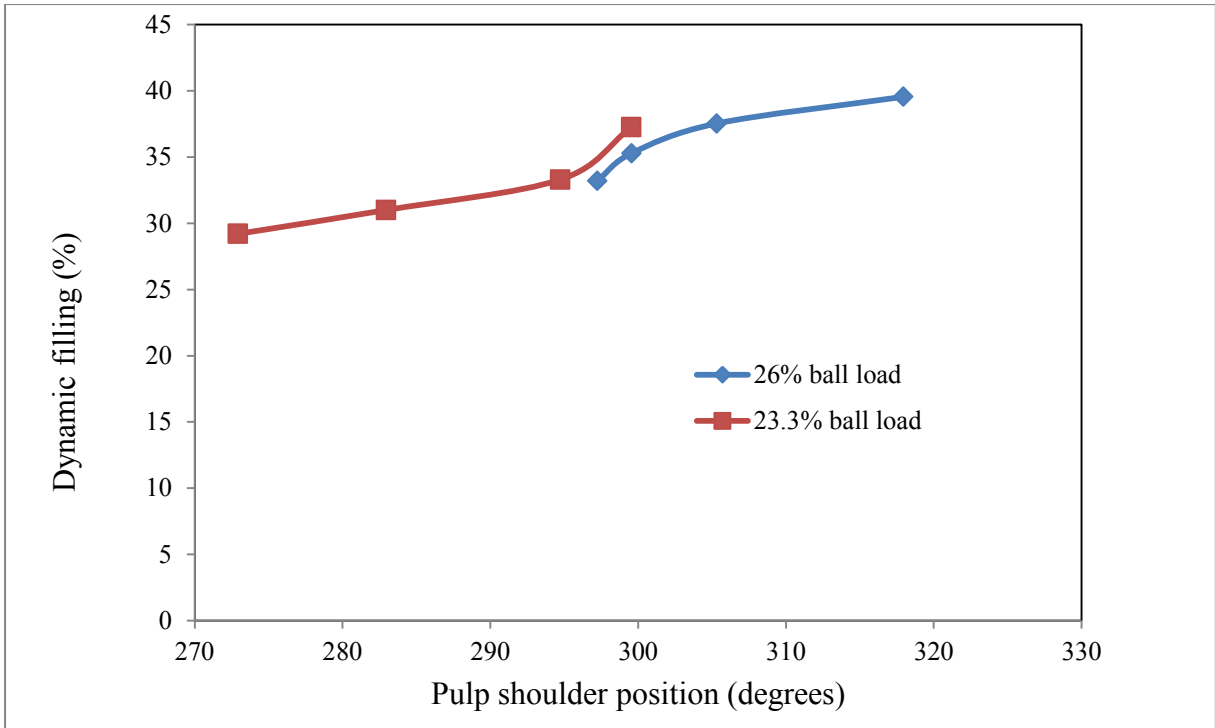


Figure 6:22-Dynamic mill filling and slurry shoulder position at varying ball load

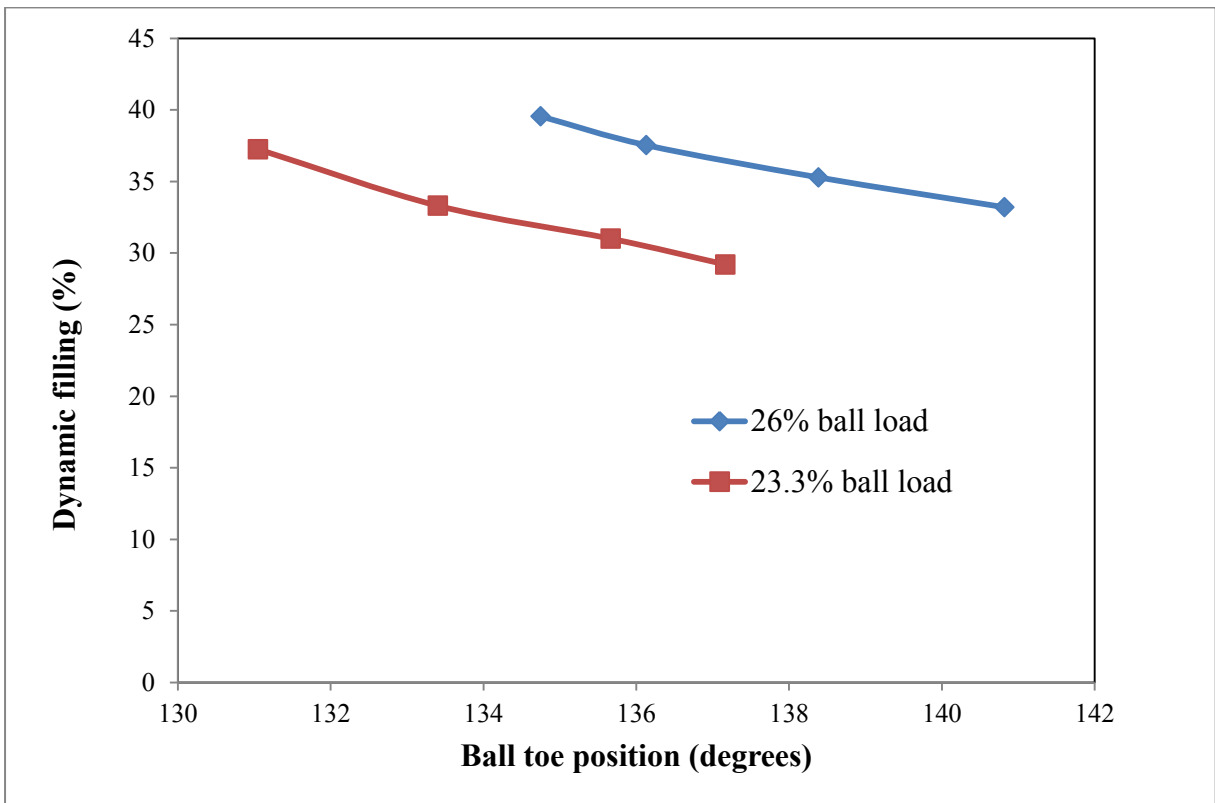


Figure 6:23-Dynamic mill filling and ball toe position at varying ball load

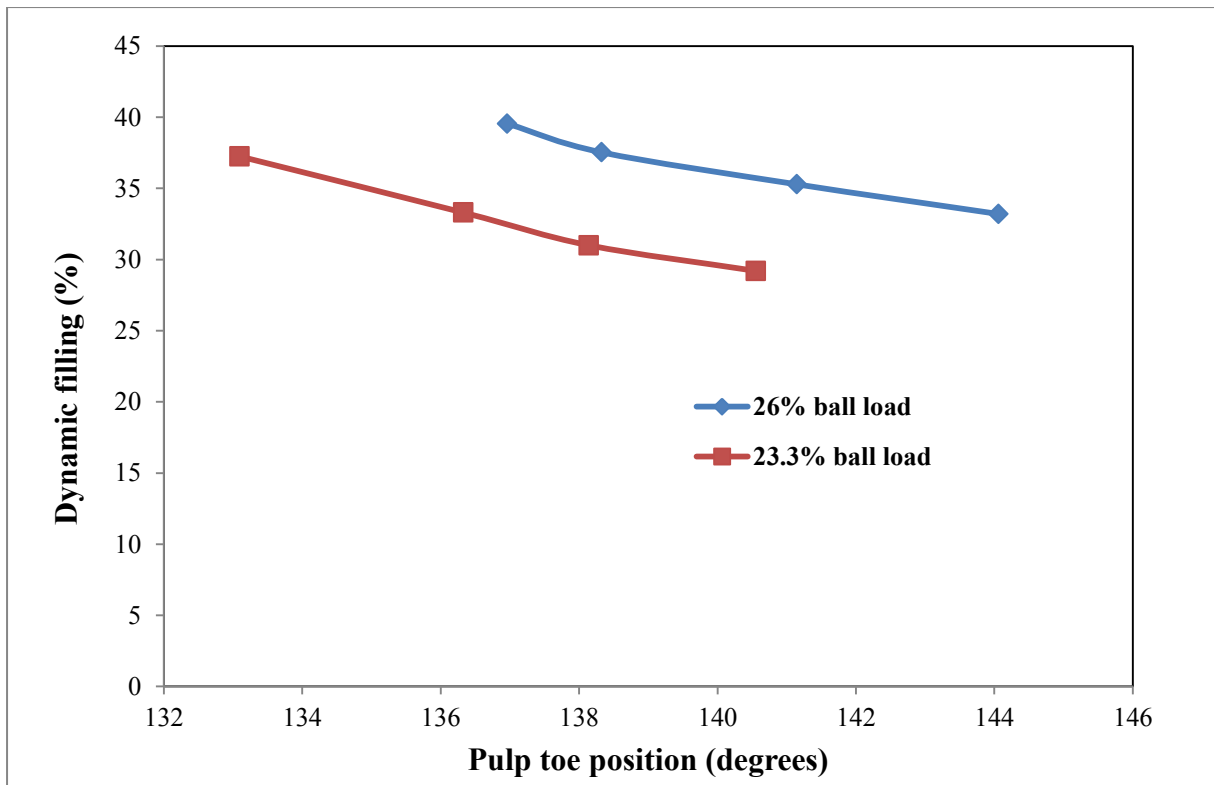


Figure 6:24-Dynamic mill filling and slurry toe angle at varying ball load

6.3.2 The relationship between ball load and the material passing percentage 75 μ m

A grind curve methodology was applied to the data obtained from the Magotteaux pilot plant for the test work where the ball load was varied. Figure 6:25 show the variation percentage of materials passing 75 μ m with dynamic mill filling at 23.3% and 26% ball load. The operating variables such as speed and slurry percent solids were kept constant while varying ball-filling degree. The grind curve used the dynamic volumetric filling measured using the toe and shoulder positions obtained from the Sensomag. It can be observed that the percentage passing 75 μ m decreased as the dynamic volumetric filling increased for both loads.

Some authors have proposed that as mill filling increases, the grind is coarser because the effective collision zones between the steel balls are already saturated with slurry (Austin *et al.*, 1984). The grind at 26% ball load was finer than that at 23.3% ball load. This was because a 26% ball load had increased contact of steel balls to charge compared to that of a 23.3% ball filling. Unlike SAG mills, increasing ball load in RoM ball mills results in better grind as a result of increased contacts of steel on steel and the slurry (Powell *et al.*, 2006, 2010, and 2012).

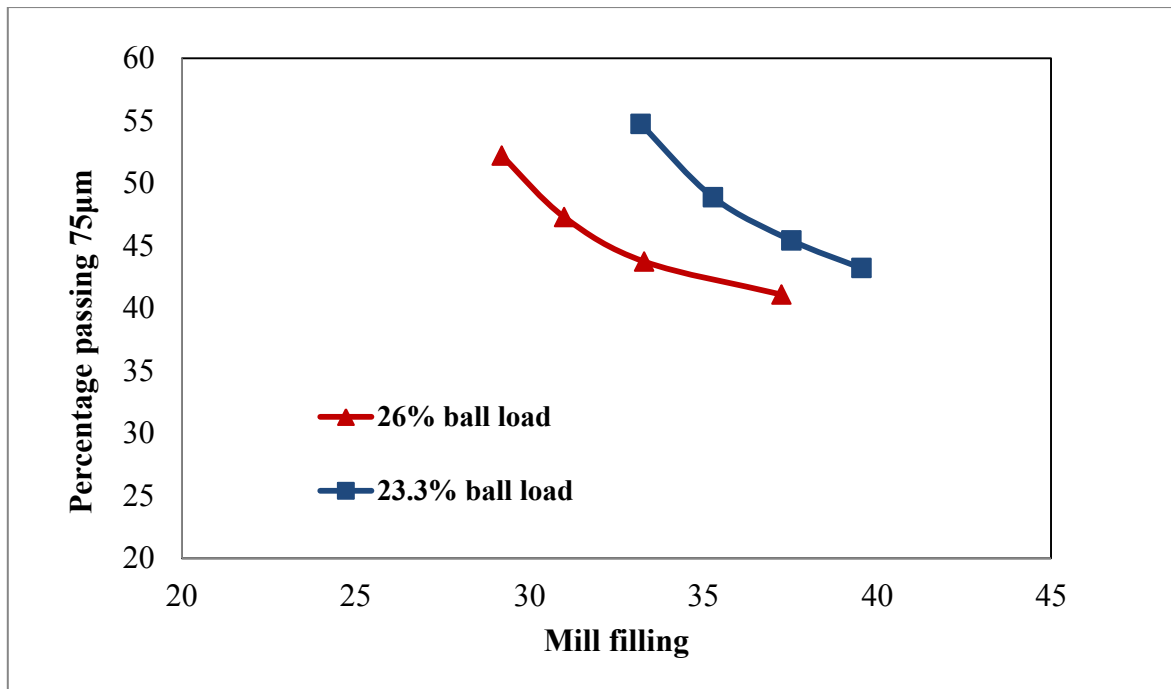


Figure 6:25-Variation of mill grind as a function of varying ball load

Figure 6:26 shows the variation of percentage of material passing 75µm with shoulder and toe position for slurry load. The toe and shoulder positions are the input in the dynamic filling calculations. It can be seen that as the grind coarsened as the shoulder position for the slurry increased. This was due to reduced contact of the steel balls with the slurry as the mill filled up.

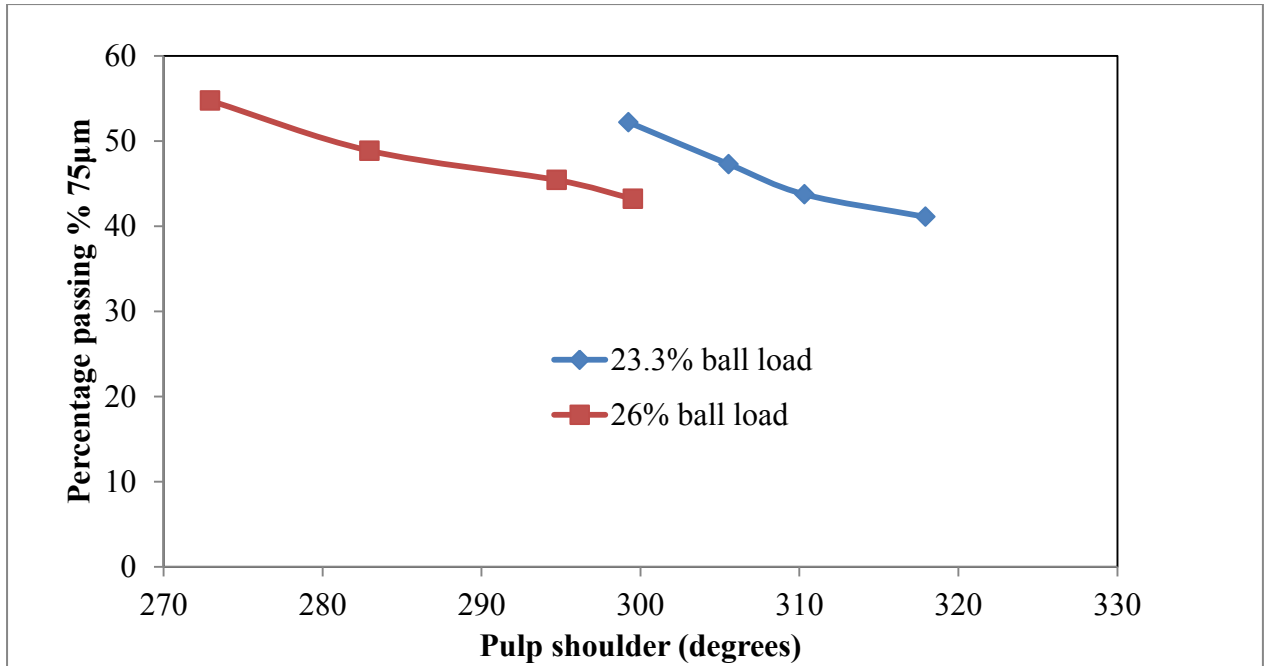


Figure 6:26- Relationship between grind and slurry shoulder at 23% and 26% ball load

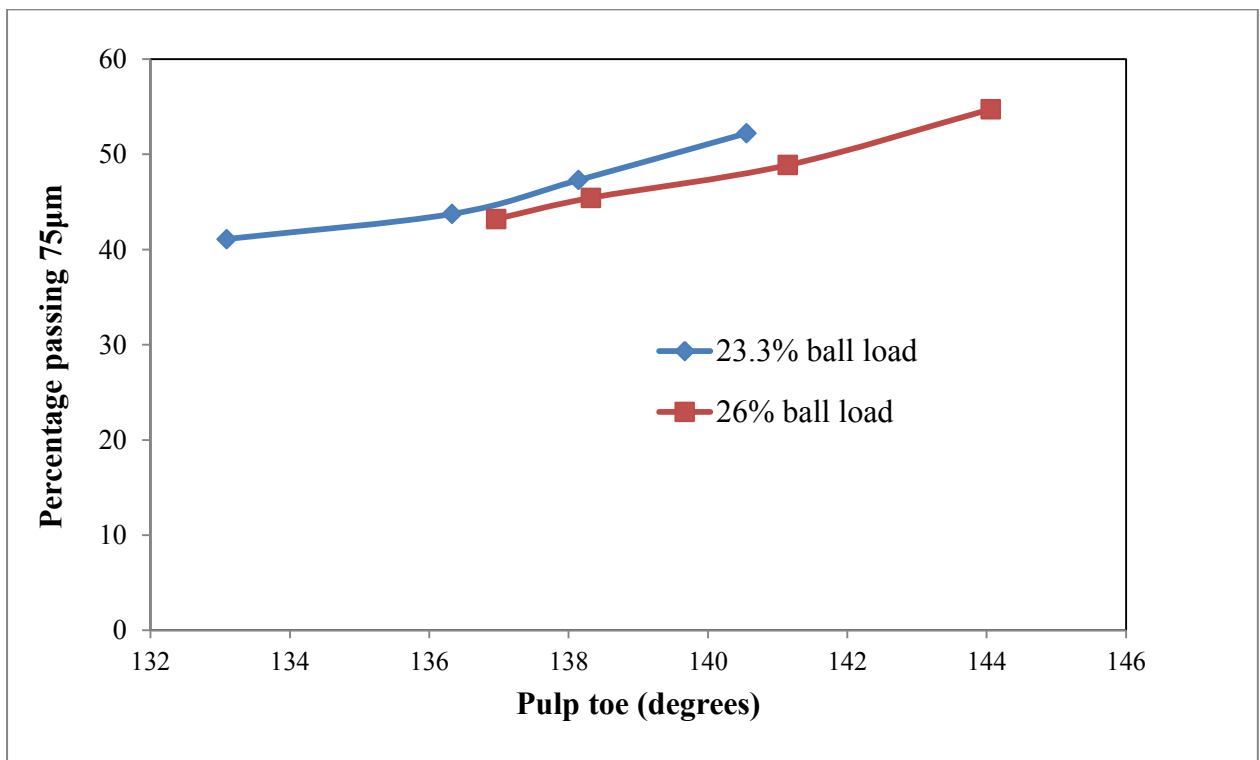


Figure 6:27- Relationship between grind and slurry toe at 23% and 26% ball load

6.4 Conclusion

The Sensomag provided the shoulder and toe positions of the mill charge and these were used to calculate the dynamic filling. The shoulder angle for the media and slurry increased with an increase in the dynamic volumetric filling. While the toe angle decreased with an increase in the dynamic volumetric filling. The highest shoulder position and lowest toe angle gave highest volumetric filling. The power draw varied with changes in the toe and shoulder positions of the mill charge. That is why these were key inputs in power model developed (Liddell, 1986; Morrell, 1993). The dynamic volumetric filling from the Sensomag output can be used for monitoring the performance of the tumbling mill. The grind got finer as the shoulder position increased, and the grind coarsened with increasing toe position.

CHAPTER SEVEN: OBSERVATIONS AND CONCLUSIONS

This study used the CSIRO acoustic and the Sensomag sensors for continuous monitoring of the tumbling mill charge at industrial and pilot scale, respectively. The sensors are used to determine the toe and shoulder positions of the mill charge. The Sensomag pilot test work investigated the influence of mill speed and ball filling degrees on the toe and shoulder positions. The acoustic sensor was used to investigate the effect of feed rate on the toe and shoulder positions. The toe and shoulder positions measured were used to calculate the dynamic volumetric filling. The corresponding static mill filling were calculated from physical measurements of the charge after each crash stop. A summary of observations and conclusions that were drawn from the study are presented in this chapter.

7.1 Summary of observations from inductive proximity and conductive sensor at the pilot plant scale

The test work performed at the pilot plant has shown that when the mill was operated at 75%, 80% and 85% of the critical speed and range ball loads shows that the Sensomag sensor can be used to estimate the toe and shoulder angles of the media and slurry.

- The dynamic volumetric filling for the slurry and the ball load was estimated (using the Morrell filling equation). The corresponding static mill filling was calculated from the crash stop. An average difference between static and dynamic volumetric filling of 2-8% was observed.
- The study performed indicated that the toe and shoulder angles for the media and slurry load vary with mill speeds in the range of 75%, 80%, and 85% critical speeds. The shoulder angles increased with an increase in the mill speed (75%-85% critical), due to the expansion in the charge. The toe angles decreased with an increase in the mill speeds possibly due to the cataracting and centrifuging of the charge on the mill shell.
- It was found that at the shoulder region, the trajectory of the slurry load is higher than that of the ball load. This trend was similar for 75% and 85% of the critical speed. This is possible since the rocks were lighter than the steel balls and hence were lifted to higher levels than the steel balls.

7.1.2 Main Conclusions

The key conclusions from the inductive proximity and conductive sensor at the pilot plant scale work are as follows.

- The test work performed in this study covered a wide range of conditions and have shown that the Sensomag sensor can be used to determine the toe and shoulder angles of the ball and slurry filling rates.
- It was found that the dynamic volumetric filling could be calculated from the toe and shoulder positions using the Morrell filling equation. A comparison between the static (measured) and dynamic volumetric filling showed a difference of 5.8%.
- It was observed that the toe angles for the slurry and ball load followed a similar trend for the 75% and 85% critical speed, respectively. The slurry toe was consistently at lower angles than the ball toe because the trajectory of the slurry was higher than that of the balls.
- The Sensomag can detect the expected changes in the toe and shoulder angles with changes in the mill speed. It was consistently found that the toe for the media and slurry decreased with an increase in the mill speed.

7.2 Summary of observations from acoustic sensor for the industrial scale test work

The acoustic sensor was used to measure the vibration signal emitted from the RoM ball mill shell by varying the feed rate at a ball load of 28%. The band power signal, toe, and shoulder angles of the mill charge were estimated from the vibration signal. The following observations were made.

- An inverse relationship was observed between the total vibration power and mill mass. The total vibration power decreased with increased in mill mass. The highest total vibration power was observed at low mill mass (~819 tons) while the lowest total vibration power occurred at high mill mass (~ 890 tons). The vibration power is used to estimate the toe and shoulder angles of the charge.
- The dynamic ball filling was calculated (using the Morrell filling equation) from the toe and shoulder angles obtained during the grind-out. The corresponding static mill filling was determined after mill grind-out. A difference of 4-8% was observed between the static and dynamic ball filling. The dynamic volumetric filling was calculated using the same method as the ball filling from the toe and shoulder

positions measured using the acoustic signals for the range of feed rates during the test work.

- A direct relationship was observed between dynamic volumetric filling and shoulder angles of the mill charge and inverse relationship was observed between the mill filling and the toe angles for the range of feed rates covered in the test work.

7.2.1 Conclusions

The key conclusions from the acoustic sensor are as follows:

- The observations indicated that the CSIRO acoustic sensor can be used to determine the toe and shoulder angles of the mill charge with 6.5% accuracy.
- The changes in the grind observed on mill products (materials passing 75 μ m) at varying volumetric filling, showed that there was an inverse relationship between volumetric filling and grind.
- The dynamic volumetric filling calculated from the toe and shoulder angles correlate well with corresponding static measurements.

REFERENCES

- AGRAWALA, S., RAJAMANI, R., SONGFACK, P. and MISHRA, B., 1997. Mechanics of media motion in tumbling mills with 3D discrete element method. *Minerals Engineering*, 10(2), pp. 215-227.
- ALATALO, J., PÅLSSON, B. and TANO, K., 2011. Influence of pebble mill operating conditions on measurements with an in-mill sensor. *Minerals & Metallurgical Processing*, 28(4).
- ALDRICH, C. and THERON, D., 2000. Acoustic estimation of the particle size distributions of sulphide ores in a laboratory ball mill. *Journal of the South African Institute of Mining and Metallurgy(South Africa)*, 100(4), pp. 243-248.
- APELT, T., ASPREY, S. and THORNHILL, N., 2002. Inferential measurement of SAG mill parameters III: inferential models. *Minerals Engineering*, 15(12), pp. 1055-1071.
- APELT, T., ASPREY, S. and THORNHILL, N., 2001. Inferential measurement of SAG mill parameters. *Minerals Engineering*, 14(6), pp. 575-591.
- AUSTIN, L., KLIMPEL, R. and LUCKIE, P., 1984. Process Engineering of Size Reduction: Ball Milling. Society of Mining Engineers of the American Institute of Mining, Metallurgical, and Petroleum engineers. *Inc, New York, NY*, , pp. 112.
- AUSTIN, L., MENACHO, J. and PEARCY, F., 1987. A general model for semi-autogenous and autogenous milling, *Proceedings of the 20th International Symposium on the Application of Mathematics and Computers in the Mineral Industries 1987*, pp. 107-126.
- BEHERA, B., MISHRA, B. and MURTY, C., 2007. Experimental analysis of charge dynamics in tumbling mills by vibration signature technique. *Minerals Engineering*, 20(1), pp. 84-91.
- CAMPBELL, J., SPENCER, S., SUTHERLAND, D., ROWLANDS, T., WELLER, K., CLEARY, P. and HINDE, A., 2001. SAG mill monitoring using surface vibrations. *Proceedings International autogenous and semiautogenous grinding technology*, , pp. 373-385.
- CAMPBELL, J., HOLMES, R., SPENCER, S., SHARP, V., DAVEY, K., BARKER, D. and PHILLIPS, P., 2003. The collection and analysis of single sensor surface vibration data to estimate operating conditions in pilot-scale and production-scale AG/SAG mills, *Proceedings: XXII International Mineral Processing Congress 2003*, pp. 280-288.
- CLEARY, P.W., 1998. Predicting charge motion, power draw, segregation and wear in ball mills using discrete element methods. *Minerals Engineering*, 11(11), pp. 1061-1080.
- CLEARY, P., 2001. Recent advances in DEM modelling of tumbling mills. *Minerals Engineering*, 14(10), pp. 1295-1319.
- CUNDALL, P.A. and STRACK, O.D., 1979. A discrete numerical model for granular assemblies. *Geotechnique*, 29(1), pp. 47-65.

- DAS, S.P., DAS, D.P., BEHERA, S.K. and MISHRA, B.K., 2011. Interpretation of mill vibration signal via wireless sensing. *Minerals Engineering*, 24(3), pp. 245-251.
- DE HAAS, B., 2008. *Method for evaluating the filling rate of a tubular rotary ball mill and device therefor*, .
- DENIZ, V. and ONUR, T., 2002. Investigation of the breakage kinetics of pumice samples as dependent on powder filling in a ball mill. *International Journal of Mineral Processing*, 67(1), pp. 71-78.
- DUPONT, J. and VIEN, A., 2001. Direct measurement and control of SAG volumetric loads using embedded sensors, *Preprints of the 2001 SME Annual Meeting 2001*, pp. 01-5.
- GIORDANO, M., CONDELLI, L. and NICOLAIS, L., 1999. Acoustic emission wave propagation in a viscoelastic plate. *Composites Science and Technology*, 59(11), pp. 1735-1743.
- GUGEL, K., PALACIOS, G., RAMIREZ, J. and PARRA, M., 2003. Improving ball mill control with modern tools based on digital signal processing (DSP) technology, *Cement Industry Technical Conference, 2003. Conference Record. IEEE-IAS/PCA 2003*, IEEE, pp. 311-318.
- HOSSEINI, P., MARTINS, S., MARTIN, T., RADZISZEWSKI, P. and BOYER, F., 2011. Acoustic emissions simulation of tumbling mills using charge dynamics. *Minerals Engineering*, 24(13), pp. 1440-1447.
- HOU, R., HUNT, A. and WILLIAMS, R., 1998. Acoustic monitoring of hydrocyclone performance. *Minerals Engineering*, 11(11), pp. 1047-1059.
- HUANG, P., JIA, M. and ZHONG, B., 2010. New Method to Measure the Fill Level of the Ball Mill I—Theoretical Analysis and DEM Simulation. *Chinese Journal of Mechanical Engineering*, (4), pp. 460.
- HUANG, P., JIA, M. and ZHONG, B., 2009. Investigation on measuring the fill level of an industrial ball mill based on the vibration characteristics of the mill shell. *Minerals Engineering*, 22(14), pp. 1200-1208.
- KAWATRA, S.K., 2006. *Advances in comminution*. SME.
- KESHAV, P., HAAS, B.D., CLERMONT, B., MAINZA, A. and MOYS, M., 2011. Optimisation of the secondary ball mill using an on-line ball and slurry load sensor—The Sensomag. *Minerals Engineering*, 24(3), pp. 325-334.
- KIANGI, K.K. and MOYS, M.H., 2006. Measurement of the load behaviour in a dry pilot mill using an inductive proximity probe. *Minerals Engineering*, 19(13), pp. 1348-1356.
- KIANGI, K.K., 2011. *Effect of particle filling and size on the behaviour of the ball load and power in a dry mill*.

- KOLACZ, J., 1997. Measurement system of the mill charge in grinding ball mill circuits. *Minerals Engineering*, 10(12), pp. 1329-1338.
- LO, Y., HERBST, J., RAJAMANI, K. and ARBITER, N., 1988. Design considerations for large diameter ball mills. *International Journal of Mineral Processing*, 22(1), pp. 75-93.
- MALEKI-MOGHADDAM, M., YAHYAEI, M. and BANISI, S., 2013. A method to predict shape and trajectory of charge in industrial mills. *Minerals Engineering*, 46, pp. 157-166.
- MALEKI-MOGHADDAM, M., YAHYAEI, M. and BANISI, S., 2013. A method to predict shape and trajectory of charge in industrial mills. *Minerals Engineering*, 46, pp. 157-166.
- MISHRA, B., 2003. A review of computer simulation of tumbling mills by the discrete element method: Part II—Practical applications. *International Journal of Mineral Processing*, 71(1), pp. 95-112.
- MISHRA, B. and RAJAMANI, R.K., 1994. Simulation of charge motion in ball mills. Part 1: experimental verifications. *International Journal of Mineral Processing*, 40(3), pp. 171-186.
- MORRELL, S., 1993. The prediction of power draw in wet tumbling mills.
- MOYS, M., 1993. A model of mill power as affected by mill speed, load volume, and liner design. *JOURNAL-SOUTH AFRICAN INSTITUTE OF MINING AND METALLURGY*, 93, pp. 135-135.
- MOYS, M. and SKORUPA, J., 1993. Measurement of the radial and tangential forces exerted by the load on a liner in a ball mill, as a function of load volume and mill speed. *International Journal of Mineral Processing*, 37(3), pp. 239-256.
- MULENGA, F.K. and MOYS, M.H., 2014. Effects of slurry filling and mill speed on the net power draw of a tumbling ball mill. *Minerals Engineering*, 56(0), pp. 45-56.
- NAPIER-MUNN, T. and WILLS, B.A., 2011. *Wills' mineral processing technology: an introduction to the practical aspects of ore treatment and mineral recovery*. Butterworth-Heinemann.
- PONTT, J., 2004. MONSAG: A new monitoring system for measuring the load filling of a SAG mill. *Minerals Engineering*, 17(11), pp. 1143-1148.
- POWELL, M. and MAINZA, A., 2006. Extended grinding curves are essential to the comparison of milling performance. *Minerals Engineering*, 19(15), pp. 1487-1494.
- POWELL, M. and MAINZA, A., 2006. Extended grinding curves are essential to the comparison of milling performance. *Minerals Engineering*, 19(15), pp. 1487-1494.
- POWELL, M., PERKINS, T. and MAINZA, A., 2011. Grindcurves applied to a range of SAG and AG mills, *Proc. SAG 2011*.
- POWELL, M., 1991. The effect of liner design on the motion of the outer grinding elements in a rotary mill. *International Journal of Mineral Processing*, 31(3), pp. 163-193.

POWELL, M., MCBRIDE, A. and GOVENDER, I., 2003. Application of DEM outputs to refining applied sag mill models, *IMPC 2003 Conference 2003*, South African Institute of Mining and Metallurgy, pp. 307-316.

POWELL, M. and NURICK, G., 1996. A study of charge motion in rotary mills Part 1—extension of the theory. *Minerals Engineering*, 9(2), pp. 259-268.

POWELL, M. and NURICK, G., 1996. A study of charge motion in rotary mills Part 2—Experimental work. *Minerals Engineering*, 9(3), pp. 343-350.

POWELL, M. and NURICK, G., 1996. A study of charge motion in rotary mills Part 2—Experimental work. *Minerals Engineering*, 9(3), pp. 343-350.

POWELL, M., VAN DER WESTHUIZEN, A. and MAINZA, A., 2009. Applying grindcurves to mill operation and optimisation. *Minerals Engineering*, 22(7), pp. 625-632.

POWELL, M., VAN DER WESTHUIZEN, A. and MAINZA, A., 2009. Applying grindcurves to mill operation and optimisation. *Minerals Engineering*, 22(7), pp. 625-632.

RAJAMANI, R., MISHRA, B., VENUGOPAL, R. and DATTA, A., 2000. Discrete element analysis of tumbling mills. *Powder Technology*, 109(1), pp. 105-112.

ROSE, H.E. and SULLIVAN, R.M.E., 1958. *A treatise on the internal mechanics of ball, tube, and rod mills*. Constable.

SHOJI, K., AUSTIN, L., SMAILA, F., BRAME, K. and LUCKIE, P.T., 1982. Further studies of ball and powder filling effects in ball milling. *Powder Technology*, 31(1), pp. 121-126.

SPENCER, S., CAMPBELL, J., SHARP, V., DAVEY, K., PHILLIPS, P., BARKER, D. and HOLMES, R., 2005. Multiple sensor surface vibrations analysis for monitoring tumbling mill performance, *Intelligence in a Small Materials World. Selected papers from The Fourth International Conference on Intelligent Processing and Manufacturing of Materials (IPMM-2003)(ed: JA Meech et al) pp 2005*, pp. 359-376.

SPENCER, S., CAMPBELL, J., WELLER, K. and LIU, Y., 1999. Acoustic emissions monitoring of SAG mill performance, *Intelligent Processing and Manufacturing of Materials, 1999. IPMM'99. Proceedings of the Second International Conference on 1999*, IEEE, pp. 939-946.

SU, Z., WANG, P., YU, X. and LV, Z., 2008. Experimental investigation of vibration signal of an industrial tubular ball mill: monitoring and diagnosing. *Minerals Engineering*, 21(10), pp. 699-710.

TANG, J., ZHAO, L., YU, W., YUE, H. and CHAI, T., 2010. Soft sensor modeling of ball mill load via principal component analysis and support vector machines. *Advances in Neural Network Research and Applications*. Springer, pp. 803-810.

TANO, K.T., 2005. Continuous monitoring of mineral processes with special focus on tumbling mills: a multivariate approach.

TANO, K.T. and PÅLSSON, B.I., 2008. Assessment of mill lifter bar deflection measurements using wavelets and discrete element methods. *Granular Matter*, 10(4), pp. 279-283.

TANO, K.T., PÅLSSON, B.I. and SELLGREN, A., 2005. On-line lifter deflection measurements showing flow resistance effects in grinding mills. *Minerals Engineering*, 18(11), pp. 1077-1085.

VAN NIEROP, M. and MOYS, M., 1997. Measurement of load behaviour in an industrial grinding mill. *Control Engineering Practice*, 5(2), pp. 257-262.

VERMEULEN, L., OHLSON DE FINE, M. and SCHAKOWSKI, F., 1984. Physical information from the inside of a rotary mill. *J.S.Afr.Inst.Min.Metall.*, 84(8), pp. 247-253.

ZHAO, L., TANG, J., YU, W., YUE, H. and CHAI, T., 2010. Modelling of mill load for wet ball mill via GA and SVM based on spectral feature, *Bio-Inspired Computing: Theories and Applications (BIC-TA)*, 2010 IEEE Fifth International Conference on 2010, IEEE, pp. 874-879.

APPENDICES

Appendix 1: Volumetric filling calculation procedure using the toe and shoulder positions of the charge

$$\theta_s = \frac{\pi}{2} - \left(\theta_T - \frac{\pi}{2} \right) \left((0.3386 + 0.1041\phi c) + (1.54 - 2.5673\phi c)J_t \right)$$

Mill filling calculation for the feed rate of 400tph

$$0.9056 = \frac{22}{14} - \left(3.8798 - \frac{22}{14} \right) \left((0.3386 + 0.1041 \times 0.75) + (1.54 - 2.5673 \times 0.75)J_t \right)$$

$$0.9056 = 1.5714 - (2.3088)(0.41668 - 0.3855J_t)$$

$$0.9056 - 1.5714 = -0.9620 + 0.8900424J_t$$

$$-0.6658 = -0.9620 + 0.8900424J_t$$

$$-0.6658 + 0.9620 = 0.8900424J_t$$

$$0.2962 = 0.8900424J_t$$

$$J_t = \frac{0.2962}{0.8900424} \times 100$$

$$J_t = 33.2\%$$

Appendix 2: The average values of the Sensomag values converted using the CSIRO acoustic reference

Test No.	Speed (%) critical)	Slurry shoulder (°)	Slurry toe (°)	Ball shoulder (°)	Ball toe (°)
1	75	48.4	231.5	47.2	237.6
2	75	54.1	226.9	52.7	235.3
3	75	58.5	224.0	58.2	230.2
4	80	64.4	226.8	64.1	230.7
5	85	63.1	232.2	63.3	235.8
6	85	65.4	229.8	66.1	230.1
7	85	72.8	228.6	74.2	229.2
8	85	75.8	226.2	76.9	225.0

Appendix 3: Size distribution of feed and discharge sample for the 75% critical speed test

Size (mm)	Feed	Discharge -2.1 tph	Discharge-1.8 tph	Discharge - 1.2 tph
180	100.00	100	100	100
120	90.59	100	100	100
90	77.69	100	100	100
63	64.06	100	100	100
45	57.15	100	100	100
31.5	51.65	100	100	100
22.4	46.72	100	100	100
16	42.72	100	100	100
11.2	38.58	99.97	99.97	99.99
8	35.20	99.85	99.89	99.95
5.6	32.51	99.67	99.75	99.9
4	30.58	99.44	99.55	99.88
2.8	28.46	99.25	99.37	99.88
2	26.40	99.02	99.1	99.88
1.4	23.76	98.66	98.91	99.78
1	20.94	98.19	98.61	99.78
0.85	19.80	97.99	97.77	99.68
0.6	17.60	97.36	96.46	99.48
0.425	14.91	96.11	93.94	98.98
0.3	12.34	91.83	87.26	97.28
0.212	9.80	82.41	76.49	92.49
0.15	7.53	73.63	65.55	86
0.106	5.82	60.01	53.51	75.21
0.075	4.32	49.63	41.95	62.82
0.053	3.29	40.39	35.02	52.33
0.038	2.74	35.79	31.18	44.24
0.025	2.50	34.38	28.72	40.24

Appendix 4: Size distribution of feed and discharge sample for the 80% and 85% critical speed test

Size (mm)	80% critical speed	85% critical speed			
	Discharge - 2.4 tph	Discharge - 1.8 tph	Discharge - 2.1 tph	Discharge - 2.4 tph	Discharge - 2.8 tph
180	100	100	100	100	100
120	100	100	100	100	100
90	100	100	100	100	100
63	100	100	100	100	100
45	100	100	100	100	100
31.5	100	100	100	100	100
22.4	100	100	100	100	100
16	100	100	100	100	100
11.2	99.98	99.99	99.99	99.99	99.99
8	99.91	99.96	99.95	99.95	99.94
5.6	99.80	99.92	99.88	99.87	99.84
4	99.36	99.84	99.77	99.68	99.72
2.8	99.01	99.74	99.64	99.47	99.61
2	98.72	99.53	99.41	99.35	99.26
1.4	98.38	99.39	99.23	99.16	98.99
1	97.95	99.22	99.03	98.93	98.6
0.85	97.72	99.11	98.87	98.68	98.24
0.6	96.95	98.7	98.28	97.9	97.07
0.425	95.41	97.68	93.33	96.57	94.72
0.3	90.61	95.11	89.9	91.54	88.2
0.212	81.95	87.75	80.88	80.68	77.99
0.15	71.68	79.73	71.83	71.07	66.54
0.106	60.05	68.11	59.53	59.5	54.25
0.075	49.82	56.85	48.4	50.66	44.84
0.053	40.08	46.79	38.85	42.69	36.93
0.038	33.37	40.19	31.79	38.04	32.71
0.025	29.94	36.37	28.93	36.56	31.47